VOLATILE METAL BOROHYDRIDE COMPLEXES: SYNTHESIS AND CHARACTERIZATION OF NEW CHEMICAL VAPOR DEPOSITION PRECURSORS

BY

JUSTIN L. MALLEK

DISSERTATION

Submitted in partial fulfillment of the requirements
for the degree of Doctor of Philosophy in Chemistry
in the Graduate College of the
University of Illinois at Urbana-Champaign, 2014

Urbana, Illinois

Doctoral Committee:

Professor Gregory Girolami, Chair
Professor John Abelson
Professor Joseph Lyding
Professor Kenneth Suslick

ABSTRACT

The complex sodium methylborohydride, $Na(H_3BCH_3)$, can be prepared in high yield (83%) by the addition of trimethylboroxine, $(H_3C)_3B_3O_3$, to sodium aluminum hydride, $NaAlH_4$. The subsequent reaction of two equivalents of sodium methylborohydride with the alkaline earth bromides; $MgBr_2$, $CaBr_2$, $SrBr_2$, and $BaBr_2$ in 1,2-dimethoxyethane, DME, affords the new alkaline earth methylborohydride DME adducts: $[Mg(H_3BCH_3)_2(DME)]_2$, $Ca(H_3BCH_3)_2(DME)_2$, $Sr(H_3BCH_3)_2(DME)_3$, and $Ba(H_3BCH_3)_2(DME)_3$. $[Mg(H_3BCH_3)_2(DME)]_2$ sublimes between 80 and 90 °C at 10 mTorr while the larger alkaline earth methylborohydrides do not sublime up to 120 °C. $[Mg(H_3BCH_3)_2(DME)]_2$ is an asymmetrically bridged dimer in the solid state where each Mg center has a terminal κ^2*H*-methylborohydride, a bridging κ^2*H*-methylborohydride, a bridging κ^1*H*-methylborohydride, and a chelating DME. The other alkaline earth methyborohydrides have two κ^3*H*-methylborohydrides and two chelating DME for the Ca complex and three chelating DME for the Sr and Ba complexes.

Rare earth methylborohydride THF adducts are prepared by the reaction of a rare earth chloride (Sc, Y, Nd, Gd, Er) with 3 to 4 equivalents of sodium methylborohydride in THF. The scandium and yttrium complexes are isolated by sublimation at 50 °C while the neodymium, gadolinium, and erbium complexes are isolated by sublimation at 60 °C. In the solid state, scandium methylborohydride has three κ^3*H*-methylborohydrides and one coordinated THF. The yttrium, gadolinium, and

erbium complexes crystallize as charge separated ion pairs: $[RE(H_3BCH_3)_2(THF)_4][RE(H_3BCH_3)_4]$, where the cation has two κ^3*H*-methylborohydrides and four coordinated THF and the anion consists of four κ^3*H*-methylborohydrides. The neodymium complex is a methylborohydride bridged dimer, $[Nd(H_3BCH_3)_3(THF)_2]_2$, where each Nd center has two κ^3*H*-methylborohydrides, two bridging κ^2*H*,κ^2*H*-methylborohydrides and two THF. In addition to the THF adducts, the neodymium DME adduct, $Nd(H_3BCH_3)_3(DME)_{1.5}$, has also been synthesized by a similar method. This complex can be sublimed under vacuum at 115 °C. The Er complex has been used in preliminary CVD experiments which demonstrate the ability to grow thin films between 250 and 350 °C using this new precursor.

The synthesis of sodium aminodiboranates with sterically bulky or electron withdrawing substituents on nitrogen has been achieved by the treating amine-borane with either BH_3·THF or by thermolysis at elevated temperatures followed by the addition of BH_3·THF, which produced μ-aminodiborane. The μ-aminodiborane can then be ring opened with NaH, similar to what has been reported by Keller for the synthesis of sodium *N*,*N*-dimethylaminodiboranate. Implementing this method, the sterically bulky aminodiboranates: sodium *N*-isopropyl-*N*-methylaminodiboranate, sodium *N*,*N*-diisopropylaminodiboranate, sodium *cis*-2,6-dimethylpiperidinyldiboranate, sodium *tert*-butylaminodiboranate, and sodium *N*-isopropylaminodiboranate have been prepared. The aminodiboranates with electron

withdrawing substituents on nitrogen: sodium *N*-benzylaminodiboranate, sodium *N*-benzyl-*N*-methylaminodiboranate, and sodium 2,2-difluoroethylaminodiboranate were also able to be prepared by the addition of BH_3·THF to the appropriate amine-borane followed by treatment with sodium hydride. Unfortunately, these aminodiboranates decompose at room temperature.

Magnesium *cis*-2,6-dimethylpiperidinyldiboranate was able to be synthesized by treatment of $MgBr_2$ with two equivalents of sodium *cis*-2,6-dimethylpiperidinyldiboranate in diethyl ether followed by sublimation at 50 °C under vacuum. The hydrolysis/thermolysis product μ-(*cis*-2,6-dimethylpiperidinyl)diborane is, however, present in the sublimate due to similar volatility to the desired magnesium product. Synthesis of magnesium *N*,*N*-diisopropylaminodiboranate was attempted by ball milling $MgBr_2$ and sodium *N*,*N*-diisopropylaminodiboranate followed by sublimation at 65 °C. Interestingly, primarily decomposition products, *N*,*N*-dimethylimine and magnesium borohydride, $Mg(BH_4)_4$, were observed by ^{11}B NMR in the reaction mixture.

Static chemical vapor deposition (CVD) has been successfully used to deposit conformal thin films of hafnium diboride, HfB_2, and iron metal from hafnium borohydride, $Hf(BH_4)_4$, and iron pentacarbonyl, $Fe(CO)_5$, respectively. Microtrenches with aspect ratios greater than 10:1 were able to be completely infilled with HfB_2 or iron and macrotrenches were able to be coated with thin films of HfB_2 which has a 40% step

coverage at an aspect ratio of 1000:1. HfB_2 thin films deposited by static CVD have a Hf:B ratio similar to films deposited using $Hf(BH_4)_4$ in an actively pumped, low pressure CVD system; although the relative hydrogen content of the film deposited by static CVD was greater. Iron thin films deposited by static CVD have an iron composition as high as 97% with approximately 1.5% carbon and oxygen each.

ACKNOWLEDGMENTS

There are a number of people who have supported me and my research throughout my graduate studies. I would like to take the opportunity to gratefully acknowledge their involvement with the work presented in this thesis.

First, I thank my advisor, Professor Gregory Girolami, for his guidance and patients over the past five years. I greatly appreciate his willingness to allow me to pursue my scientific interests while offering valuable direction. I also thank my thesis committee members, Professor John Abelson and Professor Joe Lyding for our many successful collaborations, and Professor Ken Suslick for allowing me the opportunity to teach a number of lectures while working as his teaching assistant.

Thanks to all of the past and present Girolami group members: Scott Daly, Brain Bellott, Andrew Dunbar, Luke Davis, Jennifer Steele, Noel Chang, Peter Sempsrott, Joe Macor, Brian Trinh, Tracey Hitt, Kaili Zhang, and Sumeng Liu. Your insights and suggestions were typically well received and were often extremely helpful. You were a large part of what made working in the Girolami Group such a pleasure. I also thank my collaborators: Shaista Babar, Wenijiao Wang, Pengyi Zhang, Elham Mohimi, Jae Won Do, Wei Ye, Pam Pena Martin, and especially Andrew Cloud. Andrew Cloud and I worked together on the Static CVD project. His dedication to the project, as well as his eagerness to begin new collaborations which utilize the static CVD technique has greatly contributed to making that project such a resounding success.

Thanks to all of the facilities personal who assisted me with much of the work in this thesis. I would like to especially thank Marie Keel, Beth Eves, and Rudy Laufhutte for quickly running all of the EA samples I brought to them. Thanks to Danielle Gray and Jeff Berkte for collecting the crystal data for all of the crystal structures reported in this thesis. Thanks to Don O'Brien, Rich Parrish and Dave Perry for quickly putting together every piece of glassware I could draw up and Mike Harland, as well as the rest of the machine shop staff for the assistance with the repair of our previous CVD chamber and the construction of our new one.

Thanks to the IMP office secretaries: Beth Myler, Connie Knight, Theresa Struss, and Karen Neumann. Whether it was free food in the IMP office, changes in my meeting schedule with Greg, or preparing for my final defense, you made sure I knew what was going on and when important deadlines were approaching. I will greatly miss working with you in the future.

Most importantly, thanks to my amazing parents, Kris and Pam, who have provided a lifetime of love and support. Without their guidance and dedication I would never have completed the work in this thesis. Finally, thanks to my younger brother, Aaron for teaching me patience, which has been very useful over the past few years. I hope I've set the bar high enough for you and look forward to reading your thesis in the future.

TABLE OF CONTENTS

CHAPTER 1: Volatile Metal Borohydrides: Factors Influencing Volatility and Applications as Chemical Vapor Deposition Precursors.

Applications of Volatile Molecules: Chemical Vapor Deposition

Thin films have a wide range of applications, some of which are in microelectronics,[1-6] hard coatings,[7-12] optical fibers,[13-16] composites,[17-19] nanostructured catalysts,[20-23] and microelectromechanical systems (MEMS).[24-26] Three of the most important and widely used methods of producing thin films are chemical vapor deposition, CVD,[27-30] a variant of CVD called atomic layer deposition, ALD,[12,30-33] and physical vapor deposition, PVD.[34-36] In CVD, a hot substrate is exposed to a gas-phase molecular precursor or combination of precursors. A chemical reaction occurs on the substrate, leaving behind a thin film while volatile byproducts desorb from the substrate and are removed. By varying the process conditions, it is possible to enhance or retard the nucleation and growth rates, tune the composition, and control the film morphology.[37-43]

In an ALD deposition process, molecular precursors are dosed into the system in alternating cycles. Each cycle saturates the substrate's surface with precursor, which reacts selectively with functional groups left on the substrate in a previous step, and then generates a new set of surface functional groups. For surface saturation to be complete, enough time must be given to enable a monolayer of the precursor to form

over the entire substrate surface; then the system is purged and a second precursor is dosed into the system.[44] ALD is a self-limiting process because each cycle deposits approximately a monolayer of material irrespective of the total dose. This self-limiting behavior depends on choosing deposition conditions such that each precursor is unable to deposit material unimolecularly, for example by means of a thermolysis pathway, and instead has only one available reaction channel: a selective reaction with a surface functional group generated in a previous process step.

PVD processes deposit thin films from highly reactive atomic or ionic species, which travel through a vacuum from a source to the substrate. These species are typically generated by arc ionization, evaporation, pulsed laser ablation, or sputtering. Unlike CVD and ALD, the substrate does not need to be heated during PVD because the atomic or ionic species do not undergo a chemical reaction. The highly reactive species generated during PVD will adhere to a surface with a near unity probability, which means that PVD is generally a line-of-sight technique. Under normal conditions, the reactive species cannot desorb from the substrate or diffuse on the surface.

In the manufacturing of microelectronic devices, an important step is the creation of trenches, called vias, or fins structures which are later filled or coated with metals or insulators to form wire contacts, capacitors, and other circuit components. An important parameter of vias is their aspect ratio: the depth of the relief feature divided by the width of the feature opening. The uniformity of the film deposited in vias is

described in terms of step coverage: the percent difference in film thickness between the side, top, and bottom of a structure. Step coverage is often more broadly referred to as "conformality", where a perfectly conformal film has a 100% step coverage.[45,46] Figure 1.1 shows a comparison between two vias, one with a conformal film and the other with a nonconformal film.

As microelectronic devices become smaller and length scales decrease, the aspect ratio of vias tends to increase. Due to the line-of-sight character of PVD, it is difficult to use this process to deposit conformal films on features with an aspect ratio greater than ~7:1.[6,47] Unlike the "sticky" atomic species generated during PVD, the molecular precursors used in CVD and ALD can repeatedly adsorb to and desorb from the substrate, and can diffuse in the gas phase and on the substrate surface. Ideally, every surface area element eventually is exposed to precursor and becomes coated with film. Conformal thin films have been successfully deposited by CVD in vias with aspect ratios greater than 30:1 in actively pumped, thermal CVD systems,[40,48] and on features with aspect ratios greater than 1000:1 using ALD.[49,50]

The principal advantage of ALD over an actively pumped CVD system is the elimination of the competition between the film growth rate, the rates of diffusion of precursor into relief features, and the rate at which the precursor is removed from the deposition chamber by the vacuum pump or carrier gas.

Figure 1.1. Examples of conformal (left) and nonconformal (right) film. The conformal film has a uniform thickness throughout the structure and the step coverage is 100%. The nonconformal film has less than 100% step coverage.

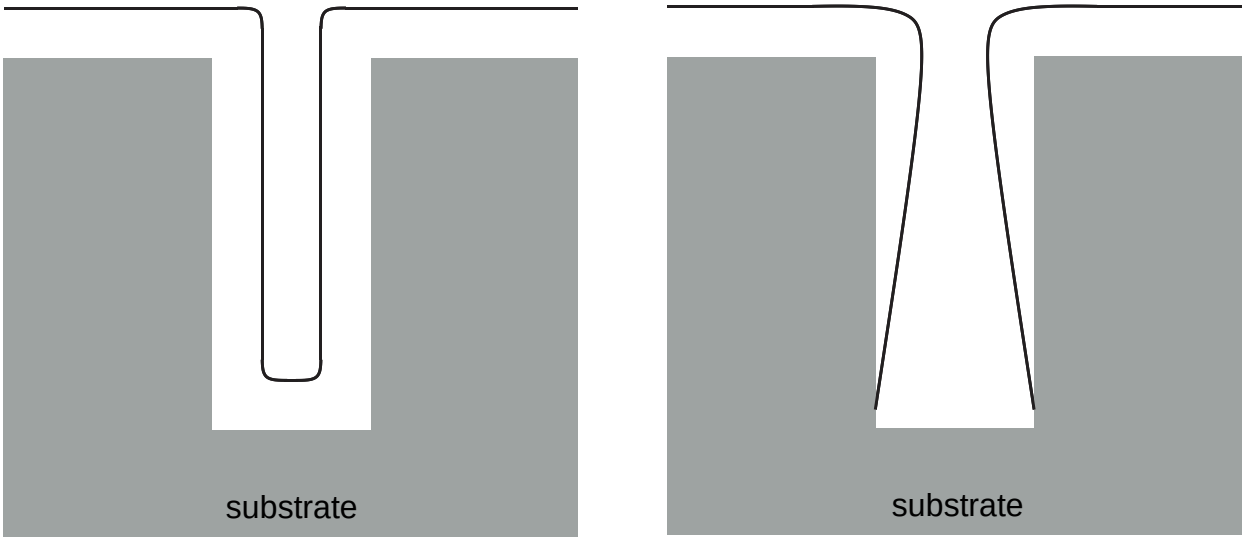

However, a disadvantage of ALD is that, when coating high aspect ratio features, the cycle times can becomes prohibitively long due to the time necessary for the precursors to diffuse into and out of a high aspect ratio feature.

In Chapter 5 of this thesis, I described the deposition of highly conformal thin films by static chemical vapor deposition. This technique employs high vapor pressure molecular precursors in a closed system, and is able to effect the conformal coating of very high aspect ratio features. For example, this technique has been used successfully to deposit thin films of hafnium diboride in a trench with a 40% step coverage at a 1000:1 aspect ratio.

Several aspects must be carefully considered when developing a CVD precursor that can produce a film with the desired composition, conformality, adhesion, and morphology. These considerations include:

- Volatility of the precursor
- Thermal stability of the precursor
- Thermolysis mechanism
- Chemical and thermal reactivity of byproducts
- Precursor and byproduct toxicity

One of the most challenging of these requirements is the identification of precursors that are highly volatile. Although several precursor delivery techniques have been developed for use with low vapor pressure precursors, such as aerosol-assisted

delivery,[27,51,52] liquid delivery,[53-55] or solid delivery systems;[56,57] films produced by these methods often exhibit poor conformality due to the limited ability of the precursor to adsorb reversibly and to diffuse on the surface. As a result, CVD with low vapor pressure precursors often affords films with conformalities little better than those obtainable by PVD.

Borohydride Chemical Vapor Deposition Precursors

Metal hydroborates, or borohydrides as they are often called, constitute an interesting class of CVD precursors, one that we have explored extensively in our research group. Among the ligands used to make such precursors are the parent borohydride anion, BH_4^-, the methylborohydride anion, $H_3BCH_3^-$, the octahydrotriborate anion, $B_3H_8^-$ and the aminodiboranates such as *N*,*N*-dimethylaminodiboranate, $[H_3B\text{-}N(CH_3)_2\text{-}BH_3]^-$. Dozens of transition metal, rare earth, and actinide complexes containing these borohydride ligands have been reported, and several of these molecules have been used successfully to deposit thin films of metals, metal borides, and metal oxides by CVD.

The bulk of this chapter will be dedicated to a discussion of the bonding, steric demands, and intermolecular interactions in metal borohydrides, with the goal of elucidating the factors that give many borohydride complexes such high vapor

pressures. Finally the chapter will conclude with an examination of thin films produced by chemical vapor deposition using borohydride containing precursors.

Borohydride Nomenclature

Before beginning the discussion of the volatility of borohydride complexes, it is worthwhile to mention the chemical nomenclature used to describe the bonding of borohydride ligands to metal centers, and the inconsistencies often found in the literature. For example, the tetrahydroborate anion, BH_4^-, is known to bond to a metal center by means of one, two, or three hydrogen bridges. To describe the number of hydrogen atoms that are interacting with a single metal center, the eta (η) nomenclature originally introduced by Cotton[58] has often been used. For example, the symbol η^3-BH_4^- is often used to describe a tetrahydroborate group bound to a single metal center by means of three hydrogen bridges. However, this nomenclature is incorrect. According to the IUPAC: Red Book IR-9.2.4.3,[59] η is used to describe hapticity, or the number of contiguous atoms in a ligand which are bound to a metal center. In contrast, the primary interactions between borohydride groups and metal centers involve the hydrogen atoms, with little, if any direct boron-metal bonding. Thus, it is appropriate to describe the interaction between BH_4^- ligands and metal centers in terms of denticity and use the kappa, κ, nomenclature, introduced by Sloan and Busch.[60] In the above

example, the descriptor κ^3H indicates that the BH_4^- ligand is tridentate and is bound to the metal center through three hydrogen bridges.

Metal Complexes of Tetrahydroborate, BH_4^-

Tetrahydroborate complexes of the non-radioactive alkali and alkaline earth metals, most of the transition metals and rare earth metals, as well as five of the actinides have been reported; these complexes are summarized in Figure 1.2. BH_4^- is the lightest and smallest polydentate ligand known. It is also unusual in its ability to coordinate in at least three ways to a single metal center, κ^1H, κ^2H, or κ^3H, depending on the degree to which the coordination sphere of the metal center is sterically saturated, as well as the number of metal orbitals available for bonding.[61-63] Additionally, borohydrides can bridge between multiple metal centers to afford oligomers and polymers. These binding modes are depicted in Figure 1.3. Alkali metal borohydrides can be directly synthesized from the elements at elevated temperatures, but other metal containing borohydride complexes must be synthesized by indirect methods.[64]

The most common method to synthesize transition metal, rare earth, and actinide borohydride complexes is by a salt metathesis reaction between the corresponding metal halide and an alkali borohydride salt.

$$MX_n + n\ LiBH_4 \longrightarrow M(BH_4)_n + n\ LiX$$

Figure 1.2. Known metal BH_4^- complexes (red) and those that are stable homoleptic monomers (yellow).

1 H Hydrogen																	2 He Helium
3 Li Lithium	4 Be Beryllium											5 B Boron	6 C Carbon	7 N Nitrogen	8 O Oxygen	9 F Fluorine	10 Ne Neon
11 Na Sodium	12 Mg Magnesium											13 Al Aluminum	14 Si Silicon	15 P Phosphorus	16 S Sulfur	17 Cl Chlorine	18 Ar Argon
19 K Potassium	20 Ca Calcium	21 Sc Scandium	22 Ti Titanium	23 V Vanadium	24 Cr Chromium	25 Mn Manganese	26 Fe Iron	27 Co Cobalt	28 Ni Nickel	29 Cu Copper	30 Zn Zinc	31 Ga Gallium	32 Ge Germanium	33 As Arsenic	34 Se Selenium	35 Br Bromine	36 Kr Krypton
37 Rb Rubidium	38 Sr Strontium	39 Y Yttrium	40 Zr Zirconium	41 Nb Niobium	42 Mo Molybdenum	43 Tc Technetium	44 Ru Ruthenium	45 Rh Rhodium	46 Pd Palladium	47 Ag Silver	48 Cd Cadmium	49 In Indium	50 Sn Tin	51 Sb Antimony	52 Te Tellurium	53 I Iodine	54 Xe Xenon
55 Cs Cesium	56 Ba Barium	57 La Lanthanum	72 Hf Hafnium	73 Ta Tantalum	74 W Tungsten	75 Re Rhenium	76 Os Osmium	77 Ir Iridium	78 Pt Platinum	79 Au Gold	80 Hg Mercury	81 Tl Thallium	82 Pb Lead	83 Bi Bismuth	84 Po Polonium	85 At Astatine	86 Rn Radon
87 Fr Francium	88 Ra Radium	89 Ac Actinium	104 Rf Rutherfordium	105 Db Dubnium	106 Sg Seaborgium	107 Bh Bohrium	108 Hs Hassium	109 Mt Meitnerium	110 Ds Darmstadtium	111 Rg Roentgenium	112 Cn Copernicium	113 Uut Ununtrium	114 Fl Flerovium	115 Uup Ununpentium	116 Lv Livermorium	117 Uus Ununseptium	118 Uuo Ununoctium

58 Ce Cerium	59 Pr Praseodymium	60 Nd Neodymium	61 Pm Promethium	62 Sm Samarium	63 Eu Europium	64 Gd Gadolinium	65 Tb Terbium	66 Dy Dysprosium	67 Ho Holmium	68 Er Erbium	69 Tm Thulium	70 Yb Ytterbium	71 Lu Lutetium
90 Th Thorium	91 Pa Protactinium	92 U Uranium	93 Np Neptunium	94 Pu Plutonium	95 Am Americium	96 Cm Curium	97 Bk Berkelium	98 Cf Californium	99 Es Einsteinium	100 Fm Fermium	101 Md Mendelevium	102 No Nobelium	103 Lr Lawrencium

Figure 1.3. Bonding modes of BH_4^- to metal centers.

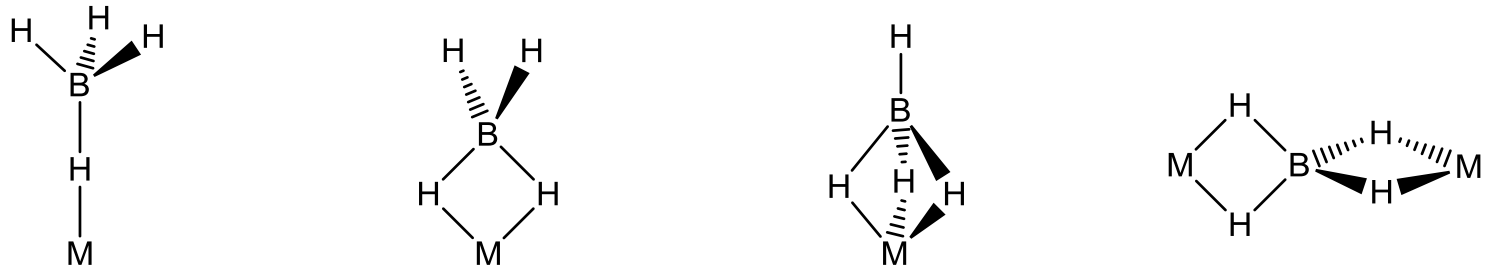

κ^1H κ^2H κ^3H κ^2H,κ^2H

Other routes used to synthesize alkali earth and metal borohydrides have been developed, such as addition of diborane to metal hydrides, metal alkyls, or metal alkoxides.[65-68]

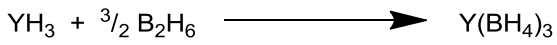

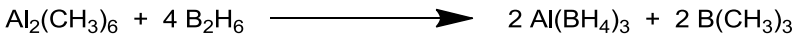

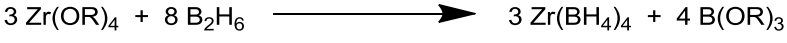

Metal Complexes of Methylborohydride, $H_3BCH_3^-$, and Other Organoborohydrides

A number of alkali, alkaline earth metal, transition metal, rare earth metal, and actinide methylborohydride complexes have been reported, including several which are reported in this thesis for the first time (Figure 1.4). Methylborohydride is a stronger reductant than BH_4^-. As a result, no mid- or late transition metal complexes containing methylborohydride are known, because these metals are easily reduced by methylborohydride to their metallic form. Salt metathesis reactions between a metal halide and alkali methylborohydride have been successful in producing alkaline earth, early transition metal, rare earth, and actinide methylborohyride complexes:

Figure 1.4. Metal $H_3BCH_3^-$ complexes; previously reported (red) and reported in this thesis (blue).

1 H Hydrogen																	2 He Helium
3 Li Lithium	4 Be Beryllium											5 B Boron	6 C Carbon	7 N Nitrogen	8 O Oxygen	9 F Fluorine	10 Ne Neon
11 Na Sodium	12 Mg Magnesium											13 Al Aluminum	14 Si Silicon	15 P Phosphorus	16 S Sulfur	17 Cl Chlorine	18 Ar Argon
19 K Potassium	20 Ca Calcium	21 Sc Scandium	22 Ti Titanium	23 V Vanadium	24 Cr Chromium	25 Mn Manganese	26 Fe Iron	27 Co Cobalt	28 Ni Nickel	29 Cu Copper	30 Zn Zinc	31 Ga Gallium	32 Ge Germanium	33 As Arsenic	34 Se Selenium	35 Br Bromine	36 Kr Krypton
37 Rb Rubidium	38 Sr Strontium	39 Y Yttrium	40 Zr Zirconium	41 Nb Niobium	42 Mo Molybdenum	43 Tc Technetium	44 Ru Ruthenium	45 Rh Rhodium	46 Pd Palladium	47 Ag Silver	48 Cd Cadmium	49 In Indium	50 Sn Tin	51 Sb Antimony	52 Te Tellurium	53 I Iodine	54 Xe Xenon
55 Cs Cesium	56 Ba Barium	57 La Lanthanum	72 Hf Hafnium	73 Ta Tantalum	74 W Tungsten	75 Re Rhenium	76 Os Osmium	77 Ir Iridium	78 Pt Platinum	79 Au Gold	80 Hg Mercury	81 Tl Thallium	82 Pb Lead	83 Bi Bismuth	84 Po Polonium	85 At Astatine	86 Rn Radon
87 Fr Francium	88 Ra Radium	89 Ac Actinium	104 Rf Rutherfordium	105 Db Dubnium	106 Sg Seaborgium	107 Bh Bohrium	108 Hs Hassium	109 Mt Meitnerium	110 Ds Darmstadtium	111 Rg Roentgenium	112 Cn Copernicium	113 Uut Ununtrium	114 Fl Flerovium	115 Uup Ununpentium	116 Lv Livermorium	117 Uus Ununseptium	118 Uuo Ununoctium

58 Ce Cerium	59 Pr Praseodymium	60 Nd Neodymium	61 Pm Promethium	62 Sm Samarium	63 Eu Europium	64 Gd Gadolinium	65 Tb Terbium	66 Dy Dysprosium	67 Ho Holmium	68 Er Erbium	69 Tm Thulium	70 Yb Ytterbium	71 Lu Lutetium
90 Th Thorium	91 Pa Protactinium	92 U Uranium	93 Np Neptunium	94 Pu Plutonium	95 Am Americium	96 Cm Curium	97 Bk Berkelium	98 Cf Californium	99 Es Einsteinium	100 Fm Fermium	101 Md Mendelevium	102 No Nobelium	103 Lr Lawrencium

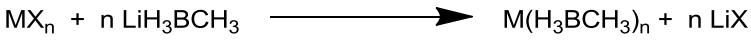

The uranium complex $U(H_3BCH_3)_4$ has been synthesized by the addition of trimethylborane, $B(CH_3)_3$, to uranium borohydride, $U(BH_4)_4$:[69]

The alkaline earth complex, $Mg(H_3BCH_3)_2$ has been claimed to be produced by the addition of borane tetrahydrofuran, BH_3·THF, to methyl-magnesium hydride, but this finding was not reproducible in our hands.[70] In addition to the methylborohydride complexes, other mono(organo)borohydride complexes of uranium have been synthesized according to the following method, where R = ethyl or phenyl groups:[71]

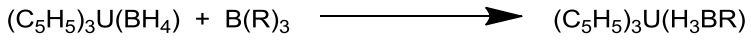

Similarly to BH_4^-, monosubstituted borohydrides can coordinate to metal centers by κ^2H and κ^3H bonding modes and can also bridge between two metal centers in a κ^2H,κ^1H or κ^2H,κ^2H fashion. Unlike BH_4, monosubstituted borohydrides cannot bridge in a κ^3H,κ^1H or κ^2H,κ^2H fashion due to the presence of the alkyl or aryl substituent. This

characteristic, which will be discussed in greater length later in this chapter, may result in increased volatility of the methylborohydride species in comparison to the polymeric BH_4^- parent complexes.

Metal Complexes of Octahydrotriborate, $B_3H_8^-$

A number of metal complexes containing the octahydrotriborate anion, $B_3H_8^-$, have been described,[72-75] but only a few of them are reported to be volatile, and of those only one has successfully been used as a CVD precursor. Magnesium octahydrotriborate, $Mg(B_3H_8)_2$, and its Lewis base adducts $Mg(B_3H_8)_2 \cdot L_2$, (L = dimethyl ether and diethyl ether) have been prepared by ball milling anhydrous $MgBr_2$ or the respective $MgBr_2$ etherate with NaB_3H_8. All three $Mg(B_3H_8)_2$ complexes sublime in vacuum between 70 and 80 °C.[76] Chromium octahydrotriborate, $Cr(B_3H_8)_2$, is the only homoleptic transition-metal $B_3H_8^-$ complex known. It is prepared by a salt metathesis/reduction reaction between $CrCl_3$ and NaB_3H_8; the initially formed chromium(III) intermediate, presumed to be $CrH(B_3H_8)_2$, converts to the chromium(II) final product and is purified by sublimation at 35 °C.[77,78]

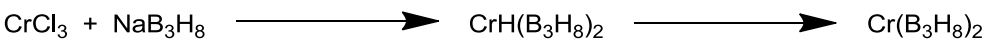

The heteroleptic complex (pentamethylcyclopentadienyl)bis(octahydrotriborate)-vanadium, Cp*V(B_3H_8)$_2$, is volatile but partially decomposes during sublimation at 70 °C.[79] The dimethyl octahydrotriborate metal complexes (H_3C)$_2$M(B_3H_8) (M = Al, Ga, and In) are highly volatile molecular species; the aluminum complex is the most volatile $B_3H_8^-$ containing complex reported, with a vapor pressure of 13 Torr at 0 °C.[80-82] The synthesis of (H_3C)$_2$In(B_3H_8) proceeds by an interesting reaction between trimethylindium, In(CH_3)$_3$, and tetraborane, B_4H_{10}, which produces the desired product and methylborane.

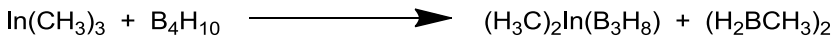

Metal Complexes of Aminodiboranates

Our group has demonstrated the ability of aminodiboranate ligands to form numerous homoleptic complexes containing alkaline earths, transition metals, rare earths, and actinides as well as a number of heteroleptic, cyclopentadienyl containing transition metal complexes.[83-96] The *N*,*N*-dimethylaminodiboranate group, DMADB, has been extensively investigated, and metal complexes containing DMADB are shown in Figure 1.5. These DMADB complexes can be synthesized by a salt metathesis reaction in an ethereal solvent or by solid state ball milling.

Figure 1.5. Metal DMADB complexes; volatile homoleptic (green), volatile heteroleptic (yellow), and nonvolatile (red).

1 H Hydrogen																	2 He Helium
3 Li Lithium	4 Be Beryllium											5 B Boron	6 C Carbon	7 N Nitrogen	8 O Oxygen	9 F Fluorine	10 Ne Neon
11 Na Sodium	12 Mg Magnesium											13 Al Aluminum	14 Si Silicon	15 P Phosphorus	16 S Sulfur	17 Cl Chlorine	18 Ar Argon
19 K Potassium	20 Ca Calcium	21 Sc Scandium	22 Ti Titanium	23 V Vanadium	24 Cr Chromium	25 Mn Manganese	26 Fe Iron	27 Co Cobalt	28 Ni Nickel	29 Cu Copper	30 Zn Zinc	31 Ga Gallium	32 Ge Germanium	33 As Arsenic	34 Se Selenium	35 Br Bromine	36 Kr Krypton
37 Rb Rubidium	38 Sr Strontium	39 Y Yttrium	40 Zr Zirconium	41 Nb Niobium	42 Mo Molybdenum	43 Tc Technetium	44 Ru Ruthenium	45 Rh Rhodium	46 Pd Palladium	47 Ag Silver	48 Cd Cadmium	49 In Indium	50 Sn Tin	51 Sb Antimony	52 Te Tellurium	53 I Iodine	54 Xe Xenon
55 Cs Cesium	56 Ba Barium	57 La Lanthanum	72 Hf Hafnium	73 Ta Tantalum	74 W Tungsten	75 Re Rhenium	76 Os Osmium	77 Ir Iridium	78 Pt Platinum	79 Au Gold	80 Hg Mercury	81 Tl Thallium	82 Pb Lead	83 Bi Bismuth	84 Po Polonium	85 At Astatine	86 Rn Radon
87 Fr Francium	88 Ra Radium	89 Ac Actinium	104 Rf Rutherfordium	105 Db Dubnium	106 Sg Seaborgium	107 Bh Bohrium	108 Hs Hassium	109 Mt Meitnerium	110 Ds Darmstadtium	111 Rg Roentgenium	112 Cn Copernicium	113 Uut Ununtrium	114 Fl Flerovium	115 Uup Ununpentium	116 Lv Livermorium	117 Uus Ununseptium	118 Uuo Ununoctium

58 Ce Cerium	59 Pr Praseodymium	60 Nd Neodymium	61 Pm Promethium	62 Sm Samarium	63 Eu Europium	64 Gd Gadolinium	65 Tb Terbium	66 Dy Dysprosium	67 Ho Holmium	68 Er Erbium	69 Tm Thulium	70 Yb Ytterbium	71 Lu Lutetium
90 Th Thorium	91 Pa Protactinium	92 U Uranium	93 Np Neptunium	94 Pu Plutonium	95 Am Americium	96 Cm Curium	97 Bk Berkelium	98 Cf Californium	99 Es Einsteinium	100 Fm Fermium	101 Md Mendelevium	102 No Nobelium	103 Lr Lawrencium

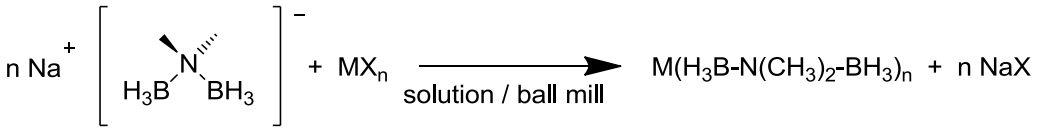

One alternative synthetic route for the synthesis of the 1,2-dimethoxyethane, DME, adduct of calcium *N*,*N*-dimethylaminodiboranate, $Ca(DMADB)_2(DME)$, has also been described: addition of calcium metal to dimethylamine borane in refluxing DME:[93]

DMADB complexes often are bound in a κ^2H,κ^2H chelating fashion to metal centers, although some exhibit a κ^2H,κ^1H or even κ^1H,κ^1H binding mode due to electronic effects (the number of empty *d*-orbitals on the metal center). A number of lanthanide DMADB complexes form dimers or polymers in the solid state, in which either one BH_3 group bridges between two metal centers, or the two BH_3 groups in one DMADB ligand interact with different metal centers.

Like borohydrides and monosubstituted borohydrides, DMADB is a strong reducing agent, and is capable of reducing metal centers by one electron, and forming the cyclic species μ-(dimethylamino)diborane, $\mu\text{-}(H_3C)_2NB_2H_5$, and hydrogen:

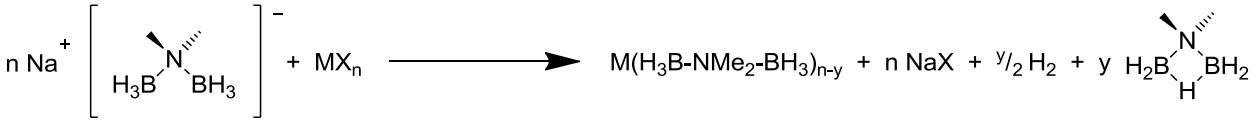

Even Ti(III) is reduced to Ti(II) by DMADB. Because of this reducing power, no homoleptic DMADB complexes of the late transition metals are known.

In addition to the *N*,*N*-dimethylamine backbone, other amines can also serve as the backbone for aminodiboranate ligands, including; ammonia, methylamine, ethylamine, ethylmethylamine, diethylamine, piperidine, and pyrrolidine.[84,86] In chapter 4 of this thesis, this ligand set will be expanded to examine the electronic effects of low pK_a (more acidic) and high pK_a (less acidic) amines, as well as the steric effects of adding sterically hindered *N*-alkyl groups to the aminodiboranate backbone.

The Nature of B-H Bonds

In order to explain the unusually high volatility of many of the borohydride complexes, it is important to examine the chemical nature of the B-H bond. The electronegativities of boron (χ = 2.04) and hydrogen (χ = 2.20) illustrate the greater affinity of hydrogen to draw electron density towards itself. The electronegative difference creates a slightly polarized B-H bond with increased electron density on

hydrogen and decreased electron density on boron.[97] An example of this effect can be seen in the charge density difference plots of beryllium borohydride (Figure 1.6).

The Mulliken population analysis is a simple way of estimating the charge distribution within a molecule or ion. For the borohydride anion, BH_4^-, the Mulliken charges are calculated to be +0.044 for boron and -0.261 for each of the four hydrogens, summing to a net -1 charge overall.[98] However, for a molecular species in which BH_4^- is bound to a metal center, some of the hydrogens will bridge to the metal center while others will be terminal. Table 1.1 contains the calculated Bader charges for certain metal bound borohydrides, which show that there is more electron density on the bridging hydrogen atoms, as expected, owing to the Coulombic effect of the positively charged metal center. It is important to note, however, that the terminal hydrogen continue to bear a partial negative, albeit, weaker charge.[99,100]

Figure 1.6. Charge density difference plots of beryllium borohydride. Positive (+) and negative (-) symbols indicate an increase and decrease in electron density relative to the free atoms, respectively.[101]

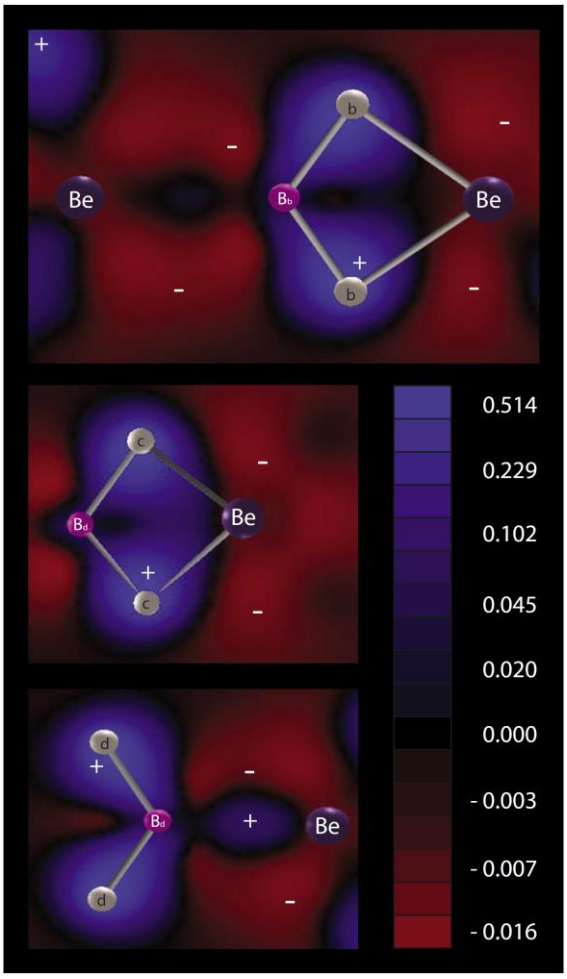

Table 1.1. Calculated Bader charges for homoleptic borohydrides.[102]

	Metal	Boron	Bridging hydrogen	Terminal hydrogen
$Al(BH_4)_3$	+2.29	+1.54	-0.64	-0.50
$Sc(BH_4)_3$	+1.85	+1.54	-0.55	-0.51
$Y(BH_4)_3$	+2.03	+1.53	-0.57	-0.51
$Zr(BH_4)_4$	+2.17	+1.52	-0.53	-0.49

Electronic Structure and Metal Interactions of Borohydrides

Before the electronic interactions between borohydrides and metal centers are discussed, it is first important to examine the electronic structure of the BH_4^- anion itself. The BH_4^- group has four occupied valence molecular orbitals, MOs, which correspond to a_1 and t_2 representations. The a_1 MO is typically neglected in the bonding scheme owing to its low (corelike) energy and consequent negligible overlap with orbitals on the metal center. The primary interaction between the metal center and BH_4^- involves the t_2 MOs on the latter; the overlap largely involves the hydrogen atom atomic orbitals, AOs. The BH_4^- orbitals involved in κ^1H, κ^2H, and κ^3H coordination modes are shown in Figure 1.7.

The electronic nature of the interaction of a MX_3 fragment with a single BH_4^- group can be analyzed as follows, in which the M-B vector defines the z axis (Figure 1.7). For a κ^1H interaction, there is only one significant bonding interaction: between the BH_4^- t_{2z} orbital and a metal orbital of a_1 symmetry. In a κ^2H interaction, two bonding interactions are possible: between the BH_4^- t_{2z} and t_{2x} orbitals and metal orbitals of a_1 and e_x symmetry, respectively. Finally, with a κ^3H interaction, the t_{2x}, t_{2y}, and t_{2z} orbitals of the BH_4^- interact with the e_x, e_y, and a_1 orbitals of the MX_3 fragment. Because of the three bonding interactions of the κ^3H bound borohydride it is considerably more thermodynamically favorable than either the κ^1H or κ^2H cases for d^0 metals.[103]

Figure 1.7. Ligand orbitals involved in κ^1H, κ^2H, and κ^3H M-BH_4 bonding modes.

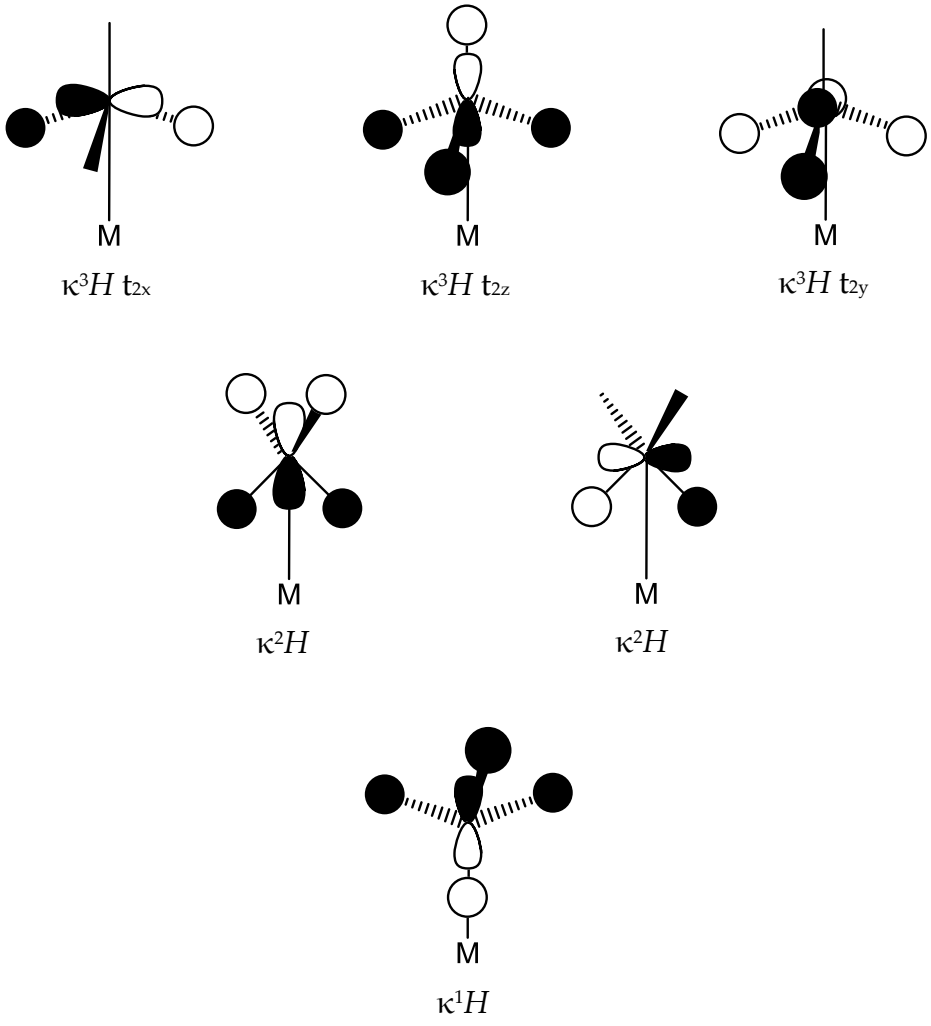

κ^3H t_{2x} κ^3H t_{2z} κ^3H t_{2y}

κ^2H κ^2H

κ^1H

Low lying a_1

The d^0 borohydride complexes $Zr(BH_4)_4$ and $Hf(BH_4)_4$ have T_d symmetry and, because each BH_4^- ligand is κ^3H, there are 12 hydrogen atoms in the inner coordination sphere of each metal. The filled BH_4^- orbitals that interact with the metal center form 12 symmetry adapted linear combinations, SALCs, that transform as $A_1 + E + T_1 + 2T_2$. The A_1, E, and T_2 SALCs are the same symmetry as the s, (d_{z^2}, $d_{x^2-y^2}$), and (p_x, p_y, p_z)/(d_{xy}, d_{xz}, d_{yz}) atomic orbitals on the metal center, respectively. In contrast, no valence orbital on the metal center transforms as T_1; as a result, 3 of the SALCs are non-bonding and only 9 donate electrons to the metal center. These $M(BH_4)_4$ complexes therefore have electron counts of 18, to which each BH_4^- contributes (on average) 4.5 bonding electrons.[104]

Figure 1.8 shows the MO diagram of $Zr(BH_4)_4$ and $Hf(BH_4)_4$ in comparison to the MO diagram of $U(BH_4)_4$, all three of which are bound κ^3H to the metal center. The percentage atomic orbital contributions to the occupied MOs of $Zr(BH_4)_4$, $Hf(BH_4)_4$, and $U(BH_4)_4$ are shown in Table 1.2. Clearly, the H 1*s* orbital of BH_4^- is the largest contributor to all of the M-BH_4 MOs, both bonding and effectively non-bonding. As expected from the AO energies, the 2*s* orbital of boron mainly contributes to the low energy $1a_1$ and $1t_2$ orbitals, and the 2*p* orbitals on boron contribute to the higher energy $1t_1$, $3t_2$, $2a_1$, 1e, and $2t_2$ orbitals. Also as expected from AO energies, the metal *d*, *p*, and *s* atomic orbitals contribute relatively little to the M-BH_4 bonding MOs of the molecule.

Figure 1.8. MO diagram of $Zr(BH_4)_4$, $Hf(BH_4)_4$, and $U(BH_4)_4$.[105]

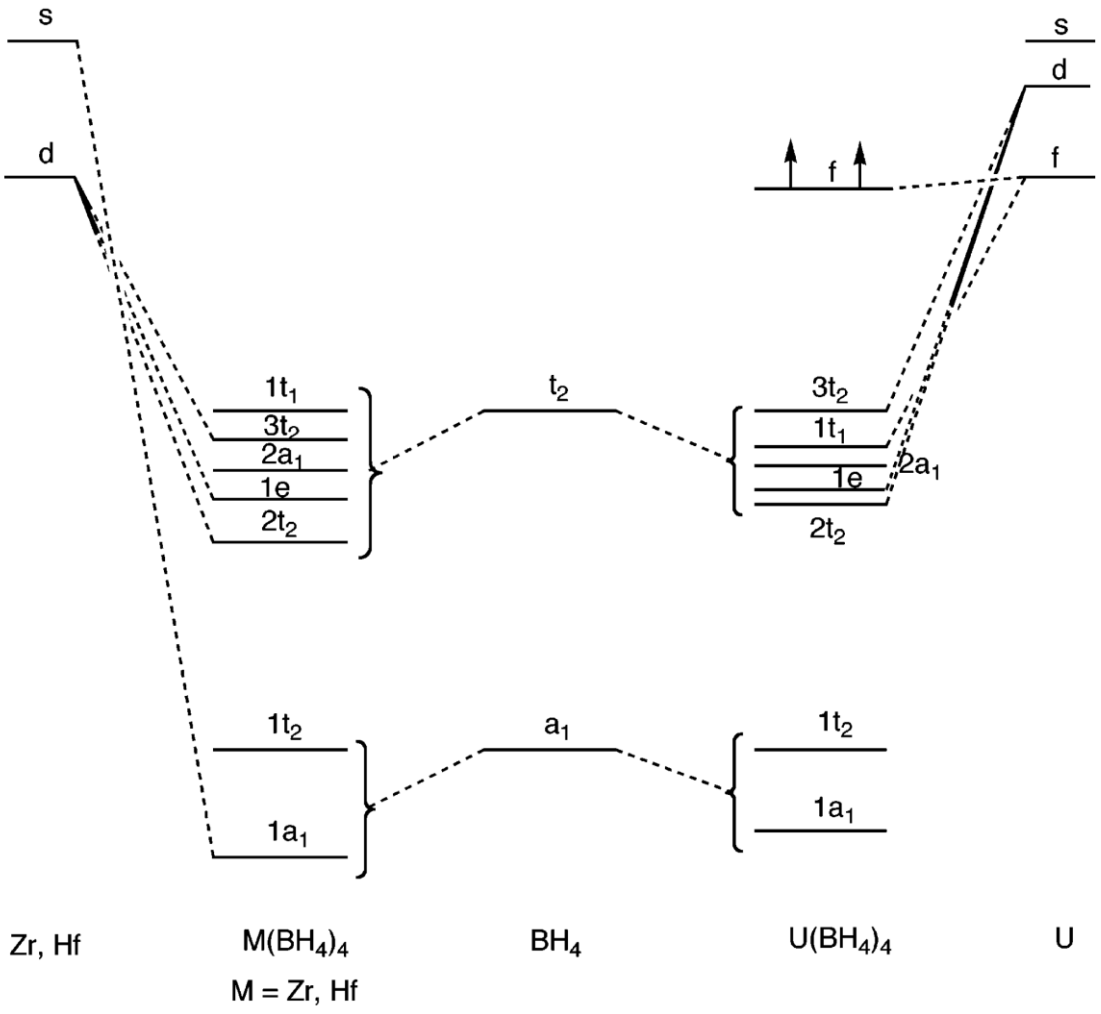

Table 1.2. Atomic orbital percentage contribution to $M(BH_4)_4$.[105]

		H 1*s*	B 2*s*	B 2*p*	M(*n*-1)*d*	M *ns*	M *np*
Zr	$1t_1$	56		32			
	$3t_2$	55		31	2		
	$2a_1$	59	7	25		3	
	1e	45		28	23		
	$2t_2$	53		24	18		
	$1t_2$	54	28		7		6
	$1a_1$	72	21			19	
Hf	$1t_1$	56		32			
	$3t_2$	56		28	2		
	$2a_1$	56	7	27		2	
	1e	44		28	23		
	$2t_2$	49		25	19		
	$1t_2$	53	27		7		7
	$1a_1$	73	22			16	

		H 1*s*	B 2*s*	B 2*p*	M(*n*-1)*d*	M *ns*	M *np*	M (*n*-2)*f*	M (*n*-1)*p*
U	f							96	
	$1t_1$	50		26				13	
	$3t_2$	58		31					
	$2a_1$	57	5	32					
	1e	54		24	18				
	$2t_2$	61		23	14				
	$1t_2$	55	26		8		3		3
	$1a_1$	78	24						

Of $Zr(BH_4)_4$, $Hf(BH_4)_4$, and $U(BH_4)_4$, the uranium complex is the only one with partially filled f orbitals. As is evident in Figure 1.8 and Table 1.2, the contribution of the f orbitals to the M-BH_4 bonding is nearly non-existent and generally is ignored.[106]

The coordination modes adopted by a BH_4^- in any particular transition metal complex can often be rationalized by determining how many empty d-orbitals are available to the BH_4^- group, sometimes modified by symmetry considerations that generate non-bonding ligand SALCs, as seen in the $M(BH_4)_4$ complexes and in complexes of stoichiometry $M(BH_4)_3(PR_3)_2$.[107-109] The are some interesting examples of complexes in which electronic factors cause considerable "unsaturation" in the coordination sphere of the metal: the *N*-methyl-*N*-ethylaminodiboranate, MEADB, complex $Cr(MEADB)_2$ is four-coordinate and square planar, and Cp*Cr(DMADB), where Cp* is pentamethylcyclopentadienyl, is five-coordinate. In both of these complexes the aminodiboranate ligands are κ^1H,κ^1H (Figure 1.9), despite the fact that there is sufficient room in the coordination sphere of the metal to adopt a higher denticity bonding mode.[94] Thus, it is reasonable to conclude that the ligand metal interactions of this molecule are controlled entirely by electronic factors.

Figure 1.9. Aminodiboranate coordination modes in Cp*Cr(DMADB) (top) and Cr(MEADB)$_2$ (bottom).[94]

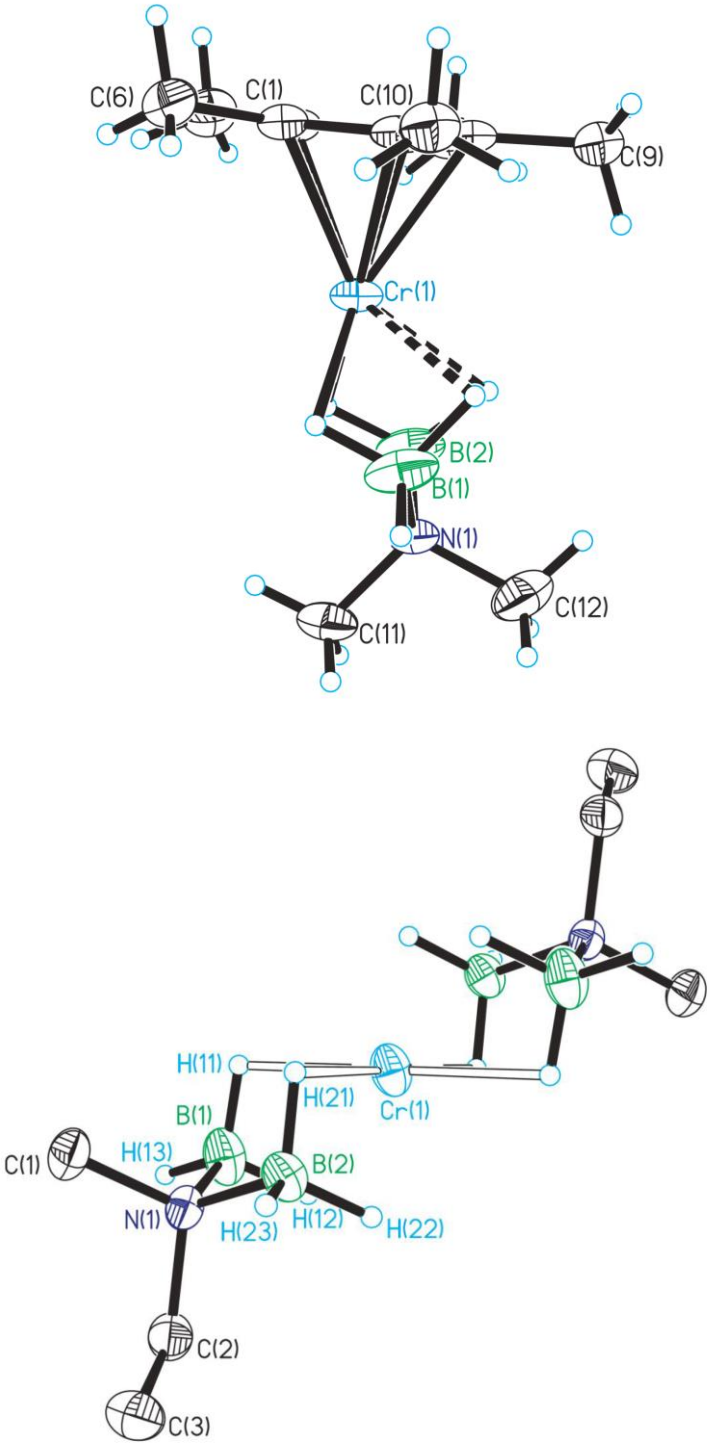

Effects on Volatility: Intermolecular Forces

Before discussing the effect of intermolecular interactions on the volatility of metal borohydride molecules, it is prudent to begin with a general overview of the types and properties of intermolecular forces. Intermolecular interactions comprise both attractive and repulsive components, which operate over distances larger than those characteristic of ionic or covalent bonds.[110]

Van der Waals forces. There are several types of intermolecular attractive forces, which go under the general name of van der Waals forces. Intermolecular forces are nonadditive; that is to say, the van der Waals forces between two molecules are, in part, influenced by neighboring molecules. There are several kinds of van der Waals forces, which are known as dipole-dipole forces, dipole-induced dipole forces, and dispersion forces.

Dipole-dipole interactions, or Keesom forces, involve interactions between permanent dipoles present in the polarized chemical bonds of adjacent molecules. Hydrogen bonds are a type of dipole-dipole interaction.

Dipole-induced dipole interactions, or Debye forces, occur when a permanent dipole of one molecule induces a dipole in a neighboring molecule.

Dispersion forces, or London forces, are caused by correlated movements of electrons in neighboring molecules and are the only intermolecular forces that are always present regardless of the properties of the molecule. Dispersion forces are

unique in that they can range from sub-interatomic distances of 0.2 nm to very large distances of over 10 nm. However, when intermolecular distances are very large, r = ~100 nm, the interaction strength of dispersion forces decreases rapidly with increasing distance, at a rate approaching r^{-7}.

Dispersion forces depend on the number and types of atoms in a molecule and become more important with increasing molecular size and may, for very large molecules, dominate even dipole-dipole interactions of polar molecules. For example, the series of halides, F_2, Cl_2, Br_2, I_2, have increasing polarizability, F_2 having the least and I_2 the most. As the halide molecules become larger and more diffuse, the dispersion force strength increases due to the increased polarizability. This results in F_2 having the lowest boiling point of the series, -188 °C and I_2 the highest, 184 °C.

Most attractive intermolecular forces are weakly anisotropic in nature; in contrast, repulsive intermolecular forces are often are highly isotropic and often heavily influence how molecules pack into crystals. These repulsive forces can arise from the Coulombic and Pauli repulsions generated by the electrons as two atoms approach one another.[111] At equilibrium, the attractive and repulsive forces are balanced, but because the repulsive forces weaken much more quickly than the attractive forces as the interatomic or intermolecular distances increase, energy is required to pull the molecules apart. The dependence of intermolecular interaction strength on distance is often explained using the Lennard-Jones potential.[112,113] This potential contains terms for

both the short-range repulsive force, which has an r^{-12} dependence on interatomic distance, and the attractive force, which has a dependence of r^{-6}. The minimum on the potential energy surface lies where the two forces are equal in magnitude.

Coulombic forces. Coulombic forces are generally long range forces where like charges, positive and positive or negative and negative are repulsive and dissimilar charges, positive and negative, are attractive. Coulombic repulsion is observed between borohydride groups due to their similar charge, which, in part, contributes to the high volatility of homoleptic metal borohydride monomers. Intermolecular interaction between a cationic metal center and the atoms of adjacent molecules can be limited by Coulombic shielding, where, for example, a borohydride anion coordinated to a cationic metal center results in a more rapid decay of the cation electric field and a diminished attractive force between the cationic metal and borohydrides coordinated to neighboring metal centers.

As an example of the role of Coulombic effects on volatility, we consider the case of fluorinated sodium *tert*-butoxides. Increasing the fluorine content of the alkoxide from trifluoro-*tert*-butoxide, $OCMe_2(CF_3)$, to hexafluoro-*tert*-butoxide, $OCMe(CF_3)_2$, and finally to perfluoro-*tert*-butoxide, $OC(CF_3)_3$, results in an increase in the volatility of the sodium salt.[114] Of the three complexes, trifluoro-*tert*-butoxide is the least volatile, subliming at 120 °C at 10^{-2} Torr and a slight decrease in sublimation temperature is observed for hexafluoro-*tert*-butoxide, subliming at 100 °C. When all methyl groups

have been substituted with trifluoromethyl groups in the perfluoro-*tert*-butoxide, there is a drastic decrease in the sublimation temperature to 30 °C at 10^{-2} Torr. This is due, in part, to the Coulombic shielding of the Na cation and the low polarizability of the CF_3 groups. In contrast, there is a much smaller increase in the sublimation temperature of the zirconium *tert*-butoxides; trifluoro-*tert*-butoxide, a liquid, distills at 60 °C, hexafluoro-*tert*-butoxide sublimes at 40 °C under 10^{-2} Torr, and perfluoro-*tert*-butoxide sublimes at 35 °C.[114] The similarity in the sublimation temperatures of zirconium hexafluoro-*tert*-butoxide and zirconium perfluoro-*tert*-butoxide can be attributed to the saturation of the coordination sphere of Zr with four *tert*-butoxy groups. The substitution of one additional CF_3 group provides only a minor increase in Coulombic shielding.

Intermolecular Interactions in Metal Borohydrides

As discussed earlier, B-H bonds are polarized, with a net negative charge on hydrogen and thus on the exterior of boron hydride ligands. This negative charge results in Coulombic repulsion between neighboring BH_4^- groups. The intermolecular Coulombic repulsions and weak van der Waals' interactions due to the low polarizability of the borohydride groups are primarily responsible for the small lattice energies (and high volatilities) of metal borohydrides such as aluminum borohydride and zirconium borohydride, only 9.6 kJ/mol and ~10 kJ/mol, respectively.[102]

Coulombic repulsions are in part responsible for the different volatilities of hafnium borohydride and hafnium methylborohydride. Both molecules are monomeric in the solid state, but hafnium borohydride sublimes readily in vacuum at 20 °C whereas hafnium methylborohydride must be heated between 30 and 40 °C before it sublimes. This difference is due, in part, to the negative charge on the terminal hydrogen atoms of BH_4^- vs. the relatively neutral hydrogen atoms on the methyl group of the methylborohydride anion. An additional factor is the increase in the London dispersion forces due to a greater number of atoms in the methylborohydride molecule.

Steric Considerations: Saturation of the Metal Coordination Sphere

The volatility of a metal complex is generally highest if it is a monomer rather than part of a polymeric network, and the degree of association in turn depends on whether or not the coordination sphere of the metal is saturated by the steric demands of its ligands. The borohydride anion is a relatively small ligand and even three or four of them are often insufficient to saturate the coordination sphere of a metal center; as a result, most binary borohydride complexes are polymeric. The effect of varying the saturation of the coordination sphere on volatility can be seen in the homoleptic actinide borohydride series, $An(BH_4)_4$ (Ac = Th, Pa, U, Np, and Pu). The borohydride complexes of the three largest actinides, Th, Pa, and U, are isostructural polymers. The structure is best represented as $An(\mu_2\text{-}\kappa^2\textit{H}\text{-}BH_4)_2(\kappa^3\textit{H}\text{-}BH_4)_2$ in which two borohydrides

bridge κ^2H,κ^2H between two metal centers, for a total of four κ^2H bound borohydrides per metal center, and the remaining two borohydrides are κ^3H bound to the metal center for a total coordination number of 14.[115,116] In contrast, the Np and Pu analogs are monomeric with four κ^3H bound borohydrides, $An(\kappa^3H\text{-}BH_4)_4$, and have a total coordination number of 12.[115,117] As the central cation becomes smaller, fewer hydrogen atoms are needed to saturate the coordination sphere and there is no need to form bonds to all four hydrogen atoms on a single BH_4 group (which is possible only if the group is bridging).

Unsurprisingly, the polymeric actinide borohydrides have significantly lower vapor pressures than the monomeric species. The reported vapor pressures of the $Th(BH_4)_4$ and $U(BH_4)_4$ polymers are 0.05 Torr at 130 °C and 0.3 Torr at 34 °C, respectively.[118,119] In contrast, the monomeric species $Np(BH_4)_4$ and $Pu(BH_4)_4$ both have vapor pressures of 10 Torr at 25 °C.[115,117] The vapor pressure of the polymeric complexes is an indicator of the strength of the $\mu_2\text{-}\kappa^2H\text{-}BH_4$ bridging interaction. It has been estimated that the free energy of the structural transformation of the solid state $U(BH_4)_4$ polymer into the 12-coordinate monomer is 2.6 kcal/mol.[120]

Table 1.3. Vapor pressure, ionic radius, and borohydride coordination modes of various tetrakisborohydrides.[115,118]

Molecule	Vapor pressure (Torr/°C)	Ionic radius (Å)	Metal coordination in the solid state
$Th(BH_4)_4$	0.05 / 130	1.05	$(\mu_2\text{-}\kappa^2H\text{-}BH_4)_2(\kappa^3H\text{-}BH_4)_2$
$U(BH_4)_4$	0.3 / 34	1.00	$(\mu_2\text{-}\kappa^2H\text{-}BH_4)_2(\kappa^3H\text{-}BH_4)_2$
$Np(BH_4)_4$	10 / 25	0.98	$(\kappa^3H\text{-}BH_4)_4$
$Pu(BH_4)_4$	10 / 25	0.96	$(\kappa^3H\text{-}BH_4)_4$
$Zr(BH_4)_4$	15 / 25	0.84	$(\kappa^3H\text{-}BH_4)_4$
$Hf(BH_4)_4$	14.9 / 25	0.83	$(\kappa^3H\text{-}BH_4)_4$

One method to prevent the dimerization or polymerization of metal borohydrides, despite the small size of this anion, is to coordinate one or more ancillary Lewis bases to the metal center. For example, a series of monoadducts $U(BH_4)_4 \cdot L$ has been reported, where L = dimethyl ether, diethyl ether, and di(*n*-propyl) ether, as has the diadduct $U(BH_4)_4(THF)_2$. Of these Lewis base adducts, the di(*n*-propyl) ether complex $U(BH_4)_4 \cdot O(n\text{-}C_3H_7)_2$ is the most volatile: it sublimes in vacuum at room temperature.[121] In contrast, the dimethyl ether and diethyl ether adducts (which are less sterically saturated) form infinite linear chains in which three of the borohydrides are bound κ^3H to uranium and the remaining borohydride is bridging κ^2H,κ^2H between adjacent uranium centers, resulting in a coordination number of 14.[122] The THF diadduct $U(BH_4)_4(THF)_2$ is a monomer in which the six ligands describe a distorted octahedron: four κ^3H-borohydrides occupy the equatorial plane and two THF ligands are trans to one another, giving this complex a coordination number of 14.[123]

Oversaturation of the coordination sphere with Lewis base adducts can change the preferred borohydride bonding mode from κ^3H to κ^2H. For example, the structure of $Th(BH_4)_4(PEt_3)_2$ is similar to that of $U(BH_4)_4(THF)_2$ described above: all four borohydrides are κ^3H coordinated to thorium. In contrast, in the monomeric thorium complex $Th(BH_4)_4(dmpe)_2$, where dmpe = 1,2-bis(dimethylphosphino)ethane, the steric demands of the two chelating dmpe ligands allow only two of the four borohydrides to coordinate κ^3H while forcing the other two to be κ^2H.[124]

There is a way to inhibit the polymerization (and thereby increase the volatility) of metal borohydride complexes without changing the saturation of the coordination sphere: by modifying the borohydride ligand so that it is less likely to bridge between two metal centers. The methylborohydride anion, $H_3BCH_3^-$, does not have the ability to bridge in the κ^2H,κ^2H fashion seen in many BH_4^- complexes, and other bridging modes are less favorable. For example, only one complex possessing a κ^2H,κ^1H bridging configuration is known, the magnesium dimer, $[Mg(\kappa^2H\text{-}H_3BCH_3)(\mu_2\text{-}\kappa^1H,\kappa^2H\text{-}H_3BCH_3)(DME)]_2$, which will be described in Chapter 2 of this thesis. Consequently, the homoleptic actinide methylborohydrides, $An(H_3BCH_3)_4$ (An = Th, U, and Np) are all monomers in the solid state.[125] with four terminal κ^3H-methylborohydride ligands (for the structures of the BH_4^- analogs see above). Whereas polymeric $Th(BH_4)_4$ has a vapor pressure of 0.05 Torr at 130 °C, in contrast monomeric $Th(H_3BCH_3)_4$ sublimes at 50 °C.[125]

Three complexes are known, $[Th(H_3BCH_3)_4]_2(OEt_2)$, $[Th(H_3BCH_3)_4(THF)]_2$, and $[Nd(H_3BCH_3)_3(THF)_2]_2$ which possess κ^2H,κ^2H bridging methylborohydride ligands (Figure 1.10 and Chapter 3 of this thesis).[126,127] Presumably, in the case of the Th complexes, the Lewis bases causes enough steric crowding around the Th center to force one of the four methylborohydrides from a κ^3H coordination, what is observed in the monomers, to a κ^2H coordination observed in these two dimers.

Figure 1.10. Solid state crystal structure of methylborohydride bridged thorium dimers.[126]

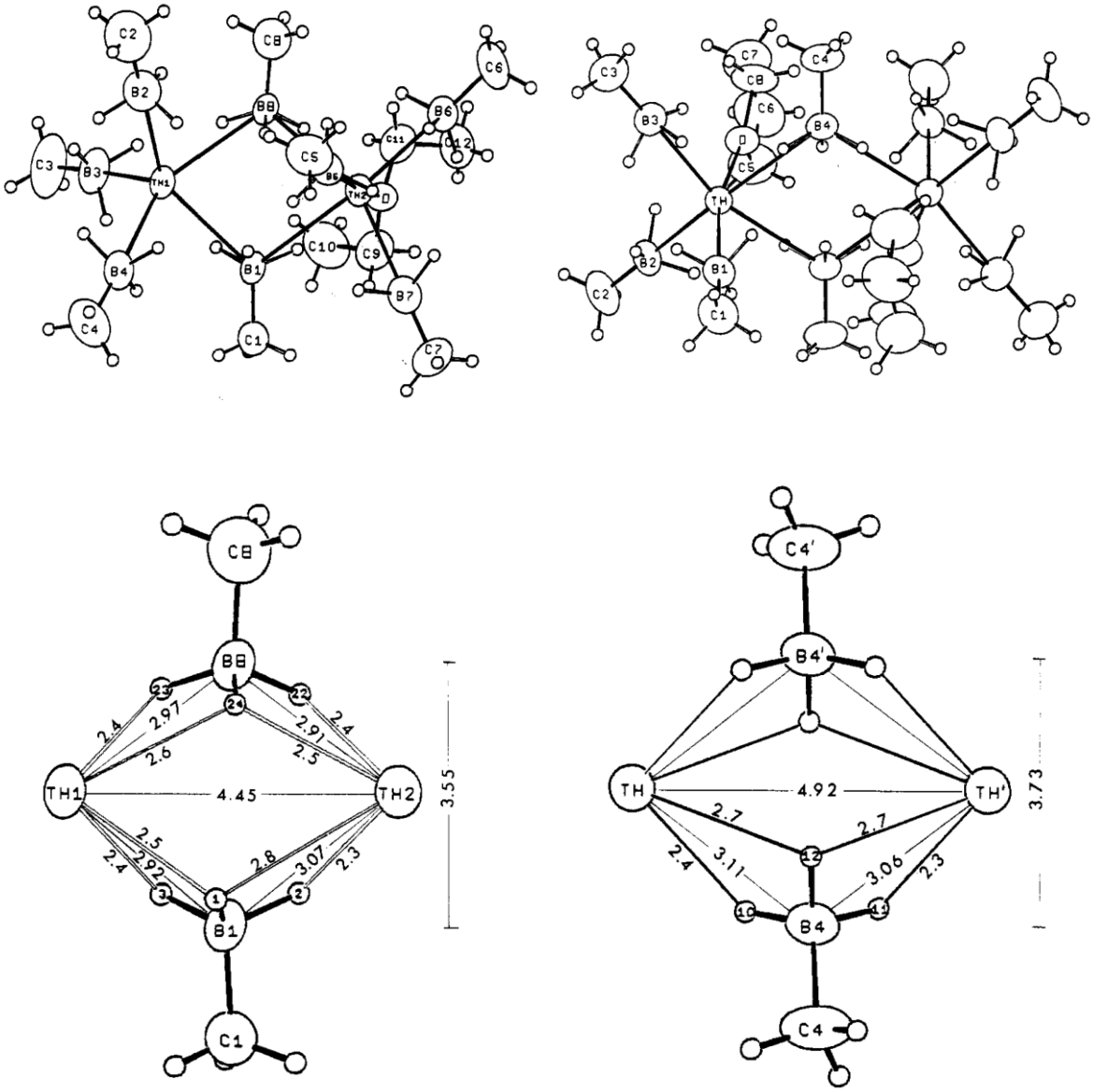

$[Th(H_3BCH_3)_4]_2Et_2O$ $[Th(H_3BCH_3)_4(THF)]_2$

Significantly, even though these complexes are dinuclear in the solid state, they are quite volatile – $Th(H_3BCH_3)_4(THF)_2$ sublimes at 100 °C and $[Nd(H_3BCH_3)_3(THF)_2]_2$ at 60 °C – evidently reversion to monomeric species must be facile.

Saturation of the $U(H_3BCH_3)_4$ coordination sphere can be accomplished by the formation of monoadducts with chelating Lewis bases such as 1,2-dimethoxyethane, *N*,*N*,*N*′,*N*′-tetramethylethylenediamine, and 1,2-bis(methylthio)ethane. In all of these $U(H_3BCH_3)_4$·L complexes the methylborohydride ligands are bound in a κ^3*H* fashion (except for a single κ^2*H* methylborohydride in the TMEDA adduct).[128]

Finally, another way to inhibit polymerization of metal borohydride complexes is to replace one or more of the borohydride ligands with sterically more demanding anions. For example, addition of TlCp to $U(BH_4)_4$ in toluene or pentane followed by sublimation at room temperature affords the monomeric complex $CpU(BH_4)_3$.[129]

Quantification of the Steric Saturation of Borohydride Complexes

In order to predict whether or not a certain metal borohydride complex will be monomeric or oligomeric/polymeric, one needs a quantitative method to assess whether or not the ligand set saturates the coordination sphere of the metal. Lobkovskii has proposed such a method, in which each ligand is assigned a steric constant, S_L, which is a normalized solid angle having units of Å^2.[130] For each ligand, L, in a complex, S_L is divided by the square of the metal-ligand distance, and the resulting quotients are

summed to give the degree of steric saturation, $\Sigma S_L/(M\text{-}L)^2$ The steric constants S_L are normalized so that the sum of the $S_L/(M\text{-}L)^2$ values equals 1 for a sterically saturated coordination sphere, although some highly crowded molecules have a Σ value that is slightly larger than 1. For any particular ligand, its steric constant is deduced from crystallographic data. Lobkovskii calculated that S_L equals 2.05 Å^2 for cyclopentadienyl (Cp), and 0.80 Å^2 for the ethers $O(C_2H_5)_2$, OC_4H_8, and $O(n\text{-}C_3H_7)_2$. The S_L value of 1,2-dimethoxyethane, DME, can be estimated to be twice that of monodentate etherates, or S_L = 1.6 Å^2.

Typically the metal-ligand distance used in these calculations is the bond length between the metal and coordinated atom of the ligand, but for κ^2H and κ^3H borohydride complexes the most relevant distance is the metal-boron distance rather than the metal-hydrogen bond lengths. For κ^2H and κ^3H borohydride ligands, S_L is 1.19 and 1.28 Å^2, respectively. We can assign identical values for the methylborohydride ligand, $H_3BCH_3^-$, because the methyl substituent should have no effect on the saturation of the inner coordination sphere.

Using these values and metal ligand distances from the literature, Σ for many of the complexes listed in the previous section of this chapter, as well as molecules reported in this thesis, have been calculated and compiled in Table 1.4.

Table 1.4. Degree of steric saturation, coordination number, and borohydride coordination modes of borohydride and methylborohydride complexes.[130,131]

Complex	Σ	Coordination number	Metal Coordination in the solid state
$Zr(BH_4)_4$	0.94	12	$(\kappa^3H\text{-}BH_4)_4$
$U(BH_4)_4$	0.99	14	$(\mu_2\text{-}\kappa^2H\text{-}BH_4)_4(\kappa^3H\text{-}BH_4)_2$
$Np(BH_4)_4$	0.85	12	$(\kappa^3H\text{-}BH_4)_4$
$U(Cp)(BH_4)_3$	0.96	12	$(\kappa^3H\text{-}BH_4)_3$
$U(BH_4)_4(Me_2O)$	1.03	14	$(\kappa^3H\text{-}BH_4)_3(\mu\text{-}\kappa^2H\text{-}BH_4)_2$
$U(BH_4)_4(Et_2O)$	1.01	14	$(\kappa^3H\text{-}BH_4)_3(\kappa^2H\text{-}BH_4)_2$
$U(BH_4)_4(THF)_2$	1.04	14	$(\kappa^3H\text{-}BH_4)_4$
$Zr(H_3BCH_3)_4$	0.93	12	$(\kappa^3H\text{-}H_3BCH_3)_4$
$Th(H_3BCH_3)_4$	0.78	12	$(\kappa^3H\text{-}H_3BCH_3)_4$
$U(H_3BCH_3)_4$	0.83	12	$(\kappa^3H\text{-}H_3BCH_3)_4$
$Np(H_3BCH_3)_4$	0.82	12	$(\kappa^3H\text{-}H_3BCH_3)_4$
$Ca(H_3BCH_3)_2(DME)_2$	0.91	10	$(\kappa^3H\text{-}H_3BCH_3)_2$
$Sr(H_3BCH_3)_2(DME)_3$	0.95	12	$(\kappa^3H\text{-}H_3BCH_3)_2$
$Ba(H_3BCH_3)_2(DME)_3$	0.87	12	$(\kappa^3H\text{-}H_3BCH_3)_2$
$Sc(H_3BCH_3)_3(THF)$	0.90	10	$(\kappa^3H\text{-}H_3BCH_3)_3$
$Nd(H_3BCH_3)_3(DME)(Et_2O)$	0.92	12	$(\kappa^3H\text{-}H_3BCH_3)_3$

Effects on Volatility: Molecular Mass

Although it is tempting to believe that volatility decreases as molecular mass increases, the relationship between volatility and mass is complex. For example, when comparing the vapor pressure of isotopically labeled molecules, the isotope effect on vapor pressure is always normal at sufficiently low temperatures: that is to say, the lighter molecule is the more volatile. However, at higher temperatures (which may still be considerably below room temperature) the isotope effect typically crosses-over from normal to inverse and the more massive molecule is more volatile.[132] This phenomenon arises because molecules of greater mass have greater translational entropy in the vapor phase vs. the condensed phase.[133]

Baertschni demonstrated that, at their boiling points, the volatilities of the molecules $CHCl_3$ and CCl_4 increase when carbon-13 is substituted for carbon-12, but decrease when chlorine-37 is substituted for chlorine-35.[134] If one assumes that the intermolecular interactions are localized to the nearest atoms of neighboring molecules, then the intermolecular interactions in carbon tetrachloride will be limited to the chlorine atoms; the central carbon atom is fully shielded. Thus, an increase in the mass of the carbon atom from 12 amu to 13 amu will mainly affect the entropy of the molecule and will cause the heavier molecules $^{13}CCl_4$ and $^{13}CHCl_3$ to be more volatile. In contrast, replacing chlorine-35 with chlorine-37 decreases the volatility because the

increased intermolecular interactions between the heavier chlorine-37 atoms overwhelms the benefit of increased entropy.[133]

This specific case is an example of the more general "super isotope effect" which relates pairs of highly symmetric molecules consisting of different central atoms, with similar atomic radii, surrounded with ligands with similar geometries.[135] This phenomenon has been observed in $Zr(BH_4)_4$ and $Hf(BH_4)_4$: the vapor pressure of the hafnium analog $Hf(BH_4)_4$ increases more rapidly with increased temperature, even though the ionic radii of the metal centers are similar, Zr^{4+} = 0.84 Å and Hf^{4+} = 0.83 Å, as are the vapor pressures at 25 °C, $Zr(BH_4)_4$ = 15 Torr and $Hf(BH_4)_4$ = 14.9 Torr. The difference in temperature dependence of their vapor pressures is a consequence of the large difference in molecular mass: $Zr(BH_4)_4$ = 150.6 amu and $Hf(BH_4)_4$ = 237.9 amu.[118,136]

In highly symmetric molecules containing central atoms of dissimilar atomic radii, the entropy effect is over-ridden by the effects of intermolecular interactions, which generally increase with the size and number of atoms in the molecule. This effect can be observed by comparing the vapor pressure of $Zr(BH_4)_4$ and $Hf(BH_4)_4$ to that of $Np(BH_4)_4$. All three molecules have the same ligand set, geometry, and oxidation state, but the 0.98 Å ionic radius of Np^{4+} is approximately 0.15 Å larger than those of Hf^{4+} and Zr^{4+}. Correspondingly, at low temperatures, near 0 °C, all three tetrakis borohydride metal complexes have similar vapor pressures (Figure 1.11), but at 25 °C the vapor

pressure of $Np(BH_4)_4$ is approximately 5 Torr lower than those of $Hf(BH_4)_4$ and $Zr(BH_4)_4$.[117,137]

Use of Borohydride Precursors in Chemical Vapor Deposition

Tetrahydroborate precursors. Of all the borohydride containing molecules which are of interest in CVD, the most widely explored are the homoleptic complexes $Zr(BH_4)_4$ and $Hf(BH_4)_4$, which are useful precursors for the growth of the corresponding metal diboride phases. The onset temperature for film growth from zirconium borohydride is 100 - 150 °C, which corresponds to an activation energy of 0.28 eV (27 kJ/mol).[138-140] There is some variation in the composition of the as-deposited films grown by thermal CVD from $Zr(BH_4)_4$. Films grown at ca. 250 °C have reported compositions of $ZrB_{1.6}$ and ZrB_2, whereas films grown at higher temperatures are boron rich with compositions near ZrB_3.[138,141] Evidently, at the flow rates used, the residence time of the diborane byproduct in the hot zone is long enough for some of it to decompose on the surface rather than be pumped away. At deposition temperatures up to 400 °C the films are smooth and amorphous, whereas at higher temperatures they are poorly crystalline and have a columnar morphology. Epitaxial ZrB_2 films have been grown on Si(111) at 900 °C by limiting the growth rate to ~1.2 nm/min.[142]

Figure 1.11. Vapor pressure curves of $Hf(BH_4)_4$, $Zr(BH_4)_4$, and $Np(BH_4)_4$.[117,137]

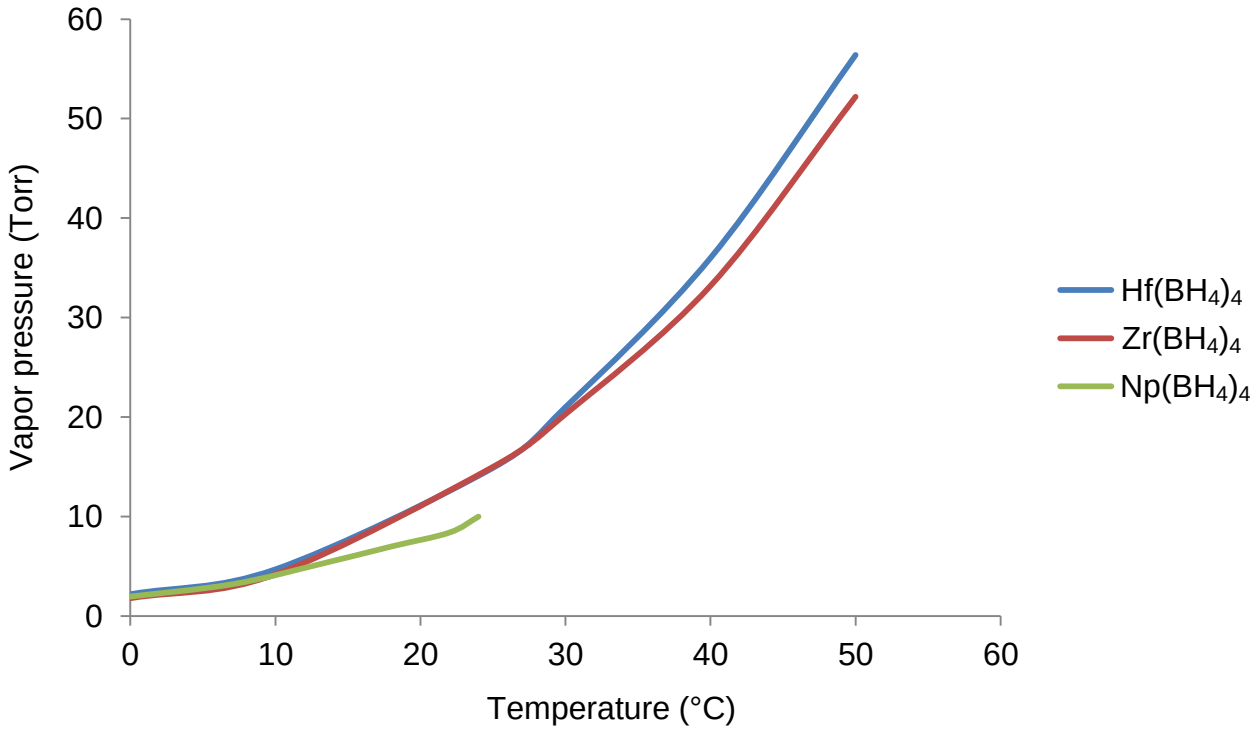

Plasma enhanced CVD of ZrB_2 from $Zr(BH_4)_4$ using hydrogen plasma has also been studied. Amorphous films are obtained at 300 °C, and crystalline films can be grown at 450 °C.[3,143] Laser induced CVD from $Zr(BH_4)_4$ on an iron substrate gives high growth rates of ZrB_2, suggesting that the transient surface temperature is relatively high. The deposits were claimed to be stoichiometric, which is atypical of high temperature growth. The authors theorize that the diborane byproduct has time to diffuse away from the reaction zone between pulses (which were 25 ns long but separated by 0.16 s), thereby suppressing reactions that deposit excess boron in the film.[138]

Hafnium borohydride has a growth onset temperature of approximately 200 °C, which corresponds to an activation energy of 0.43 eV (41 kJ/mol).[139] Films deposited at 250 °C were dense and smooth whereas films grown at 400 °C were columnar and rough; at both temperatures the films are amorphous. Films deposited at 500 °C and above are crystalline with a preferred crystallographic orientation dependent on growth temperature.[144] Postannealing of the films between 200 and 300 °C transforms the microstructure from amorphous to nanocrystalline, and the films become microcrystalline when annealed at temperatures above 600 °C. Unlike the zirconium boride films deposited from $Zr(BH_4)_4$, films deposited from $Hf(BH_4)_4$ have the desired 2:1 ratio of Hf/B over a wide temperature range, 200 - 900 °C.[145]

Using $Hf(BH_4)_4$ in plasma enhanced CVD produces results similar to those of $Zr(BH_4)_4$ in that the film composition is sensitive to substrate temperature. The Hf content decreases and the B content increases with increased temperature.[143] Multiphase ternary films of Hf-B-N have been deposited by in several ways. Film growth by thermal CVD below 350 °C results in deposition of HfB_2 even with NH_3 present, whereas films grown above 350 °C are multiphase and contain HfN_x ($x > 1$) and a BN phase.[146] Films grown by PECVD with N_2 result in films which contain HfB_2, HfN, and BN.[9]

Attempts to deposit MgB_2 from magnesium borohydride, $Mg(BH_4)_2$ have, to date, have been unsuccessful. A range of growth temperatures, up to 700 °C, have been investigated. Films grown from $Mg(BH_4)_2$ have an oxide rich surface layer rich in Mg. Sputtering away the oxide overlayer reveals a film consisting almost entirely of boron, most likely due to loss of Mg to the vacuum during deposition because of this element's high vapor pressure at elevated temperatures .[147,148]

The aluminum precursors $Al(BH_4)_3$ and $AlH_2(BH_4)\cdot N(CH_3)_3$ have been used to deposit aluminum-containing thin films by CVD. Aluminum tris(borohydride) affords aluminum boride thin films at temperatures between 300 and 430 °C, although the aluminum content ranges from 19% to 77%; this precursor has also been used to deposit aluminum oxide thin films, Al_2O_3, at approximately 330 °C with the addition of O_2 as an oxygen source.[149] Aluminum films of greater than 99% purity have been deposited from

$AlH_2(BH_4)\cdot N(CH_3)_3$ at room temperature on substrates which have been pretreated with titanium tetrachloride.[149-151]

Titanium diboride, TiB_2, thin films have been deposited from $Ti(BH_4)_3(DME)$ at 200 °C. Although there is a thin oxide overlayer the bulk of the film is stoichiometric with a Ti/B ratio of 1:2.[141]

Substituted borohydride precursors. Although several volatile methylborohydride complexes as well as other monosubstituted borohydride complexes have been reported,[69,125,126,152,153] none have previously been investigated as CVD or ALD precursors. An investigation of rare earth methylborohydride complexes as CVD precursors is reported in Chapter 3 of this thesis.

Octahydrotriborate precursors. The only metal $B_3H_8^-$ complex that has been explored as a CVD precursor is $Cr(B_3H_8)_2$. Amorphous and conformal thin films of CrB_2 could be deposited at temperatures as low as 200 °C; above 500 °C excess boron was present in the films due to decomposition of the boron hydride byproducts.[139,154] The idealized reaction stoichiometry for this precursor is shown below.

N,N-Dimethylaminodiboranate precursors. Homoleptic magnesium, titanium, yttrium, and praseodymium *N*,*N*-dimethylaminodiboranate (DMADB) complexes have

been used to deposit thin films of oxides and borides by CVD. Magnesium oxide, MgO, has been deposited from $Mg(DMADB)_2$ and water at substrate temperatures between 225 °C and 800 °C. At low temperatures, the films are conformal (35:1 aspect ratio), smooth, amorphous, and highly pure.[48] Depositions conducted at the higher temperatures afford films with columnar structures and increased crystallinity. Similarly, yttrium oxide, Y_2O_3, and titanium oxide, TiO_2, have been deposited from $Y(DMADB)_3$ and $Ti(DMADB)_2$, respectively, using water as a co-reactant.[155] Hydrolysis of the DMADB ligand most likely proceeds by the idealized reaction shown below.

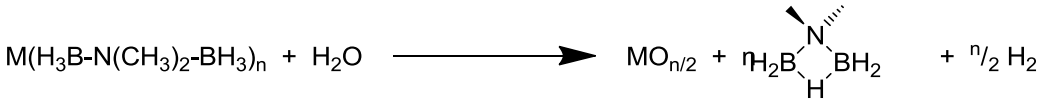

The byproduct μ-(dimethylamino)diborane, $(H_3C)_2NB_2H_5$, is a volatile liquid at STP. At higher temperatures, this complex may disproportionate into (*N*,*N*-dimethylamino)borane, $H_2BN(CH_3)_2$, and diborane.

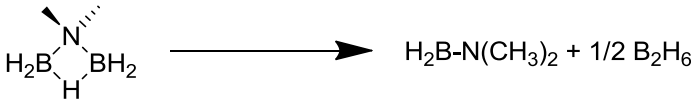

Attempts to employ $Ti(DMADB)_2$ as a single source precursor at 300 °C did not afford TiB_n, but instead give films with the stoichiometry of $TiB_{1.2}C_{1.2}N_{0.6}$, indicating the

uncontrolled decomposition of the DMADB ligand.[155] Titanium doped magnesium boride films have been successfully prepared by the co-deposition of $Mg(DMADB)_2$ and $Ti(DMADB)_2$. Films deposited at 350 °C have the stoichiometry $Mg_{0.88}Ti_{0.19}B_2$.[155] Unfortunately, these films were not superconducting at low temperatures. Finally, films of PrB_n have been prepared using $Pr(DMADB)_3$ as a single source precursor. Films deposited at 300 °C were amorphous and contained a Pr/B ratio of 1:5.[86]

Various iron boride phases can be deposited from boron-containing iron carbonyl clusters. $HFe_4(CO)_{12}BH_2$ and $HFe_3(CO)_9BH_4$ afford films containing slightly more boron than the 4:1 and 3:1 Fe/B ratios of the precursor molecules. For example, films deposited from $HFe_3(CO)_9BH_4$ at 160 °C are amorphous and have a Fe/B ratio of 3.4 with approximately 5% carbon and 3% oxygen (the latter being present as B_2O_3); at temperatures above 400 °C, the deposited films are crystalline.[156,157] In contrast, films deposited from $HFe_3(CO)_{10}BH_2$ at 180 °C contain mostly iron, 85 to 88%, with a small amount of carbon, 1 to 2%, and similar amounts of boron and oxygen, 4 to 5% and 7 to 8%, respectively, again as B_2O_3. These films are amorphous as-deposited but become crystalline when annealed above 500 °C. Finally, the two complexes $B_2H_6Fe_2(CO)_6$ and $[B_2H_4Fe_2(CO)_6]_2$, both of which contain 1:1 Fe/B ratios, afford amorphous films between 175 and 250 °C. Films deposited from $B_2H_6Fe_2(CO)_6$ at 170 °C had a Fe/B ratio of 1.3 which increased to 1.7 when the deposition temperature was increased to 250 °C. These films crystallize to a mixture of Fe_2B and FeB when they are annealed at 600 °C.[158]

Summary

Several aspects of borohydride chemistry are of interest in the context of CVD: these ligands exhibit a range of binding modes and electronic interactions with metal centers, their negative charge enables the formation of electrically neutral complexes of positively charged metal centers and creates Coulombic repulsions between adjacent molecules in the solid state, and they have low polarizabilities, which reduces the strengths of attractive intermolecular London dispersion forces. These properties, among others, contribute to the unusually high vapor pressures observed in many metal borohydrides.

References

(1) Cote, D. R.; Nguyen, S. V.; Cote, W. J.; Pennington, S. L.; Stamper, A. K.; Podlesnik, D. V. *IBM J. Res. Dev.* **1995**, *39*, 837-864.

(2) Smith, R. C.; Ma, T.; Hoilien, N.; Tsung, L. Y.; Bevan, M. J.; Colombo, L.; Roberts, J.; Campbell, S. A.; Gladfelter, W. L. *Adv. Mater. Opt. Electron.* **2000**, *10*, 105-114.

(3) Sung, J.; Goedde, D. M.; Girolami, G. S.; Abelson, J. R. *J. Appl. Phys.* **2002**, *91*, 3904-3911.

(4) Leskelä, M.; Kukli, K.; Ritala, M. *J. Alloys Compd.* **2006**, *418*, 27-34.

(5) Vasilev, V. Y.; Repinsky, S. M. *Russ. Chem. Rev.* **2005**, *74*, 413-441.

(6) Rossnagel, S. M. *IBM J. Res. Dev.* **1999**, *43*, 163-179.

(7) Sproul, W. D. *J. Vac. Sci. Technol., A* **1994**, *12*, 1595-1601.

(8) Hauert, R.; Patscheider, J. *Adv. Eng. Mater.* **2000**, *2*, 247-259.

(9) Jayaraman, S.; Gerbi, J. E.; Yang, Y.; Kim, D. Y.; Chatterjee, A.; Bellon, P.; Girolami, G. S.; Chevalier, J. P.; Abelson, J. R. *Surf. Coat. Technol.* **2006**, *200*, 6629-6633.

(10) Chatterjee, A.; Jayaraman, S.; Gerbi, J. E.; Kumar, N.; Abelson, J. R.; Bellon, P.; Polycarpou, A. A.; Chevalier, J. P. *Surf. Coat. Technol.* **2006**, *201*, 4317-4322.

(11) Chatterjee, A.; Kumar, N.; Abelson, J. R.; Bellon, P.; Polycarpou, A. A. *Wear* **2008**, *265*, 921-929.

(12) Doll, G. L.; Mensah, B. A.; Mohseni, H.; Scharf, T. W. *J. Therm. Spray Technol.* **2010**, *19*, 510-516.

(13) Dianov, E. M.; Golant, K. M.; Khrapko, R. R.; Kurkov, A. S.; Tomashuk, A. L. *J. Lightwave Technol.* **1995**, *13*, 1471-1474.

(14) Shiue, S.; He, J.; Pan, L.; Huang, S. *Thin Solid Films* **2002**, *406*, 210-214.

(15) Watekar, P. R.; Ju, S.; Han, W. *J. Non-Cryst. Solids* **2008**, *354*, 1453-1459.

(16) Felice, V.; Dussardier, B.; Jones, J. K.; Monnom, G.; Ostrowsky, D. B. *Opt. Mater.* **2001**, *16*, 269-277.

(17) Biener, J.; Baumann, T.; Wang, Y.; Nelson, E.; Kucheyev, S.; Hamza, A.; Kemell, M.; Ritala, M.; Leskelä, M. *Nanotechnology* **2007**, *18*, 055303.

(18) Ponja, S.; Sathasivam, S.; Chadwick, N.; Kafiza, A.; Bawaked, S. M.; Obaid, A. Y.; Al-Thabaiti, S.; Basahel, S. N.; Parkin, I. P.; Carmalt, C. J. *J. Mater. Chem., A* **2013**, *1*, 6271-6278.

(19) Zhang, Z.; Bian, J.; Bi, K.; Liu, Y.; Zhang, D.; Qin, F.; Liu, H.; Miao, L. *Appl. Phys. Lett.* **2013**, *103*, 212105.

(20) Faust, M.; Enders, M.; Bruns, M.; Bräse, S.; Gao, K.; Seipenbusch, M. *Surf. Coat. Technol.* **2013**, *230*, 284-289.

(21) Kay, A.; Cesar, I.; Grätzel, M. *J. Am. Chem. Soc.* **2006**, *128*, 15714-15721.

(22) Tahir, A. A.; Wijayantha, K. G. U. *J. Photochem. Photobiol., A* **2010**, *216*, 119-125.

(23) King, J. S.; Wittstock, A.; Biener, J.; Kucheyev, S. O.; Wang, Y. M.; Baumann, T. F.; Giri, S. K.; Hamza, A. V.; Baeumer, M.; Bent, S. F. *Nano Lett.* **2008**, *8*, 2405-2409.

(24) Mayer, T. M.; Elam, J. W.; George, S. M.; Kotula, P. G.; Goeke, R. S. *Appl. Phys. Lett.* **2003**, *82*, 2883.

(25) Nistorica, C.; Liu, J.; Gory, I.; Skidmore, G.; Mantiziba, F.; Gnade, B.; Kim, J. *J. Vac. Sci. Technol., A* **2005**, *23*, 836.

(26) Zhu, X.; Aslam, D. *Diamond Relat. Mater.* **2006**, *15*, 254-258.

(27) Choy, K. L. *Prog. Mater. Sci.* **2003**, *48*, 57-170.

(28) Hampden-Smith, M. J.; Kodas, T. T. *Chem. Vap. Deposition* **1995**, *1*, 8-23.

(29) Hampden-Smith, M. J.; Kodas, T. T. *Chem. Vap. Deposition* **1995**, *1*, 39-48.

(30) Crowell, J. E. *J. Vac. Sci. Technol., A* **2003**, *21*, S88-S95.

(31) George, S. M. *Chem. Rev.* **2010**, *110*, 111-131.

(32) Choy, K. L. *ECS Trans.* **2009**, *25*, 59-65.

(33) Knisley, T. J.; Kalutarage, L. C.; Winter, C. H. *Coord. Chem. Rev.* **2013**, *257*, 3222-3231.

(34) Helmersson, U.; Lattemann, M.; Bohlmark, J.; Ehiasarian, A. P.; Gudmundsson, J. T. *Thin Solid Films* **2006**, *513*, 1-24.

(35) Konstantinidis, S.; Snyders, R. *Eur. Phys. J. - Appl. Phys.* **2011**, *56*, 24002.

(36) Reinhold, E.; Faber, J. *Surf. Coat. Technol.* **2011**, *206*, 1653-1659.

(37) Kumar, N.; Yanguas-Gil, A.; Daly, S. R.; Girolami, G. S.; Abelson, J. R. *Appl. Phys. Lett.* **2009**, *95*, 144107.

(38) Kumar, N.; Yanguas-Gil, A.; Daly, S. R.; Girolami, G. S.; Abelson, J. R. *J. Am. Chem. Soc.* **2008**, *130*, 17660-17661.

(39) Yanguas-Gil, A.; Kumar, N.; Yang, Y.; Abelson, J. R. *J. Vac. Sci. Technol., A* **2009**, *27*, 1244-1248.

(40) Babar, S.; Kumar, N.; Zhang, P.; Abelson, J. R.; Dunbar, A. C.; Daly, S. R.; Girolami, G. S. *Chem. Mater.* **2013**, *25*, 662-667.

(41) Abelson, J. R. *ECS Trans.* **2010**, *33*, 307-319.

(42) Matsuzaki, T.; Funakubo, H. *J. Appl. Phys.* **1999**, *86*, 4559-4564.

(43) Ludviksson, A.; Nooney, M.; Bruno, R.; Bailey, A.; Kodas, T. T.; Hampden-Smith, M. J. *Chem. Vap. Deposition* **1998**, *4*, 129-132.

(44) Puurunen, R. L. *J. Appl. Phys.* **2005**, *97*, 121301.

(45) Belyansky, M. *Handbook of Thin Film Deposition (Third Edition)*; Seshan, K., Ed.; William Andrew Publishing: Oxford, 2012, 89-125.

(46) Cheng, L.; McVittie, J. P.; Saraswat, K. C. *Appl. Phys. Lett.* **1991**, *58*, 2147-2149.

(47) Rossnagel, S. M. *J. Vac. Sci. Technol., B.* **1998**, *16*, 2585-2608.

(48) Wang, W.; Yang, Y.; Yanguas Gil, A.; Chang, N.; Girolami, G.; Abelson, J. *Appl. Phys. Lett.* **2013**, *102*, 101605.

(49) Kucheyev, S. O.; Biener, J.; Wang, Y. M.; Baumann, T. F.; Wu, K. J.; van Buuren, T.; Hamza, A. V.; Satcher, J. H.; Elam, J. W.; Pellin, M. J. *Appl. Phys. Lett.* **2005**, *86*, 083108.

(50) Elam, J.; Xiong, G.; Han, C. Y.; Wang, H. H.; Birrell, J. P.; Welp, U.; Hryn, J. N.; Pellin, M. J.; Baumann, T. F.; Poco, J. F.; Satcher Jr., J. H. *Journal of Nanomaterials* **2006**, *2006*, 1-5.

(51) Meng, G.; Song, H.; Dong, Q.; Peng, D. *Solid State Ionics* **2004**, *175*, 29-34.

(52) Marchand, P.; Hassan, I. A.; Parkin, I. P.; Carmalt, C. J. *Dalton Trans.* **2013**, *42*, 9406-9422.

(53) Lee, J.; Rhee, S. *Electrochem. Solid-State Lett.* **1999**, *2*, 510-511.

(54) Lee, J.; Kim, J.; Rhee, S.; Yang, D.; Kim, D.; Yang, C.; Han, Y.; Hwang, C. *J. Vac. Sci. Technol., A* **2000**, *18*, 2400-2403.

(55) Senzaki, Y.; Hochberg, A. K.; Norman, J. A. T. *Adv. Mater. Opt. Electron.* **2000**, *10*, 93-103.

(56) Shin, J. C.; Lee, J. M.; Hong, S.; Cho, H. J.; Kim, K. S.; Hwang, C. S.; Kim, H. J. *J. Vac. Sci. Technol., A* **1998**, *16*, 2591-2594.

(57) Hong, E.; Shin, J. C.; Choi, J.; Hwang, C. S.; Kim, H. J. *J. Mater. Res.* **2000**, *15*, 1284-1290.

(58) Cotton, F. A. *J. Am. Chem. Soc.* **1968**, *90*, 6230-6232.

(59) IUPAC *Nomenclature of Inorganic Chemistry (Red Book)* Cambridge (UK), 2005.

(60) Sloan, T. E.; Busch, D. H. *Inorg. Chem.* **1978**, *17*, 2043-2047.

(61) Marks, T. J.; Kolb, J. R. *Chem. Rev.* **1977**, *77*, 263-293.

(62) Holah, D. G.; Hughes, A. N.; Maciaszek, S.; Magnuson, V. R. *J. Chem. Soc., Chem. Commun.* **1983**, 1308-1309.

(63) Takusagawa, F.; Fumagalli, A.; Koetzle, T. F.; Shore, S. G.; Schmitkons, T.; Fratini, A. V.; Morse, K. W.; Wei, C.; Bau, R. *J. Am. Chem. Soc.* **1981**, *103*, 5165-5171.

(64) Friedrichs, O.; Buchter, F.; Borgschulte, A.; Remhof, A.; Zwicky, C. N.; Mauron, P.; Bielmann, M.; Züttel, A. *Acta Mater.* **2008**, *56*, 949-954.

(65) Schlesinger, H. I.; Sanderson, R. T.; Burg, A. B. *J. Am. Chem. Soc.* **1940**, *62*, 3421-3425.

(66) Nöth, H. *Angew. Chem.* **1961**, *73*, 371-383.

(67) Remhof, A.; Borgschulte, A.; Friedrichs, O.; Mauron, P.; Yan, Y.; Züttel, A. *Scripta Mater.* **2012**, *66*, 280-283.

(68) Hagemann, H.; Cerny, R. *Dalton Trans.* **2010**, *39*, 6006-6012.

(69) Schlesinger, H. I.; Brown, H. C.; Horvitz, L.; Bond, A. C.; Tuck, L. D.; Walker, A. O. *J. Am. Chem. Soc.* **1953**, *75*, 222-224.

(70) Goel, A. *Indian J. Chem.* **1978**, *16*, 491-494.

(71) Marks, T. J.; Kolb, J. R. *J. Am. Chem. Soc.* **1975**, *97*, 27-33.

(72) Lippard, S. J.; Melmed, K. M. *Inorg. Chem.* **1969**, *8*, 2755-2762.

(73) Burns, I. D.; Hill, A. F.; Williams, D. J. *Inorg. Chem.* **1996**, *35*, 2685-2687.

(74) Beall, H.; Gaines, D. F. *Inorg. Chim. Acta* **1999**, *289*, 1-10.

(75) Beckett, M. A.; Brassington, D. S.; Coles, S. J.; Gelbrich, T.; Hursthouse, M. B. *Polyhedron* **2003**, *22*, 1627-1632.

(76) Kim, D. Y.; Yang, Y.; Abelson, J. R.; Girolami, G. S. *Inorg. Chem.* **2007**, *46*, 9060-9066.

(77) Goedde, D. M.; Girolami, G. S. *J. Am. Chem. Soc.* **2004**, *126*, 12230-12231.

(78) Goedde, D. M.; Windler, G. K.; Girolami, G. S. *Inorg. Chem.* **2007**, *46*, 2814-2823.

(79) Kim, D. Y.; Girolami, G. S. *J. Am. Chem. Soc.* **2006**, *128*, 10969-10977.

(80) Dain, J. C.; Downs, A. J.; Rankin, D. W. H. *J. Chem. Soc., Dalton Trans.* **1981**, *12*, 2465-2470.

(81) Aldridge, S.; Downs, A. J.; Parsons, S. *Chem. Commun.* **1996**, *17*, 2055-2056.

(82) Borlin, J.; Gaines, D. F. *J. Am. Chem. Soc.* **1972**, *94*, 1367-1369.

(83) Kim, D. Y. Ph.D. Thesis, University of Illinois at Urbana-Champaign, **2007**.

(84) Bellott, B. J. Ph.D. Thesis, University of Illinois at Urbana-Champaign, **2010**.

(85) Daly, S.; Girolami, G. *Chem. Commun.* **2010**, *46*, 407-408.

(86) Daly, S. R. Ph.D. Thesis, University of Illinois at Urbana-Champaign, **2010**.

(87) Daly, S. R.; Bellott, B. J.; Kim, D. Y.; Girolami, G. S. *J. Am. Chem. Soc.* **2010**, *132*, 7254-7255.

(88) Daly, S. R.; Girolami, G. S. *Inorg. Chem.* **2010**, *49*, 5157-5166.

(89) Daly, S. R.; Girolami, G. S. *Inorg. Chem.* **2010**, *49*, 4578-4585.

(90) Daly, S. R.; Piccoli, P. M. B.; Schultz, A. J.; Todorova, T. K.; Gagliardi, L.; Girolami, G. S. *Angew. Chem. Int. Ed.* **2010**, *49*, 3379-3381.

(91) Dunbar, A. C. Ph.D. Thesis, University of Illinois at Urbana-Champaign, **2011**.

(92) Daly, S. R.; Bellott, B. J.; Nesbit, M. A.; Girolami, G. S. *Inorg. Chem.* **2012**, *51*, 6449-6459.

(93) Dunbar, A. C.; Girolami, G. S. *Inorg. Chem.* **2013**, *53*, 888-896.

(94) Steele, J. L. Ph.D. Thesis, University of Illinois at Urbana-Champaign, **2013**.

(95) Daly, S. R.; Kim, D. Y.; Yang, Y.; Abelson, J. R.; Girolami, G. S. *J. Am. Chem. Soc.* **2010**, *132*, 2106-2107.

(96) Daly, S. R.; Kim, D. Y.; Girolami, G. S. *Inorg. Chem.* **2012**, *51*, 7050-7065.

(97) De Proft, F.; Martin, J. M. L.; Geerlings, P. *Chem. Phys. Lett.* **1996**, *250*, 393-401.

(98) Hegstrom, R. A.; Palke, W. E.; Lipscomb, W. N. *J. Chem. Phys.* **1967**, *46*, 920-922.

(99) Galvez-Ruiz, J. C.; Sanchez, M. *J. Mol. Struct. - Theochem.* **2009**, *908*, 114-116.

(100) Zhou, X.; Qian, Q.; Zhou, J.; Xu, B.; Tian, Y.; Wang, H. *Phys. Rev., B* **2009**, *79*, 212102.

(101) van Setten, M. J.; de Wijs, G. A.; Brocks, G. *Phys. Rev., B* **2008**, *77*, 165115.

(102) Łodziana, Z. *Phys. Rev., B* **2010**, *81*, 144108.

(103) Hitchcock, A. P.; Hao, N.; Werstiuk, N. H.; McGlinchey, M. J.; Ziegler, T. *Inorg. Chem.* **1982**, *21*, 793-798.

(104) Davison, A.; Wreford, S. S. *Inorg. Chem.* **1975**, *14*, 703.

(105) Green, J. C.; de Simone, M.; Coreno, M.; Jones, A.; Pritchard, H. M. I.; McGrady, G. S. *Inorg. Chem.* **2005**, *44*, 7781-7793.

(106) Green, M. L. H.; Wong, L. *J. Chem. Soc., Chem. Commun.* **1989**, 571-573.

(107) Lledos, A.; Duran, M.; Jean, Y.; Volatron, F. *Inorg. Chem.* **1991**, *30*, 4440-4445.

(108) Volatron, F.; Duran, M.; Lledos, A.; Jean, Y. *Inorg. Chem.* **1993**, *32*, 951-954.

(109) Goedde, D. M.; Girolami, G. S. *Inorg. Chem.* **2006**, *45*, 1380-1388.

(110) Karle, J.; Huang, L. *J. Mol. Struct.* **2003**, *647*, 9-16.

(111) Gavezzotti, A. *Synlett* **2002**, 201-214.

(112) Jones, J. R. *Proc. R. Soc. London, Ser. A* **1924**, *106*, 463-477.

(113) Hirschfelder, J. O.; Curtis, C. F.; Bird, R. B. *Molecular Theory of Gases and Liquids*; Wiley: New York, 1964.

(114) Samuels, J. A.; Folting, K.; Huffman, J. C.; Caulton, K. G. *Chem. Mater.* **1995**, *7*, 929-935.

(115) Banks, R. H.; Edelstein, N. M.; Rietz, R. R.; Templeton, D. H.; Zalkin, A. *J. Am. Chem. Soc.* **1978**, *100*, 1957-1958.

(116) Bernstein, E. R.; Hamilton, W. C.; Keiderling, T. A.; Placa, S. J. L.; Lippard, S. J.; Mayerle, J. J. *Inorg. Chem.* **1972**, *11*, 3009-3016.

(117) Banks, R. H.; Edelstein, N. M.; Spencer, B.; Templeton, D. H.; Zalkin, A. *J. Am. Chem. Soc.* **1980**, *102*, 620-623.

(118) Hoekstra, H. R.; Katz, J. J. *J. Am. Chem. Soc.* **1949**, *71*, 2488-2492.

(119) Schlesinger, H. I.; Brown, H. C. *J. Am. Chem. Soc.* **1953**, *75*, 219-221.

(120) Banks, R. H.; Edelstein, N. M. *ACS Symp. Ser.* **1980**, *131*, 331-348.

(121) Zalkin, A.; Rietz, R. R.; Templeton, D. H.; Edelstein, N. M. *Inorg. Chem.* **1978**, *17*, 661-663.

(122) Rietz, R. R.; Zalkin, A.; Templeton, D. H.; Edelstein, N. M.; Templeton, L. K. *Inorg. Chem.* **1978**, *17*, 653-658.

(123) Rietz, R. R.; Edelstein, N. M.; Ruben, H. W.; Templeton, D. H.; Zalkin, A. *Inorg. Chem.* **1978**, *17*, 658-666.

(124) Dunbar, A. C.; Gozum, J. E.; Girolami, G. S. *J. Organomet. Chem.* **2010**, *695*, 2804-2808.

(125) Shinomoto, R.; Gamp, E.; Edelstein, N. M.; Templeton, D. H.; Zalkin, A. *Inorg. Chem.* **1983**, *22*, 2351-2355.

(126) Shinomoto, R.; Brennan, J. G.; Edelstein, N. M.; Zalkin, A. *Inorg. Chem.* **1985**, *24*, 2896-2900.

(127) Mallek, J. L.; Girolami, G. S. Chapter 5 of this thesis. Manuscript in preparation.

(128) Shinomoto, R.; Zalkin, A.; Edelstein, N. M.; Zhang, D. *Inorg. Chem.* **1987**, *26*, 2868-2872.

(129) Baudry, D.; Charpin, P.; Ephritikhine, M.; Folcher, G.; Lambard, J.; Lance, M.; Nierlich, M.; Vigner, J. *J. Chem. Soc., Chem. Commun.* **1985**, 1553-1554.

(130) Lobkovskii, E. B. *J. Struct. Chem.* **1983**, *24*, 224-230.

(131) Goedde, D. M. Ph.D. Thesis, University of Illinois at Urbana-Champaign, **1995**.

(132) Höpfner, A. *Angew. Chem. Int. Ed.* **1969**, *8*, 689-699.

(133) Bradley, D. C. *Nature* **1954**, *173*, 260-261.

(134) Baertschi, P.; Kuhn, W.; Kuhn, H. *Nature* **1953**, *171*, 1018-1020.

(135) Bradley, D. C. *Nature* **1954**, *174*, 323-323.

(136) Shannon, R. D. *Acta Crystallogr., Sect. A* **1976**, *A32*, 751-767.

(137) Hoekstra, H. R.; Katz, J. J. *J. Am. Chem. Soc.* **1949**, *71*, 2488-2492.

(138) Rice, G. W.; Woodin, R. L. *J. Am. Ceram. Soc.* **1988**, *71*, C181-C183.

(139) Jayaraman, S. Ph.D. Thesis, University of Illinois at Urbana-Champaign, **2005**.

(140) Wayda, A. L.; Schneemeyer, L. F.; Opila, R. L. *Appl. Phys. Lett.* **1988**, *53*, 361-363.

(141) Jensen, J. A.; Gozum, J. E.; Pollina, D. M.; Girolami, G. S. *J. Am. Chem. Soc.* **1988**, *110*, 1643-1644.

(142) Tolle, J.; Roucka, R.; Tsong, I. S. T.; Ritter, C.; Crozier, P. A.; Chizmeshya, A. V. G.; Kouvetakis, J. *Appl. Phys. Lett.* **2003**, *82*, 2398-2400.

(143) Reich, S.; Suhr, H.; Hankó, K.; Szepes, L. *Adv. Mater.* **1992**, *4*, 650-653.

(144) Jayaraman, S.; Yang, Y.; Kim, D. Y.; Girolami, G. S.; Abelson, J. R. *J. Vac. Sci. Technol., A* **2005**, *23*, 1619-1625.

(145) Yang, Y.; Jayaraman, S.; Kim, D. Y.; Girolami, G. S.; Abelson, J. R. *Chem. Mater.* **2006**, *18*, 5088-5096.

(146) Kumar, N.; Noh, W.; Daly, S. R.; Girolami, G. S.; Abelson, J. R. *Chem. Mater.* **2009**, *21*, 5601-5606.

(147) Crociani, L.; Rossetto, G.; Kaciulis, S.; Mezzi, A.; El-Habra, N.; Palmieri, V. *Chem. Vap. Deposition* **2007**, *13*, 414-419.

(148) Greenbank, J. C.; Argent, B. B. *Transactions of the Faraday Society* **1965**, *61*, 655-664.

(149) Glass Jr., J. A.; Kher, S. S.; Spencer, J. T. *Chem. Mater.* **1992**, *4*, 530-538.

(150) Ryu, S.; Cho, J.; Cho, Y.; Lee, J.; Choi, J.; Lee, D.; Cho, K.; Kim, T. In *IEEE International Symposium on Semiconductor Manufacturing* 2006, p 397-400.

(151) Kang, S.; Park, Y.; Kim, Y.; Shin, Y.; Yun, J. *J. Electrochem. Soc.* **2009**, *156*, H333-H339.

(152) Shinomoto, R. S. Ph.D. Thesis, University of California, Berkely, **1984**.

(153) Shinomoto, R.; Zalkin, A.; Edelstein, N. M. *Inorg. Chim. Acta* **1987**, *139*, 97-101.

(154) Jayaraman, S.; Klein, E. J.; Yang, Y.; Kim, D. Y.; Girolami, G. S.; Abelson, J. R. *J. Vac. Sci. Technol., A* **2005**, *23*, 631-633.

(155) Yang, Y. Ph.D. Thesis, University of Illinois at Urbana-Champaign, **2007**.

(156) Amini, M. M.; Fehlner, T. P.; Long, G. J.; Politowski, M. *Chem. Mater.* **1990**, *2*, 432-438.

(157) Thimmappa, B. H. S.; Fehlner, T. P.; Long, G. J.; Pringle, O. A. *Chem. Mater.* **1991**, *3*, 1148-1152.

(158) Jun, C.; Fehlner, T. P.; Long, G. J. *Chem. Mater.* **1992**, *4*, 440-446.

CHAPTER 2: Synthesis and Characterization of Sodium Methylborohydride and the 1,2-Dimethoxyethane Adducts of Magnesium, Calcium, Strontium, and Barium Methylborohydride.

Introduction

Magnesium diboride, MgB_2, was first synthesized in 1953 by Jones and Marsh[1] and made international headlines when it was found to be a high temperature superconductor in 2001.[2] Although superconductors with higher critical temperatures have been described,[3] MgB_2 still has the highest critical temperature (39 K) of all known intermetallic superconductors. Thin films of MgB_2 have highly attractive properties for use in superconducting electronics such as superconducting radio frequency cavities[4-6] and Josephson junctions[7-10] due to the high critical current density and long coherence length of MgB_2.[11-15] The relatively low upper critical field and the rapid suppression of the critical current density by a high magnetic field, however, are factors that limit the performance of pure MgB_2 thin films in these applications.[16-18]

The deposition of MgB_2 thin films has been achieved by a wide array of techniques, including hybrid physical-chemical vapor deposition (HPCVD),[19,20] aerosol deposition of pre-synthesized MgB_2 powder,[21] co-evaporation of boron and magnesium,[22,23] co-sputtering of boron and magnesium,[24] pulsed laser deposition,[25] molecular beam epitaxy,[26] deposition of a magnesium thin film over a boron thin film

followed by post-annealing,[27] and deposition of a boron thin film followed by annealing in magnesium vapor.[28] However, none of these methods is suitable for the deposition of highly conformal thin films, which are required for use in microelectronic devices. Utilization of a volatile precursor or precursors in thermal chemical vapor deposition, CVD, may greatly improve the conformality of as-deposited thin films compared to the previously described methods due to the ability of a molecular precursor to adsorb and desorb from the surface multiple times before decomposing into a non-volatile solid and volatile byproducts.

To date, however, attempts to grow MgB_2 films from single source precursors by CVD have been unsuccessful. Among the precursors that have been investigated for the CVD of MgB_2 are magnesium borohydride, $Mg(BH_4)_2$,[29] magnesium octahydrotriborate, $Mg(B_3H_8)_2$,[30] magnesium *N*,*N*-dimethylaminodiboranate, $Mg(H_3B\text{-}N(CH_3)_2\text{-}BH_3)_2$, $Mg(DMADB)_2$,[31] and the 3-boryl propyl compounds, $Mg(C_3H_6\text{-}BC_8H_{14})_2$ and $Mg(C_3H_6\text{-}B(C_6H_{11})_2)_2$.[32] Because $Mg(BH_4)_2$ has a polymeric structure[33] this precursor must be heated to over 230 °C under vacuum before it sublimes.[34] Films deposited from $Mg(BH_4)_2$ at 500 °C (10 mTorr) have an oxide overlayer rich in magnesium and an underlying MgB_n phase that is highly depleted of magnesium. $Mg(DMADB)_2$, the most volatile magnesium precursor known (800 mTorr at 25 °C) and the less volatile $Mg(B_3H_8)_2$ also afford magnesium-depleted films by CVD. The most promising approach so far is the use of $Mg(DMADB)_2$ in tandem with 10% $Ti(DMADB)_2$ which

serves as a CVD co-reactant and catalyst. This combination produces high-purity, crystalline films with the correct metal-to-boron stoichiometry of $(Mg_{0.88}Ti_{0.19})B_2$. These films are not superconducting, however, because of the titanium doping.[35]

Many attempts have been made to improve the high-field performance of MgB_2, including irradiation[36] and doping with carbon,[37] zirconium bodride,[38] silicon,[39] copper,[40] rubidium, cesium,[41] silicon carbide,[42] and aluminum.[43] Some of the best results were observed when MgB_2 is doped with carbon; the upper critical field and critical current density increases while the critical temperature and maximum critical current decreases slightly.[37] Several methods to dope thin films of MgB_2 with carbon have been developed, including sintering MgB_2 and carbon at high temperatures and pressures,[44,45] deposition of a carbon-doped boron thin film followed by annealing in magnesium vapor,[46] annealing magnesium with B_4C,[47] and co-deposition of carbon during HPCVD.[18] With the exception of HPCVD, all of these methods require an extra annealing step at elevated temperatures which often leads to only a portion of the carbon being doped into the MgB_2 lattice while the rest collects at the grain boundaries where it forms resistive phases.

An alternative approach to deposit carbon-doped MgB_2 thin films is to design a CVD precursor with carbon and boron containing ligands. There has been one attempt to implement this idea, but the attempt did not afford conformal carbon doped MgB_2. The 3-borylpropyl compounds, $Mg(C_3H_6\text{-}BC_8H_{14})_2$ and $Mg(C_3H_6\text{-}B(C_6H_{11})_2)_2$, which

sublime between 60 and 125 °C, afford films but only at substrate temperatures above 500 °C. Although the magnesium-to-boron ratios obtained at a deposition temperature of 800 °C are approximately 1:2, the absolute magnesium content was less than 7 atomic percent. Most of the film, over 45 atomic percent, consisted of carbon.

Here we describe a new potential CVD precursor for MgB_2 thin films: the 1,2-dimethoxyethane, DME, adduct of magnesium methylborohydride, $Mg(H_3BCH_3)_2(DME)$, **1**. The methyl substituent on boron impedes polymerization by blocking the κ^2H,κ^2H borohydride bridging mode seen in in many of the metal borohydride complexes. In addition, the presence of the Lewis base DME further inhibits polymerization by helping to saturate the coordination sphere. The syntheses of methylborohydrides of the heavier alkaline earth metals are also described: the calcium complex, $Ca(H_3BCH_3)_2(DME)_2$, **2**; the strontium complex, $Sr(H_3BCH_3)_2(DME)_3$, **3**; and the barium complex, $Ba(H_3BCH_3)_2(DME)_3$, **4**.

Results and Discussion

Synthesis of Sodium Methylborohydride, $Na(H_3BCH_3)$. We have synthesized the previously unknown sodium methylborohydride, $Na(H_3BCH_3)$, by a synthetic route similar to that used to prepare lithium methylborohydride, $Li(H_3BCH_3)$.[48,49]

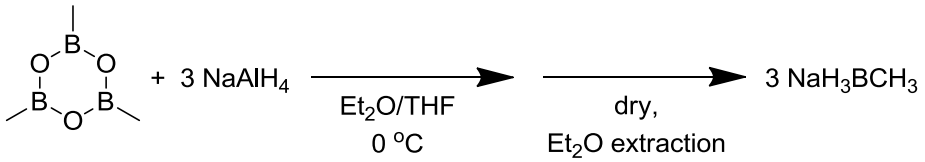

Trimethylboroxine, $B_3O_3(CH_3)_3$, is slowly added to a slurry of sodium aluminum hydride, $NaAlH_4$, in diethyl ether, Et_2O, and tetrahydrofuran, THF. Workup affords $Na(H_3BCH_3)$ as a white solid in 83% yield. The complex is soluble in Et_2O and THF.

Synthesis of $Mg(H_3BCH_3)_2(DME)$, $Ca(H_3BCH_3)_2(DME)$, $Sr(H_3BCH_3)_2(DME)_3$, and $Ba(H_3BCH_3)_2(DME)_3$. It has been reported that $Mg(H_3BCH_3)_2$ can be synthesized by the addition of BH_3·THF to $Mg(CH_3)H$, although the product was not isolated from the reaction mixture.[50] We tried to synthesize the unsolvated complex $Mg(H_3BCH_3)_2$ by ball milling $MgBr_2$ and $Na(H_3BCH_3)$, but no sublimate was collected upon heating the reaction mixture up to 120 °C under vacuum. We also find $MgBr_2$ does not react with $Li(H_3BCH_3)$ in DME at room temperature over 12 hrs, as judged by the lack of change in the ^{11}B NMR chemical shift.[51-53] When the mixture is heated to reflux for 24 hrs the $Li(H_3BCH_3)$ begins to decompose. Finally, the reaction of $MgBr_2$ and $Na(H_3BCH_3)$ in THF also gives no products that can be sublimed in vacuum.

Fortunately, we find that the reaction of $MgBr_2$ and $Na(H_3BCH_3)$ in DME for 72 hrs affords a white slurry from which a white solid can be obtained by filtration and

removal of the solvent from the filtrate. Heating the white solid under vacuum at 80 to 90 °C affords a white sublimate of $Mg(H_3BCH_3)_2(DME)$, **1**, in 86% yield.

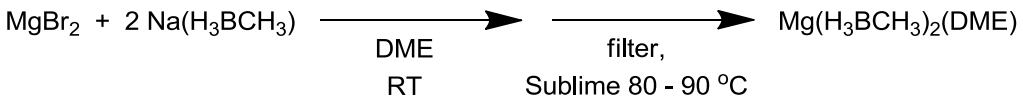

Complex **1** can be crystallized by layering pentane over a saturated diethyl ether solution. Slow diffusion over 5 to 7 days at room temperature affords colorless needles. Some related Lewis base adducts of $Mg(BH_4)_2L_n$ are known, where L = tetrahydrofuran,[54,55] diglyme,[56] *tert*-butylamine, piperidine, benzylamine,[57] and *N*,*N*,*N*′,*N*′-tetramethylethylenediamine.[58]

Calcium, strontium, and barium methylborohydride complexes can be prepared by treating MBr_2 (M = Ca, Sr, Ba) with $Na(H_3BCH_3)$ in DME for 20 hrs. Filtration and concentration of the reaction solution, followed by cooling to -20 °C, affords colorless crystals of the methylborohydride products $Ca(H_3BCH_3)_2(DME)_2$, **2**; $Sr(H_3BCH_3)_2(DME)_3$, **3**; and $Ba(H_3BCH_3)_2(DME)_3$, **4**.

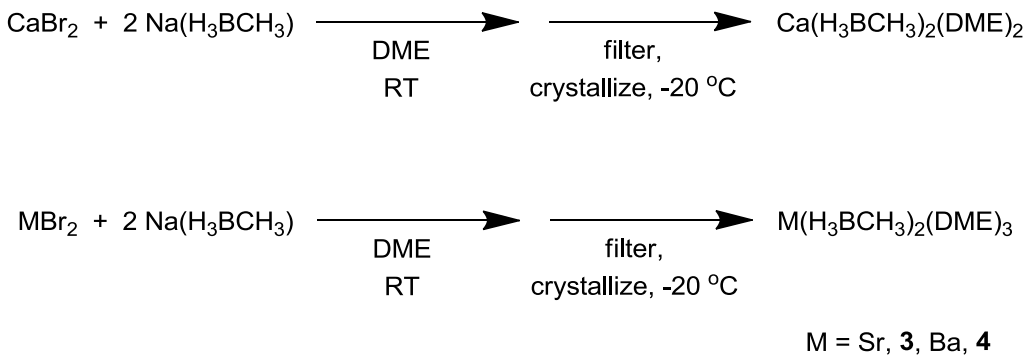

Crystals of the strontium and barium complexes lose some of the coordinated DME ligands when they are dried. Less desolvation is seen for the barium complex, presumably owing to the larger radius of barium (Sr^{2+} 131 pm; Ba^{2+} 147 pm) and a lesser amount of steric crowding in this complex.

Complexes **1** – **4** and $Na(H_3BCH_3)$ are air and water sensitive, requiring handling and storage in an inert atmosphere. They also appear to be thermally robust with only a small amount of decomposition observed from $Na(H_3BCH_3)$ after storing at room temperature for approximately 1 year.

NMR Spectra. The ^1H NMR spectrum of $Na(H_3BCH_3)$ in THF contains the expected 1:1:1:1 quartet (J_{HB} = 75 Hz) for the protons of the BH_3 group. The components of the quartet are further split into a 1:3:3:1 quartet (J_{HB} = 6 Hz) by coupling to the methyl protons. The methyl protons appear as a 1:4:7:8:7:4:1 septet that is actually a binomial quartet of 1:1:1:1 quartets (J_{HB} = J_{HH} = 6 Hz). Additional ^1H NMR resonances from the ^{10}B containing isotopologue, $H_3{}^{10}BCH_3^-$, can be observed as a 1:1:1:1:1:1:1 septet

(J_{HB} = 25 Hz) which is further split into a 1:3:3:1 quartet (J_{HB} = 6 Hz). In contrast, the ^{1}H NMR resonances of **1** - **4** in THF are broad and do not show the finer splitting, presumably as a result of chemical exchange.

The ^{11}B NMR spectrum of Na(H_3BCH_3) in THF contains a single 1:3:3:1 resonance at δ -33.6, which is slightly shielded with respect to the δ -30.9 chemical shift reported for Li(H_3BCH_3).[53] Similarly, the alkaline earth methylborohydride complexes each exhibit a single ^{11}B NMR resonance in THF. The chemical shifts become increasingly deshielded from δ -31.6 for Mg, **1**, to δ -26.9 for Ca, **2**, to δ -25.6 for Sr, **3**, and to δ -21.5 for Ba, **4**.

IR Spectra. The IR spectrum of Na(H_3BCH_3) contains two strong *v*B-H stretches at 2226 and 2170 cm^{-1}; these two bands can be assigned to the A_1 and E modes, respectively, of the methylborohydride group.[59-61] The 2170 cm^{-1} band corresponds to the 2167 cm^{-1} frequency reported for Li(H_3BCH_3).[51] The IR spectrum of the Ca complex **2** also contains two principal features in the *v*B-H stretching region at 2191 and 2143 cm^{-1}. Similarly, strong *v*B-H stretches are observed at 2204 and 2149 cm^{-1} for the Sr complex **3** and at 2173 and 2133 cm^{-1} for the Ba complex **4**.

The IR spectrum of the Mg complex **1** has the most complicated *v*B-H region of the four alkaline earth methylborohydrides complexes. This finding is consistent with the fact, which we will show below, that **1** is a dimer, [Mg(κ^2*H*-H_3BCH_3)(μ$_2$-κ^2*H*,κ^1*H*-H_3BCH_3)(DME)]$_2$; half of the methylborohydride groups are bound in a κ^2*H* fashion and

are terminal on Mg, and half are bound in a κ^2H,κ^1H fashion and bridge between the two Mg centers. The most intense absorptions are at 2339 and 2093 cm^{-1} and less intense shoulders are seen at 2321, 2173, and 2152 cm^{-1}.

Crystal Structures. In the solid state, $Mg(H_3BCH_3)_2(DME)$, **1**, is a methylborohydride-bridged dimer. If one regards each Mg-H interaction as occupying one coordination site, each magnesium atom is 7-coordinate and is bound to one chelating DME molecule, a single terminal κ^2H-methylborohydride group (Mg···B, 2.436(2) Å), and two bridging methylborohydride groups. The latter are bound unsymmetrically, and form a κ^2H interaction (Mg···B, 2.506(2) Å) with one magnesium center and a κ^1H interaction (Mg···B, 2.733(2) Å) with the other; the two Mg···B distances differ by 0.23 Å. Overall, the coordination geometry about each Mg center can be viewed as a distorted pentagonal bipyramid, with the two axial sites being occupied by the atoms O(1) and the κ^1H hydrogen atom from the bridging methylborohydride group.

Only three other complexes with bridging methylborohydride groups are known, the f-metal complexes $[Th(H_3BCH_3)_4]_2{\cdot}OEt_2$, $[Th(H_3BCH_3)_4(THF)]_2$, and $[Nd(H_3BCH_3)_3(THF)_2]_2$.[62,63] Whereas in **1**, the bridging methylborohydride groups are bound in a κ^2H,κ^1H fashion, in the thorium and neodymium complexes, the methylborohydrides are bound in a κ^2H,κ^2H fashion in which the two Th···B and Nd···B distances differ up to 0.15 Å and 0.063 Å, respectively.

The calcium complex $Ca(H_3BCH_3)_2(DME)_2$, **2**, is monomeric in the solid state. If one regards each Ca-H interaction as occupying one coordination site, the calcium center is 10-coordinate with two κ^3*H*-methylborohydrides (Ca···B, 2.617(3) Å) and two chelating DME molecules. The four oxygen and two boron atoms describe a distorted *cis*-octahedron about the calcium center.

Crystals of $Sr(H_3BCH_3)_2(DME)_3$, **3**, and $Ba(H_3BCH_3)_2(DME)_3$, **4**, are isomorphous. If, as before, one regards each M-H interaction as occupying one coordination site, both the strontium and barium centers are 12 coordinate, and are ligated by three chelating DME molecules and two κ^3*H*-methylborohydrides (Sr···B, 2.865(3) Å, Ba···B, 3.002(3) Å). Alternately, the oxygen and boron atoms define a distorted hexagonal bipyramid. The DME ligands occupy the equatorial vertices, and the boron atoms occupy the axial vertices. The B···Sr···B angle in **3** is 177.94(9)° and the B···Ba···B angle in **4** is 178.35(8)°. The small deviation of the B···M···B angle (M = Sr, Ba) away from 180° is presumed to be the result of crystal packing. The distortion of the hexagonal bipyramidal geometry in **3** and **4** involves a twisting of each of the DME molecules by 21.5° and 20.4°, respectively, so that the six oxygen atoms are alternately above and below the mean MO_6 plane.

According to Raymond and Pauling's structural definition of ionicity,[64] complexes **2** – **4** are primarily ionic because the sum of the ionic radius of the metal[65] and the 1.36 Å effective ionic radius of the κ^3*H*-methylborohydride group[66,67] is less than the metal-boron distance, which is 2.62 Å for **2**, 2.86 Å for **3**, and 3.00 Å for **4**.

Conclusions

Four new alkaline earth methylborohydride complexes with chelating DME molecules, as well as sodium methylborohydride, have been synthesized and characterized. The magnesium complex, $Mg(H_3BCH_3)_2(DME)$, can be sublimed between 80 and 90 °C under vacuum, which makes it a potential CVD candidate for the deposition of superconducting thin films of carbon doped magnesium diboride.

Experimental

All operations were carried out in vacuum or under argon using standard Schlenk and glove box techniques. All glassware was dried in an oven at 150 °C, assembled hot, and allowed to cool under a vacuum before use. Pentane, diethyl ether, tetrahydrofuran, and 1,2-dimethoxyethane were distilled under nitrogen from sodium/benzophenone and degassed with argon immediately before use. Anhydrous $MgBr_2$, anhydrous $CaBr_2$, anhydrous $SrBr_2$, anhydrous $BaBr_2$, 90% pure $NaAlH_4$, and trimethylboroxine ($C_3H_9B_3O_3$) were purchased (Aldrich) and used as received.

Elemental analyses were carried out by the University of Illinois Microanalytical Laboratory. Crystal data was collected by the University of Illinois X-Ray Facility. The IR spectra were recorded on a Perkin Elmer Spectrum One infrared spectrometer as Nujol mulls between NaCl salt plates. The ^{1}H and ^{11}B NMR spectra were obtained on a

Varian Unity 400 instrument at 9.4 T. The chemical shifts are reported in δ units (positive shifts to high frequency) relative to $SiMe_4$ (^1H NMR) or $BF_3{\cdot}Et_2O$ (^{11}B NMR).

Sodium methylborohydride, $Na(H_3BCH_3)$. To a gray suspension of $NaAlH_4$ (5.8g, 107.4 mmol) in diethyl ether (50 mL) and THF (25 mL) at 0 °C was added trimethylboroxine (5 mL, 35.8 mmol). The slurry was stirred for 1 hr and allowed to settle. The solution was filtered, and the gray solid was washed with two aliquots of diethyl ether, (50 mL). The colorless filtrate and washings were combined and taken to dryness in vacuum. The resulting white solid was dissolved in diethyl ether (ca. 50 mL). The solution was filtered to afford a colorless filtrate, and the filtrate was taken to dryness in vacuum to afford a white solid. The solid was washed with pentane (2 × 50 mL) and dried in vacuum. Yield: 4.64g (83%). Mp. >275 °C. Anal. Calcd. for $Na(H_3BCH_3)$: Na, 44.3; B, 20.9; C, 23.2; H, 11.7. Found: Na, 44.5; B, 20.7; C, 23.4; H, 11.5. ^1H NMR (d_8-THF): δ -0.47 (1:4:7:8:7:4:1 septet, $^2J_{HB} = {}^3J_{HH} = 6$ Hz, 3H, BCH_3), 0.13 (1:1:1:1 qq, $^1J_{HB} = 75$ Hz, $^3J_{HH} = 6$ Hz, 3H, BH_3). ^{11}B NMR (d_8-THF): δ -33.6 (1:3:3:1 q, $^1J_{BH} = 75$ Hz). IR (Nujol, cm^{-1}): 2576 w, 2355 m, 2325 m, 2226 vs, 2170 vs, 1864 w, 1729 w, 1332 m, 1285 s, 1173 s, 1033 s, 694 w.

Bis(methylborohydride)(1,2-dimethoxyethane)magnesium(II), $Mg(H_3BCH_3)_2$-(DME), 1. A mixture of $MgBr_2$ (1.24 g, 6.74 mmol) and $Na(H_3CBH_3)$ (0.70 g, 13.5 mmol) was stirred in DME for 72 hrs. The resulting white suspension was filtered to afford a colorless filtrate, which was dried in vacuum to afford a white solid. The solid was

ground to a powder and sublimed onto a cold finger at 80 – 85 °C and 10^{-2} Torr over 3 days, affording a white sublimate. Yield: 1.0 g (86%). Mp. 95 – 97 °C Anal. Calcd. for $Mg(H_3BCH_3)_2(DME)$: Mg, 14.1; B, 12.6; C, 41.9; H, 12.9. Found: Mg, 13.8; B, 12.2; C, 42.2; H, 13.1. ^1H NMR (d_8-THF): δ -0.42 (m, 6H, BCH_3), 0.29 (1:1:1:1 q, $^1J_{HB}$ = 72 Hz, 6H, BH_3), 3.26 (s, 6H, OCH_3), 3.42 (s, 4H, OCH_2). ^{11}B NMR (d_8-THF): δ -31.6 (1:3:3:1 q, $^1J_{BH}$ = 74 Hz). IR (Nujol, cm^{-1}): 3024 w, 2321 s, 2239 s, 2173 sh, 2152 sh, 2093 s, 1973 sh, 1394 sh, 1368 sh, 1298 m, 1277 m, 1244 m, 1192 m, 1136 s, 1115 m, 1099 s, 1052 vs, 1009 m, 872 s, 830 m.

Bis(methylborohydride)bis(1,2-dimethoxyethane)calcium(II), $Ca(H_3BCH_3)_2$-$(DME)_2$, 2. A mixture of $CaBr_2$ (0.385 g, 1.93 mmol) and $Na(H_3CBH_3)$ (0.20 g, 3.86 mmol) was stirred in DME for 20 hrs. The white suspension was filtered, and the colorless filtrate was concentrated in vacuum to ca. 5 mL and cooled -20 °C to afford prisms, which were collected and dried in vacuum. Yield: 0.179g (33%). Mp. 134 - 135 °C Anal. Calcd. for $Ca(H_3BCH_3)_2(DME)_2$: Ca, 14.4; B, 7.78; C, 43.2; H, 11.6. Found: Ca, 14.1; B, 7.46; C, 43.2; H, 11.6. ^1H NMR (d_8-THF): δ -0.42 (br s, 6H, BCH_3), 0.48 (1:1:1:1 q, $^1J_{HB}$ = 75 Hz, 6H, BH_3), 3.29 (s, 6H, OCH_3), 3.45 (s, 4H, OCH_2). ^{11}B NMR (d_8-THF): δ -26.9 (1:3:3:1 q, $^1J_{BH}$ = 75 Hz). IR (Nujol, cm^{-1}): 3010 m, 2364 w, 2457 w, 2261 m, 2191 s, 2143 vs, 1977 w, 1933 w, 1413 w, 1291 s, 1244 s, 1227 sh, 1192 s, 1113 s, 1067 vs, 1023 s, 864 s, 834 m, 804 w.

Bis(methylborohydride)tris(1,2-dimethoxyethane)strontium(II), $Sr(H_3BCH_3)_2$-$(DME)_3$, 3. A mixture of $SrBr_2$ (0.385 g, 1.56 mmol) and $Na(H_3CBH_3)$ (0.20 g, 3.86 mmol) was stirred in DME for 20 hrs. The white suspension was filtered and the colorless

filtrate was concentrated in vacuum to ca. 20 mL and cooled to -20 °C to afford colorless prisms. The prisms were collected and dried in vacuum, during which process approximately 1.25 equivalents of DME is lost. Yield of the desolvated product: 0.306 g (65%). Mp. >275 C. Anal. Calcd. for $Sr(H_3BCH_3)_2(DME)_{1.75}$: Sr, 28.9; B, 7.13; C, 35.7; H, 9.81. Found: Sr, 28.6; B, 7.08; C, 34.7; H, 9.35. ^{1}H NMR (d_8-THF): δ -0.45 (br s, BCH_3), 0.44 (1:1:1:1 q, $^1J_{HB}$ = 74 Hz, BH_3), 3.26 (s, OCH_3), 3.42 (s, OCH_2). ^{11}B NMR (d_8-THF): δ -25.6 (1:3:3:1 q, $^1J_{BH}$ = 75 Hz). IR (Nujol, cm^{-1}): 3003 w, 2246 m, 2204 m, 2149 s, 1369 m, 1301 m, 1286 m, 1267 m, 1240 m, 1193 m, 1157 m, 1116 m, 1093 m, 1064 s, 1027 m, 1012 w, 856 s, 834 w.

Bis(methylborohydride)tris(1,2-dimethoxyethane)barium(II), $Ba(H_3BCH_3)_2$-$(DME)_3$, 4. A mixture of $BaBr_2$ (0.573 g, 1.93 mmol) and $Na(H_3CBH_3)$ (0.20 g, 3.86 mmol) was stirred in DME for 20 hrs. The white suspension was filtered and the colorless filtrate was concentrated in vacuum to ca. 30 mL and cooled to -20 °C to afford colorless prisms. The prisms were collected and dried in vacuum, during which process approximately 0.75 equivalents of DME is lost. Yield of the desolvated product: 0.601 g (80%). Mp. >275 °C. Anal. Calcd. for $Ba(H_3BCH_3)_2(DME)_{2.25}$: Ba, 34.5; B, 5.43; C, 33.2; H, 8.74. Found: Ba, 34.5; B, 5.46; C, 33.2; H, 8.78. ^{1}H NMR (d_8-THF): δ -0.45 (br s, BCH_3), 0.78 (1:1:1:1 q, $^1J_{HB}$ = 75 Hz, BH_3), 3.27 (s, OCH_3), 3.43 (s, OCH_2). ^{11}B NMR (d_8-THF): δ -21.5 (1:3:3:1 q, $^1J_{BH}$ = 76 Hz). IR (Nujol, cm^{-1}): 2374 w, 2318 m, 2248 m, 2173 s, 2133 s, 1367 m,

1305 m, 1278 m, 1240 m, 1227 m, 1189 s, 1107 s, 1067 vs, 1021 m, 983 m, 855 s, 836 w, 800 w.

Crystallographic Studies.[68] Single crystals of **1** were obtained by layering pentane over a saturated diethyl ether solution. Single crystals of **2**, **3**, and **4** were obtained by cooling a saturated solution of DME to -20 °C. The single crystals were mounted on a nylon loop with Krytox oil (DuPont), and immediately cooled to less than -100 °C in a cold nitrogen gas stream on the diffractometer. Standard peak search and indexing procedures followed by least square refinement yielded the cell dimensions given in Table 2.1. Data were collected with an area detector by using the measurement parameters listed in Table 2.1. The measured intensities were reduced to structure factor amplitudes and their estimated standard deviations by correction for background, Lorentz, and polarization effects. Systematically absent reflections were deleted and symmetry equivalent reflections were averaged to yield the sets of unique data. A face-indexed absorption correction was applied.

All structures were solved using the SHELXTL software package, followed by least-squares refinement and difference Fourier calculations. Non-hydrogen atoms were refined with independent anisotropic displacement parameters. All the hydrogen atoms attached to boron were located in the E-map and their locations were refined by restraining the B-H bond distance to be equivalent within 0.01 Å unless otherwise noted. Other hydrogen atoms were placed in "idealized positions" with the idealized

methyl groups allowed to rotate about their respective C-X axes to find the best least-squares positions. Hydrogen atoms attached to boron were assigned independent isotropic displacement parameters; the displacement parameters for other hydrogen atoms were set equal to 1.3 times that of the attached carbon atom (for methylene groups) or 1.5 times that of the attached carbon atom (for methyl groups). Successful convergence was indicated by the maximum shift/error of less than 0.01 for the last cycle of least squares refinement. Aspects of the refinements unique to each structure are detailed below.

$Mg(H_3BCH_3)_2(DME)$, 1. The monoclinic lattice and systematic absences $0k0$ ($k \neq 2n$) and $h0l$ ($h + l \neq 2n$) were uniquely consistent with the space group $P2_1/n$. B-H bond distances for all methylborohydride groups were unconstrained. An isotropic extinction parameter refined to a final value of $x = 6.79 \times 10^{-6}$ (3.58×10^{-6}), where F_c is multiplied by the factor $k[1 + F_c^2 x\lambda^3/\sin 2\theta]^{-1/4}$ with k being the overall scale factor. The quantity minimized by the least-squares program was $\Sigma w(F_o^2 - F_c^2)^2$, where $w = \{[\sigma(F_o)]^2 + (0.0475P)^2 + 0.07P\}^{-1}$ and $P = (F_o^2 + 2F_c^2)/3$. The largest peak in the final Fourier difference map (0.15 e $Å^{-3}$) was located 0.81 Å from H2B.

$Ca(H_3BCH_3)_2(DME)_2$, 2. The orthorhombic lattice and systematic absences $0kl$ ($k \neq 2n$), $h0l$ ($l \neq 2n$), and $hk0$ ($h + k \neq 2n$) were uniquely consistent with the space group $Pbcn$. An isotropic extinction parameter was refined to a final value of $x = 2.63 \times 10^{-6}$ (4.1×10^{-7}), where F_c is multiplied by the factor $k[1 + F_c^2 x\lambda^3/\sin 2\theta]^{-1/4}$ with k being the overall

scale factor. The quantity minimized by the least-squares program was $\Sigma w(F_o^2 - F_c^2)^2$, where $w = \{[\sigma(F_o)]^2 + (0.0549P)^2 + 1.55P\}^{-1}$ and $P = (F_o^2 + 2F_c^2)/3$. The largest peak in the final Fourier difference map (0.65 e Å^{-3}) was located 0.92 Å from C3.

$Sr(H_3BCH_3)_2(DME)_3$, 3. The orthorhombic lattice and systematic absences $0kl$ ($k \neq 2n$), $h0l$ ($l \neq 2n$), and $hk0$ ($h + k \neq 2n$) were uniquely consistent with the space group *Pbcn*. An isotropic extinction parameter was refined to a final value of $x = 6.1 \times 10^{-7}$ (4.2×10^{-7}), where F_c is multiplied by the factor $k[1 + F_c^2 x\lambda^3/\sin 2\theta]^{-1/4}$ with k being the overall scale factor. The quantity minimized by the least-squares program was $\Sigma w(F_o^2 - F_c^2)^2$, where $w = \{[\sigma(F_o)]^2\}^{-1}$. The largest peak in the final Fourier difference map (0.45 e Å^{-3}) was located 1.13 Å from Sr1.

$Ba(H_3BCH_3)_2(DME)_3$, 4. The orthorhombic lattice and systematic absences $0kl$ ($k \neq 2n$), $h0l$ ($l \neq 2n$), and $hk0$ ($h + k \neq 2n$) were uniquely consistent with the space group *Pbcn*. The quantity minimized by the least-squares program was $\Sigma w(F_o^2 - F_c^2)^2$, where $w = \{[\sigma(F_o)]^2 + (0.0296P)^2\}^{-1}$ and $P = (F_o^2 + 2F_c^2)/3$. The largest peak in the final Fourier difference map (0.29 e Å^{-3}) was located 1.11 Å from H12.

Table 2.1. Crystallographic data for the new methylborohydride complexes **1 – 4**.

	1	**2**	**3**	**4**
Formula	$Mg_2B_4C_{12}H_{44}O_4$	$CaB_2C_{10}H_{32}O_4$	$SrB_2C_{14}H_{42}O_6$	$BaB_2C_{14}H_{42}O_6$
FW (g mol^{-1})	322.154	278.057	415.720	465.427
T (K)	193 (2)	173 (2)	193 (2)	193 (2)
λ (Å)	0.71073	1.54178	0.71073	0.71073
Crystal system	monoclinic	orthorhombic	orthorhombic	orthorhombic
Space group	$P2_1/n$	*Pbcn*	*Pbcn*	*Pbcn*
a (Å)	8.5561(6)	10.2074(3)	10.6152(15)	10.7573(9)
b (Å)	16.1998(11)	11.9213(4)	13.3686(19)	13.6236(11)
c (Å)	9.6164(7)	14.5361(5)	16.5592(2)	16.6543(13)
β(deg)	116.234(4)	90	90	90
V, (Å^3)	1195.61(2)	1768.83(10)	2349.92(6)	2440.74(3)
Z	2	4	4	4
ρ_{calc} (g cm^{-3})	0.923	1.044	1.175	1.267
μ (mm^{-1})	0.109	3.06	2.31	1.65
Max./min transm. factors	0.994, 0.930	0.566, 0.387	0.965, 0.582	0.948, 0.764
Data/restraints/params	2276/0/129	1618/0/94	2286/0/121	2467/0/121
GOF on F^2	1.081	1.067	0.862	1.113
R_1 [$I > 2\sigma(I)$]	0.0386	0.0488	0.0276	0.0223
wR_2 (all data)	0.1123	0.1300	0.0732	0.0642
max, min $\Delta\rho_{electron}$ (e · Å^{-3})	0.15, -0.17	0.65, -0.51	0.43, -0.44	0.29, -0.93

Table 2.2. Selected distances and angles for $[Mg(H_3BCH_3)_2(DME)]_2$, **1**.

Distances (Å)			
Mg(1)···B(1)	2.436(2)	B(1)-C(1)	1.600(3)
Mg(1)···B(2)	2.733(2)	B(1)-H(11)	1.13(1)
Mg(1A)···B(2)	2.506(2)	B(1)-H(12)	1.14(2)
Mg(1)-O(1)	2.112(1)	B(1)-H(13)	1.08(2)
Mg(1)-O(2)	2.075(1)	B(2)-C(2)	1.604(2)
Mg(1)-H(11)	1.92(1)	B(2)-H(21)	1.15(1)
Mg(1)-H(12)	1.99(2)	B(2)-H(22)	1.14(1)
Mg(1)-H(21)	1.97(2)	B(2)-H(23)	1.14(1)
Mg(1)-H(22)	2.53(1)		
Angles (deg)			
B(1)···Mg(1)···B(2)	96.92(7)	O(1)-Mg(1)···B(1)	91.93(6)
H(11)-B(1)···Mg(1)	50.3(8)	O(2)-Mg(1)···B(1)	118.54(6)
H(12)-B(1)···Mg(1)	53.9(8)	O(1)-Mg(1)···B(1A)	88.20(5)
H(21)-B(2)···Mg(1)	38.5(7)	O(2)-Mg(1)···B(1A)	107.14(5)
H(22)-B(2)···Mg(1)	67.5(6)	O(1)-Mg(1)···B(2)	171.11(5)
H(22)-B(2)···Mg(1A)	56.0(7)	O(2)-Mg(1)···B(2)	98.02(5)
H(23)-B(2)···Mg(1A)	51.2(8)	O(1)-Mg(1)-O(2)	76.91(4)

Table 2.3. Selected distances and angles for $Ca(H_3BCH_3)_2(DME)_2$, **2**.

Distances (Å)			
Ca(1)···B(1)	2.617(3)	Ca(1)-H(13)	2.40(3)
Ca(1)-O(1)	2.463(2)	B(1)-C(1)	1.605(4)
Ca(1)-O(2)	2.416(2)	B(1)-H(11)	1.13(2)
Ca(1)-H(11)	2.47(3)	B(1)-H(12)	1.13(2)
Ca(1)-H(12)	2.34(3)	B(1)-H(13)	1.13(2)
Angles (deg)			
B(1)···Ca(1)···B(1A)	104.3(1)	O(1)-Ca(1)···B(1A)	90.92(8)
H(11)-B(1)···Ca(1)	70(1)	O(2)-Ca(1)···B(1)	93.62(8)
H(12)-B(1)···Ca(1)	63(2)	O(2)-Ca(1)···B(1A)	110.14(8)
H(13)-B(1)···Ca(1)	66(2)	O(1)-Ca(1)-O(2)	65.67(7)
O(1)-Ca(1)···B(1)	157.84(9)		

Table 2.4. Selected distances and angles for $Sr(H_3BCH_3)_2(DME)_3$, **3**.

Distances (Å)			
Sr(1)···B(1)	2.865(3)	Sr(1)-H(13)	2.66(2)
Sr(1)-O(1)	2.746(1)	B(1)-C(1)	1.586(3)
Sr(1)-O(2)	2.724(2)	B(1)-H(11)	1.06(1)
Sr(1)-O(3)	2.767(1)	B(1)-H(12)	1.06(1)
Sr(1)-H(11)	2.62(2)	B(1)-H(13)	1.06(1)
Sr(1)-H(12)	2.61(2)		
Angles (deg)			
B(1)···Sr(1)···B(1A)	177.94(9)	O(2)-Sr(1)···B(1)	79.82(6)
H(11)-B(1)···Sr(1)	66(1)	O(3)-Sr(1)···B(1)	102.65(5)
H(12)-B(1)···Sr(1)	65(1)	O(1)-Sr(1)-O(2)	61.42(5)
H(13)-B(1)···Sr(1)	68(1)	O(1)-Sr(1)-O(3)	117.06(5)
O(1)-Sr(1)···B(1)	99.37(6)	O(2)-Sr(1)-O(3)	65.76(4)

Table 2.5. Selected distances and angles for $Ba(H_3BCH_3)_2(DME)_3$, **4**.

Distances (Å)			
Ba(1)···B(1)	3.002(3)	Ba(1)-H(13)	2.77(2)
Ba(1)-O(1)	2.859(2)	B(1)-C(1)	1.601(3)
Ba(1)-O(2)	2.859(2)	B(1)-H(11)	1.11(1)
Ba(1)-O(3)	2.893(2)	B(1)-H(12)	1.11(1)
Ba(1)-H(11)	2.75(2)	B(1)-H(13)	1.17(1)
Ba(1)-H(12)	2.72(2)		
Angles (deg)			
B(1)···Ba(1)···B(1A)	178.35(8)	O(2)-Ba(1)···B(1)	80.81(5)
H(11)-B(1)···Ba(1)	66.0(8)	O(3)-Ba(1)···B(1)	79.81(5)
H(12)-B(1)···Ba(1)	64.7(8)	O(1)-Ba(1)-O(2)	58.70(6)
H(13)-B(1)···Ba(1)	67(1)	O(1)-Ba(1)-O(3)	174.77(5)
O(1)-Ba(1)···B(1)	98.60(6)	O(2)-Ba(1)-O(3)	116.07(4)

Figure 2.1. Molecular structure of $[Mg(H_3BCH_3)_2(DME)]_2$, **1**. The 35 % probability density surfaces are shown; hydrogen atoms are represented by arbitrarily sized spheres or are omitted for clarity.

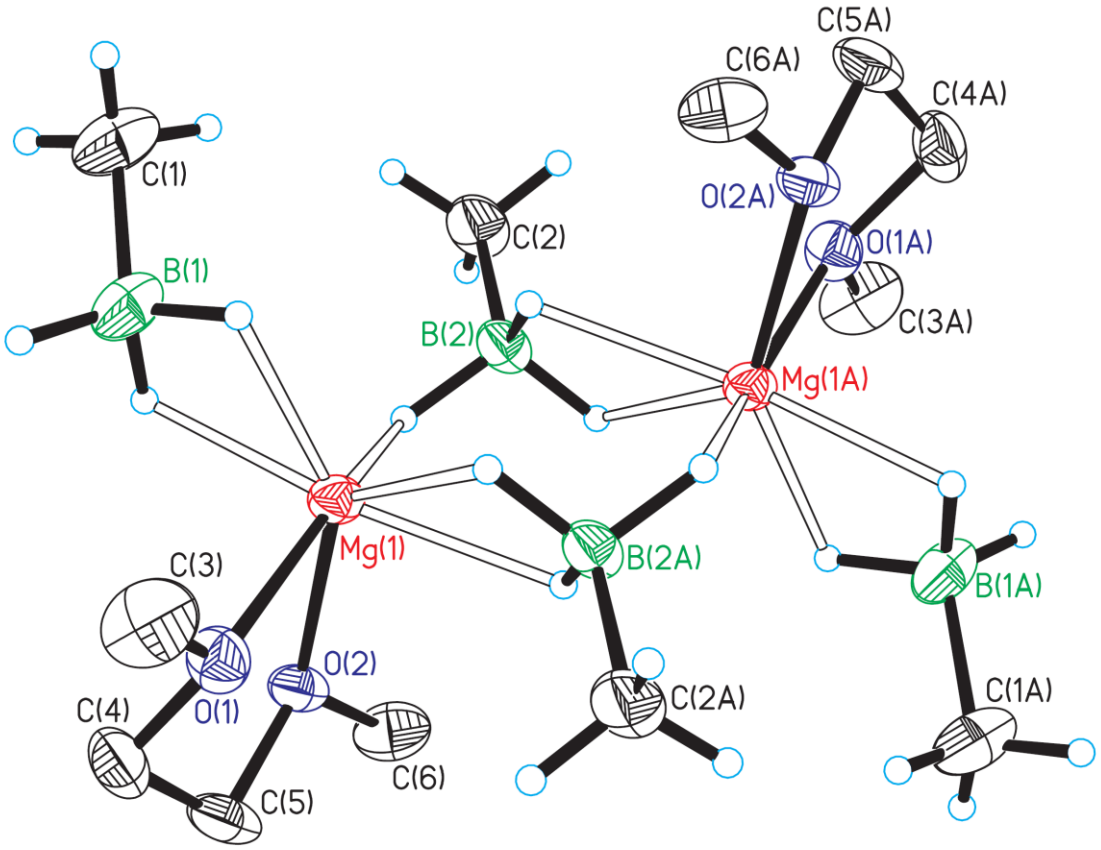

Figure 2.2. Methylborohydride bridge of $[Mg(H_3BCH_3)_2(DME)]_2$, **1**. The 35 % probability density surfaces are shown; hydrogen atoms are represented by arbitrarily sized spheres.

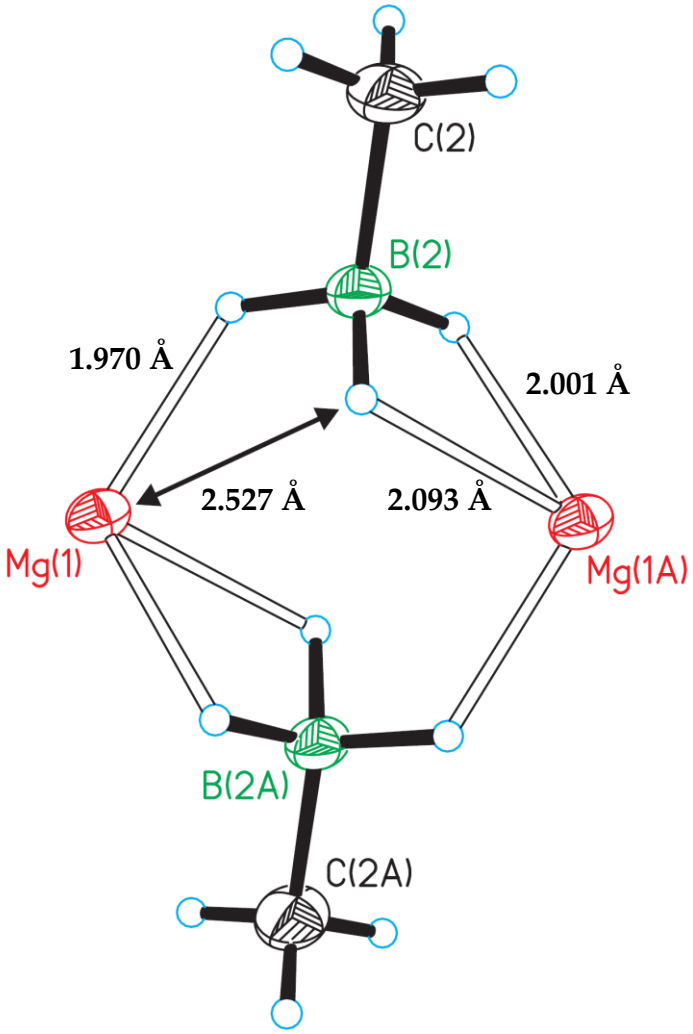

Figure 2.3. Molecular structure of $Ca(H_3BCH_3)_2(DME)_2$, **2**. The 35 % probability density surfaces are shown; hydrogen atoms are represented by arbitrarily sized spheres or are omitted for clarity.

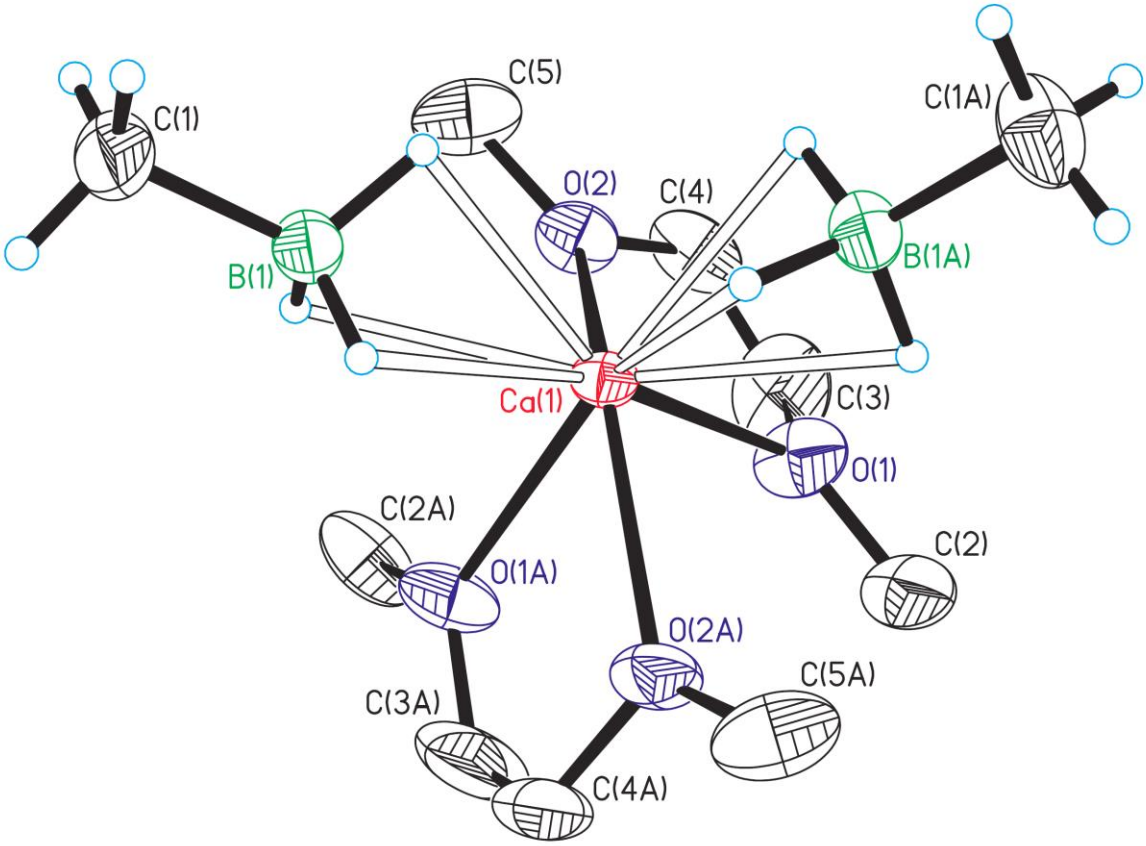

Figure 2.4. Molecular structure of $Sr(H_3BCH_3)_2(DME)_3$, **3**. The 35 % probability density surfaces are shown; hydrogen atoms are represented by arbitrarily sized spheres or are omitted for clarity.

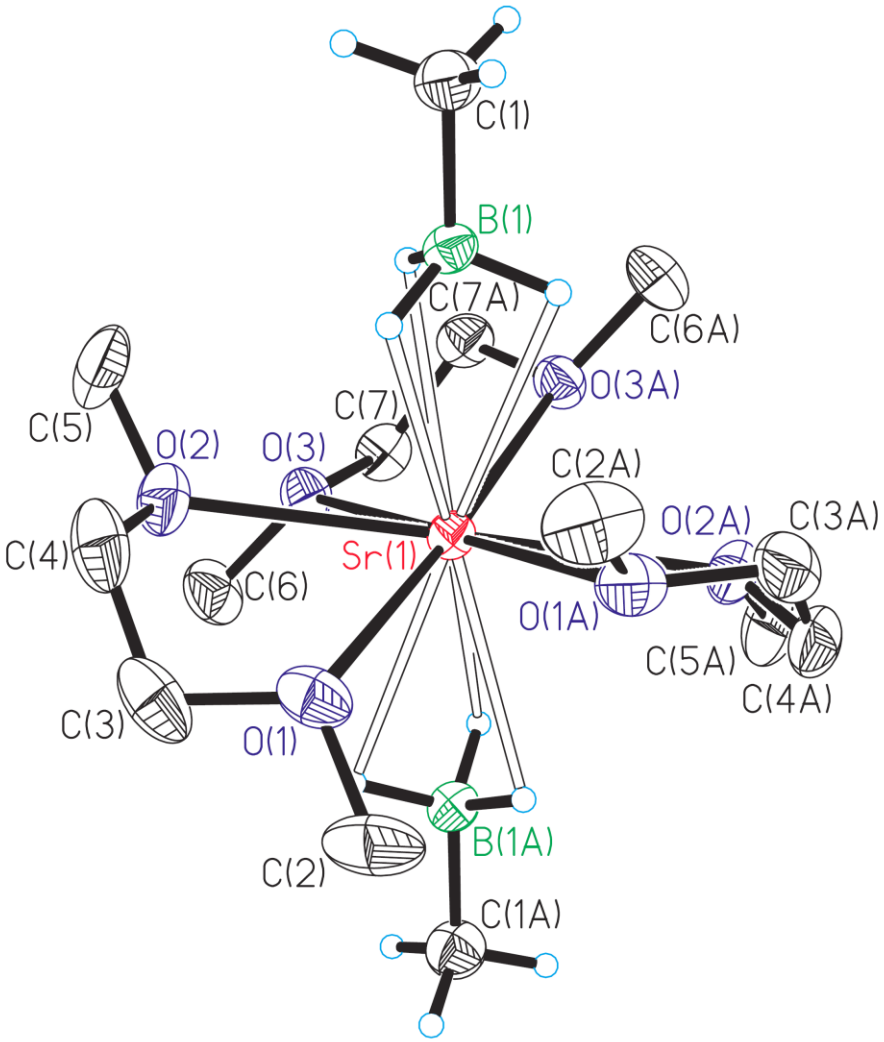

Figure 2.5. Molecular structure of $Ba(H_3BCH_3)_2(DME)_3$, **4**. The 35 % probability density surfaces are shown; hydrogen atoms are represented by arbitrarily sized spheres or are omitted for clarity.

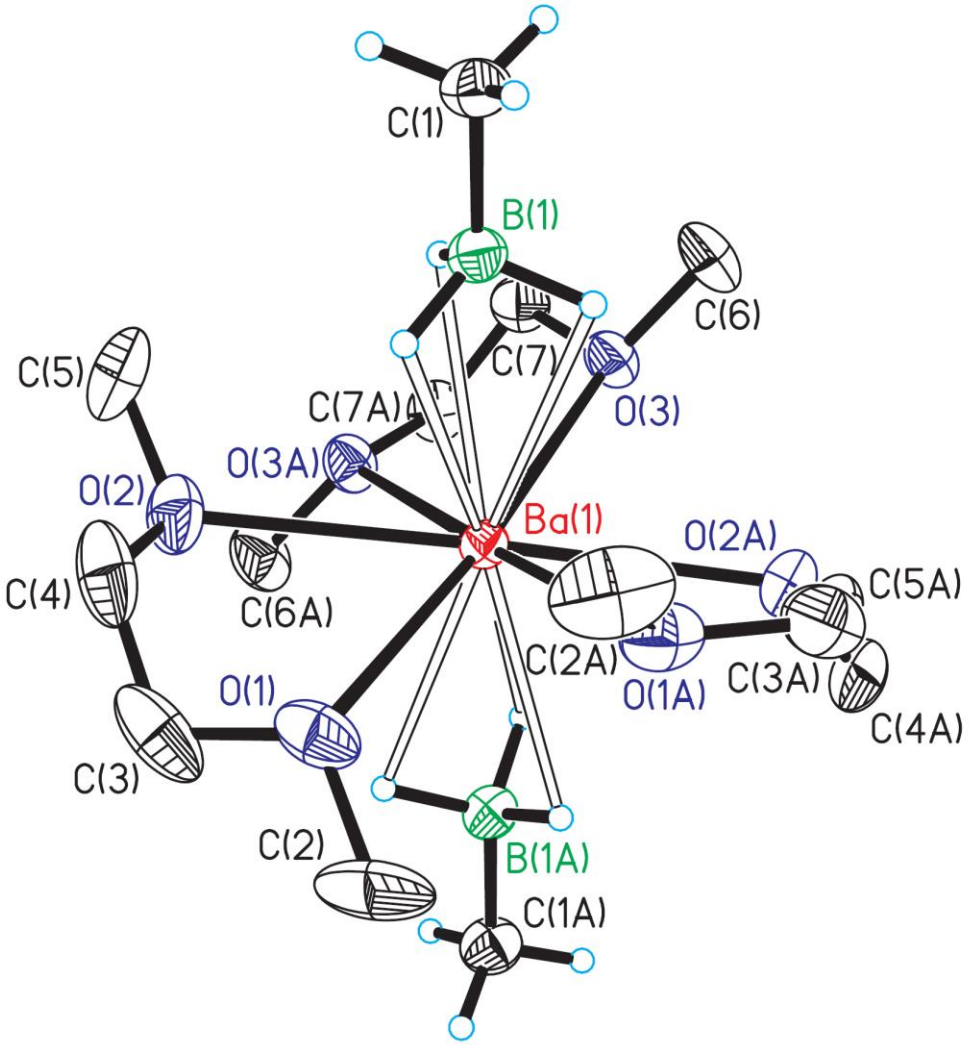

References

(1) Jones, M. E.; Marsh, R. E. *J. Am. Chem. Soc.* **1954**, *76*, 1434-1436.

(2) Nagamatsu, J.; Nakagawa, N.; Muranaka, T.; Zenitani, Y.; Akimitsu, J. *Nature* **2001**, *410*, 63-64.

(3) Wu, M. K.; Ashburn, J. R.; Torng, C. J.; Hor, P. H.; Meng, R. L.; Gao, L.; Huang, Z. J.; Wang, Y. Q.; Chu, C. W. *Phys. Rev. Lett.* **1987**, *58*, 908-910.

(4) Zhuang, C.; Tan, T.; Krick, A.; Lei, Q.; Chen, K.; Xi, X. X. *J. Supercond. Novel Magn.* **2013**, *26*, 1563-1568.

(5) He, F.; Xie, D.; Feng, Q.; Liu, K. *Supercond. Sci. Technol.* **2012**, *25*, 065003.

(6) Collings, E. W.; Sumption, M. D.; Tajima, T. *Supercond. Sci. Technol.* **2004**, *17*, S595-S601.

(7) Cunnane, D.; Galan, E.; Chen, K.; Xi, X. X. *Appl. Phys. Lett.* **2013**, *103*, 212603.

(8) Wang, S.; Zhou, Z.; Yang, F.; Yang, J.; Fu, X. *Appl. Mech. Mater.* **2011**, *130-134*, 908-912.

(9) Costache, M. V.; Moodera, J. S. *Appl. Phys. Lett.* **2010**, *96*, 082508.

(10) Chen, K.; Zhuang, C. G.; Li, Q.; Zhu, Y.; Voyles, P. M.; Weng, X.; Redwing, J. M.; Singh, R. K.; Kleinsasser, A. W.; Xi, X. X. *Appl. Phys. Lett.* **2010**, *96*, 042506.

(11) Xu, M.; Kitazawa, H.; Takano, Y.; Ye, J.; Nishida, K.; Abe, H.; Matsushita, A.; Tsujii, N.; Kido, G. *Appl. Phys. Lett.* **2001**, *79*, 2779-2781.

(12) Tsuda, S.; Yokoya, T.; Kiss, T.; Takano, Y.; Togano, K.; Kito, H.; Ihara, H.; Shin, S. *Phys. Rev. Lett.* **2001**, *87*, 177006.

(13) Schmidt, H.; Zasadzinski, J. F.; Gray, K. E.; Hinks, D. G. *Phys. Rev. Lett.* **2002**, *88*, 127002.

(14) Welp, U.; Rydh, A.; Karapetrov, G.; Kwok, W. K.; Crabtree, G. W.; Marcenat, C.; Paulius, L. M.; Lyard, L.; Klein, T.; Marcus, J.; Blanchard, S.; Samuely, P.; Szabo, P.; Jansen, A. G. M.; Kim, K. H. P.; Jung, C. U.; Lee, H. S.; Kang, B.; Lee, S. I. *Physica. C, Superconductivity* **2003**, *385*, 154-161.

(15) Xu, S. Y.; Li, Q.; Wertz, E.; Hu, Y. F.; Pogrebnyakov, A. V.; Zeng, X. H.; Xi, X. X.; Redwing, J. M. *Phys. Rev. B: Condens. Matter.* **2003**, *68*, 224501.

(16) Canfield, P. C.; Crabtree, G. W. *Physics Today* **2003**, *56*, 34-40.

(17) Zeng, X. H.; Pogrebnyakov, A. V.; Zhu, M. H.; Jones, J. E.; Xi, X. X.; Xu, S. Y.; Wertz, E.; Li, Q.; Redwing, J. M.; Lettieri, J.; Vaithyanathan, V.; Schlom, D. G.; Liu, Z.; Trithaveesak, O.; Schubert, J. *Appl. Phys. Lett.* **2003**, *82*, 2097-2099.

(18) Dai, W.; Ferrando, V.; Pogrebnyakov, A. V.; Wilke, R. H. T.; Chen, K.; Weng, X.; Redwing, J.; Bark, C.; Eom, C.; Zhu, Y.; Voyles, P. M.; Rickel, D.; Betts, J. B.; Mielke, C. H.; Gurevich, A.; Larbalestier, D. C.; Li, Q.; Xi, X. X. *Supercond. Sci. Technol.* **2011**, *24*, 125014.

(19) Zeng, X.; Pogrebnyakov, A. V.; Kotcharov, A.; Jones, J. E.; Xi, X. X.; Lysczek, E. M.; Redwing, J. M.; Xu, S.; Li, Q.; Lettieri, J.; Schlom, D. G.; Tian, W.; Pan, X.; Liu, Z. *Nat. Mater.* **2002**, *1*, 35-38.

(20) Yang, J.; Wang, S.; Yang, F. S.; Zhang, Z. P.; Ding, Z.; Fu, X. H. *Physica C.* **2007**, *467*, 1-3.

(21) Sinha, B. B.; Chung, K. C. *J. Supercond. Novel Magn.* **2013**, *26*, 1507-1511.

(22) Plecenik, A.; Satrapinsky, L.; Kúš, P.; Gazi, S.; Beňačka, S.; Vávra, I.; Kostič, I. *Physica. C, Superconductivity* **2001**, *363*, 224-230.

(23) Okuma, S.; Togo, S.; Amemori, K. *Phys. Rev. B: Condens. Matter.* **2003**, *67*, 172508.

(24) Fabretti, S.; Thomas, P.; Meinert, M.; Imort, I.; Thomas, A. *J. Supercond. Novel Magn.* **2013**, *26*, 1879-1882.

(25) Brinkman, A.; Mijatovic, D.; Rijnders, G.; Leca, V.; Smilde, H. J. H.; Oomen, I.; Golubov, A. A.; Roesthuis, F.; Harkema, S.; Hilgenkamp, H.; Blank, D. H. A.; Rogalla, H. *Physica. C, Superconductivity* **2001**, *353*, 1-4.

(26) Ueda, K.; Naito, M. *Appl. Phys. Lett.* **2001**, *79*, 2046-2048.

(27) Zhou, Z.; Yang, F.; Yang, J.; Wang, S.; Fu, X. *Adv. Mat. Res.* **2012**, *479-481*, 1781-1785.

(28) Kang, W. N.; Kim, H.; Choi, E.; Jung, C. U.; Lee, S. *Science* **2001**, *292*, 1521-1523.

(29) Crociani, L.; Rossetto, G.; Kaciulis, S.; Mezzi, A.; El-Habra, N.; Palmieri, V. *Chem. Vap. Deposition* **2007**, *13*, 414-419.

(30) Kim, D. Y.; Yang, Y.; Abelson, J. R.; Girolami, G. S. *Inorg. Chem.* **2007**, *46*, 9060-9066.

(31) Kim, D. Y.; Girolami, G. S. *Inorg. Chem.* **2010**, *49*, 4942-4948.

(32) Mathur, S.; Rügamer, T.; Braunschweig, H.; D'Andola, G. *Z. Anorg. Allg. Chem.* **2007**, *633*, 2459-2462.

(33) Her, J.; Stephens, P. W.; Gao, Y.; Soloveichik, G. L.; Rijssenbeek, J.; Andrus, M.; Zhao, J. *Acta Crystallogr., Sect. B: Struct. Sci.* **2007**, *63*, 561-568.

(34) Plesek, J.; Heřmánek, S. *Collect. Czech. Chem. Commun.* **1966**, *31*, 3845-3858.

(35) Yang, Y. Ph.D. Thesis, University of Illinois at Urbana-Champaign, **2007**.

(36) Pallecchi, I.; Ferrando, V.; Tarantini, C.; Putti, M.; Ferdeghini, C.; Zhu, Y.; Voyles, P. M.; Xi, X. X. *Supercond. Sci. Technol.* **2009**, *22*, 015023.

(37) Pogrebnyakov, A. V.; Xi, X. X.; Redwing, J. M.; Vaithyanathan, V.; Schlom, D. G.; Soukiassian, A.; Mi, S. B.; Jia, C. L.; Giencke, J. E.; Eom, C. B.; Chen, J.; Hu, Y. F.; Cui, Y.; Li, Q. *Appl. Phys. Lett.* **2004**, *85*, 2017-2019.

(38) Bhatia, M.; Sumption, M. D.; Collings, E. W.; Dregia, S. *Appl. Phys. Lett.* **2005**, *87*, 042505.

(39) Zhao, Y.; Ionescu, M.; Horvat, J.; Li, A. H.; Dou, S. X. *Los Alamos National Laboratory, Preprinit Arhive, Condensed Matter* **2003**, 1-7.

(40) Yao, Q. W.; Wang, X. L.; Soltanian, S.; Li, A. H.; Horvat, J.; Dou, S. X. *Ceram. Int.* **2004**, *30*, 1603-1606.

(41) Singh, R. K.; Shen, Y.; Gandikota, R.; Wright, D.; Carvalho, C.; Rowell, J. M.; Newman, N. *Los Alamos National Laboratory, Preprinit Arhive, Condensed Matter* **2007**, 1-7.

(42) Dou, S. X.; Braccini, V.; Soltanian, S.; Klie, R.; Zhu, Y.; Li, S.; Wang, X. L.; Larbalestier, D. *J. Appl. Phys.* **2004**, *96*, 7549-7555.

(43) Angst, M.; Budko, S. L.; Wilke, R. H. T.; Canfield, P. C. *Phys. Rev. B: Condens. Matter.* **2005**, *71*, 144512.

(44) Lee, S.; Masui, T.; Yamamoto, A.; Uchiyama, H.; Tajima, S. *Physica. C, Superconductivity* **2003**, *397*, 7-13.

(45) Kazakov, S. M.; Karpinski, J.; Jun, J.; Geiser, P.; Zhigadlo, N. D.; Puzniak, R.; Mironov, A. V. *Los Alamos National Laboratory, Preprinit Arhive, Condensed Matter* **2003**, 1-6.

(46) Wilke, R. H. T.; Bud'ko, S. L.; Canfield, P. C.; Finnemore, D. K.; Suplinskas, R. J.; Hannahs, S. T. *Phys. Rev. Lett.* **2004**, *92*, 217003.

(47) Ribeiro, R. A.; Budko, S. L.; Petrovic, C.; Canfield, P. C. *Physica. C, Superconductivity* **2003**, *384*, 227-236.

(48) Srebnik, M.; Cole, T. E.; Ramachandran, P. V.; Brown, H. C. *J. Org. Chem* **1989**, *54*, 6085-6096.

(49) Dias, H. V. R.; Wang, X. *Polyhedron* **2004**, *23*, 2533-2539.

(50) Goel, A. B. *Indian J. Chem.* **1978**, *16*, 491-494.

(51) Brown, H. C.; Cole, T. E.; Srebnik, M.; Kim, K. *J. Org. Chem.* **1986**, *51*, 4925-4930.

(52) Biffar, W.; Noth, H.; Sedlak, D. *Organometallics* **1983**, *2*, 579-585.

(53) Singaram, B.; Cole, T. E.; Brown, H. C. *Organometallics* **1984**, *3*, 774-777.

(54) Noeth, H. *Zeitschrift für Naturforschung. Teil b, Anorganische Chemie, Organische Chemie* **1982**, *37B*, 1499-1503.

(55) Lobkovskii, É. B.; Titov, L. V.; Psikha, S. B.; Antipin, M. Y.; Struchkov, Y. T. *J. Struct. Chem.* **1982**, *23*, 644-646.

(56) Lobkovskii, É. B.; Titov, L. V.; Levicheva, M. D.; Chekhlov, A. N. *J. Struct. Chem.* **1990**, *31*, 506-508.

(57) Bremer, M.; Nöth, H.; Warchhold, M. *Eur. J. Inorg. Chem.* **2003**, *2003*, 111-119.

(58) Soloveichik, G. L.; Andrus, M.; Lobkovsky, E. B. *Inorg. Chem.* **2007**, *46*, 3790-3791.

(59) Marks, T. J.; Kolb, J. R. *Chem. Rev.* **1977**, *77*, 263-293.

(60) Marks, T. J.; Kennelly, W. J.; Kolb, J. R.; Shimp, L. A. *Inorg. Chem.* **1972**, *11*, 2540-2546.

(61) Banks, R. H.; Edelstein, N. *J. Chem. Phys.* **1980**, *73*, 3589-3599.

(62) Shinomoto, R.; Brennan, J. G.; Edelstein, N. M.; Zalkin, A. *Inorg. Chem.* **1985**, *24*, 2896-2900.

(63) Mallek, J. L.; Girolami, G. S. Chapter 5 of this thesis. Manuscript in preparation.

(64) Raymond, K. N.; Eigenbrot Jr., C. W. *Acc. Chem. Res.* **1980**, *13*, 276-283.

(65) Shannon, R. D. *Acta Crystallogr., Sect. A* **1976**, *A32*, 751-767.

(66) Edelstein, N. *Inorg. Chem.* **1981**, *20*, 297-299.

(67) Shinomoto, R. S. Ph.D. Thesis, University of California, Berkely, **1984**.

(68) Brumaghim, J. L.; Priepot, J. G.; Girolami, G. S. *Organometallics* **1999**, *18*, 2139-2144.

CHAPTER 3: Synthesis and Characterization of Scandium, Yttrium, Neodymium, Gadolinium, and Erbium Methylborohydride and the Deposition of Erbium Containing Thin Films by Chemical Vapor Deposition.

Introduction

Rare earth metals (Sc, Y, La – Lu) have a wide array of applications, and find important uses in catalytic converters,[1-3] ceramics,[4-6] phosphors,[7-9] batteries,[10-12] lighting (LED),[13-15] magnets,[16-18] superconductors,[19-21] piezoelectric devices,[22-24] thermionic emitters,[25,26] high κ dielectrics,[27-32] buffer layers,[33,34] thermophotovoltaics,[27,35] and optical coatings.[36-38] Chemical vapor deposition, CVD, and atomic layer deposition, ALD, are increasingly attractive methods to fabricate thin films containing rare earths, especially for the deposition of films on microstructured or nanostructured surfaces. For example, the superconductor $YBa_2CuO_{7-\delta}$ can be deposited as a thin film by CVD using $Y(thd)_3$, $Ba(thd)_2$, and $Cu(thd)_2$, (thd = 2,2,6,6-tetramethyl-3,5-heptanedione), with H_2O or N_2O as the oxygen source.[39-45]

For CVD and ALD processes, volatile precursors are required; an in depth discussion of this topic can be found in Chapter 1 of this thesis. A substantial body of literature has been published pertaining to rare earth CVD and ALD precursors over the past 30 years, including a number of reviews.[46-57] Rare earth metal precursors can be divided into three primary classes based on the ligand sets used: organometallic

ligands, bulky ligands, and polydentate ligands. Predominant among the organo-rare earth complexes are those that contain cyclopentadienyl (Cp) and substituted Cp ligands.[58-64] Cp_3M molecules are reactive toward water and can be used to grow rare earth oxide thin films. The volatility of this class of precursors is often low, however, and the precursor typically must be heated to relatively high temperatures to obtain satisfactory transport rates.

Complexes containing bulky monodentate ligands, such as disilylamides[65-67] and tertiary alkoxides,[66,68-70] constitute another class of volatile rare earth CVD precursors. Although disilylamide complexes are highly reactive with water, they do not cleanly decompose into rare earth oxides. Rather, a silicon impurity is typically found in the film. To form volatile rare earth complexes, tertiary alkoxides typically either bear a bulky alkyl substituent or are functionalized with an ether group which can coordinate to the metal center, inhibiting intermolecular interactions. Rare earth alkoxides have the ability to deposit oxide thin films even in the absence of an oxygen source due to the decomposition of the precursor ligand. However, when films are grown at lower temperatures with an oxygen source, the growth rates are typically low.

Complexes bearing polydentate ligands, such as β-diketonates,[71-73] β-ketoiminates,[74,75] amidinates,[76-78] guanidinates,[79,80] and aminodiboranates,[81-84] constitute the largest and most structurally diverse class of rare earth CVD precursors. Some representatives of this class have reasonably high vapor pressures. For example,

$La(hfa)_3(diglyme)$, (hfa = 1,1,1,5,5,5-hexafluoropentane-2,4-dione), sublimes between 65 and 70 °C at 10^{-3} Torr. The volatility of many of these complexes is a result of metal coordination sphere saturation which limits the intermolecular interactions between neighboring molecules. Deposition of rare earth oxide thin films can be accomplished with O_2 or H_2O as the oxidant with a number of these precursors.

One other ligand that often forms volatile metal complexes is borohydride. Binary metal borohydride complexes often are volatile if they are able to saturate the coordination sphere (i.e., provided that the metal is not too large and its oxidation state is not too small), because they can shield the metal center Coulombically, they are not very polarizable, and the negative charges on the hydrogen atoms creates intermolecular repulsions between neighboring molecules. Somewhat surprisingly, relatively few volatile rare earth metal borohydrides have been described. The scandium complex, $Sc(BH_4)_3(THF)$, (THF = tetrahydrofuran), sublimes at 80 °C in vacuum.[85] The yttrium complex, $Y(BH_4)_3(THF)_3$ sublimes at 90 °C in vacuum with the loss of one THF molecule, forming the charge-separated ion pair $[Y(BH_4)_2(THF)_4][Y(BH_4)_4]$.[86] For rare earth metals with relatively small ionic radii (M = Gd, Tb, Dy, Ho, Er, Tm, and Yb), the $M(BH_4)_3(DME)$ complexes are volatile only at high temperatures, 150 to 190 °C.[87] Many rare earth complexes with one, two, or three borohydrides per metal center have been reported, although most of these decompose

rather than sublime or are volatile only at high temperature, which limits their use as CVD precursors.[88-105]

Closely related to the complexes above are methylborohydride complexes of the rare earths. The mono(diethyl etherate) complexes $M(H_3BCH_3)_3(Et_2O)$, M = Ho, Yb, and Lu, sublime at 50 °C under vacuum, whereas the $M(H_3BCH_3)_3(THF)$ analogs sublime at 100 °C under vacuum.[106,107] Surprisingly, there are no reports of the use of these molecules as CVD or ALD precursors. Not only do they have lower sublimation temperatures than the majority of rare earth precursors, they are also react readily with water, and thus ought to be useful as CVD precursors for metal oxide thin films, with concomitant formation of methylborane and hydrogen gas.

$$2\ M(H_3BCH_3)L_n + 3\ H_2O \longrightarrow M_2O_3 + 6\ H_2BCH_3 + 2n\ L + 6\ H_2$$

Here I describe a number of new potential CVD precursors for the rare earths: the tetrahydrofuran adducts of scandium methylborohydride, $Sc(H_3BCH_3)_3(THF)$, **1**; yttrium methylborohydride, $Y(H_3BCH_3)_3(THF)_2$, **2**; neodymium methylborohydride, $Nd(H_3BCH_3)_3(THF)_2$, **3**; gadolinium methylborohydride, $Gd(H_3BCH_3)_3(THF)_2$, **4**; and erbium methylborohydride, $Er(H_3BCH_3)_3(THF)_2$, **5**. Also described is the synthesis of the 1,2-dimethoxyethane adduct of neodymium methylborohydride, $Nd(H_3BCH_3)_3(DME)_{1.5}$, **3′**.

Results and Discussion

Syntheses of $Sc(H_3BCH_3)_3(THF)$, $Y(H_3BCH_3)_3(THF)_2$, $Nd(H_3BCH_3)_3(THF)_2$, $Gd(H_3BCH_3)_3(THF)_2$, and $Er(H_3BCH_3)_3(THF)_2$. Scandium, yttrium, neodymium, gadolinium, and erbium methylborohydride complexes can be prepared by treating MCl_3 (M = Sc, Y, Nd, Gd, Er) with $Na(H_3BCH_3)$ in THF for 48 hrs. Filtration of the reaction solution followed by removal of THF from the filtrate in vacuum affords a tacky solid which is sublimed at 50 °C for the Sc and Y complexes, $Sc(H_3BCH_3)_3(THF)$, **1**, $Y(H_3BCH_3)_3(THF)_2$, **2**, and at 60 °C for the neodymium, gadolinium, and erbium complexes $Nd(H_3BCH_3)_3(THF)_2$, **3**, $Gd(H_3BCH_3)_3(THF)_2$, **4**, $Er(H_3BCH_3)_3(THF)_2$, **5**.

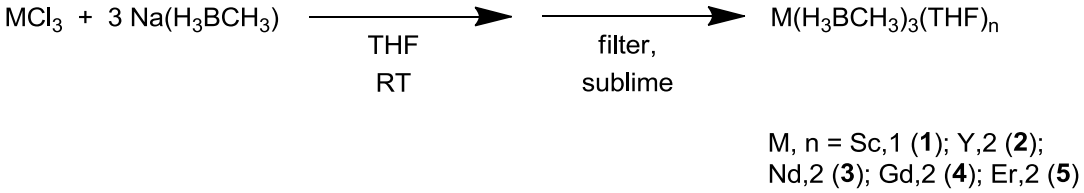

The pink sublimate, both powder and crystals, of the Er complex, **5**, can be re-sublimed at 60 °C although a small amount (< 15%) of pale pink, non-volatile solid remains, presumably due to thermal decomposition. The other rare earth methylborohydride THF adducts probably behave similarly, although we did not investigate this point in detail.

Synthesis of $Nd(H_3BCH_3)_3(DME)_{1.5}$. Treatment of $NdCl_3$ with three equivalents of $Na(H_3BCH_3)$ in DME for 48 hrs, followed by sublimation from the dried reaction products at 115 °C affords the complex $Nd(H_3BCH_3)_3(DME)_{1.5}$, **3′**.

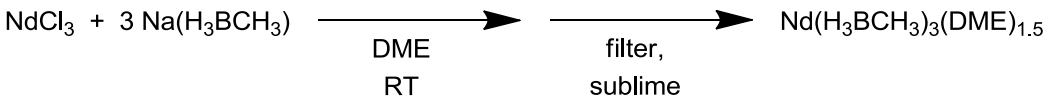

Attempts were made to synthesize the gadolinium and erbium DME analogs by the same synthetic route. However, no volatile material could be collected upon heating the dried reaction mixture to 120 °C under vacuum.

Complexes **1** – **5** and **3′** are air and water sensitive and must be handled under inert atmospheres. They appear to decompose thermally at room temperature, albeit slowly over a period of months.

Attempts to synthesize praseodymium, samarium, and europium methylborohydride complexes. The reaction between praseodymium chloride, $PrCl_3$ and $Na(H_3BCH_3)$ in THF resulted in a green solid which could not be sublimed at 60 °C under vacuum. Sublimation at 90 °C afforded a small amount of green sublimate. The elemental analysis of the sublimate corresponds to the stoichiometry $Pr(H_3BCH_3)_3(THF)_{1.6}$. The relatively low volatility of this complex suggests that it is a polymer or salt in the solid state.

Stirring samarium chloride, $SmCl_3$, with sodium methylborohydride in THF or DME resulted in no reaction as determined by ^{11}B NMR spectroscopy. This finding agrees with a previous report that no sublimate was obtained from the analogous reaction of samarium chloride with lithium methylborohydride in diethyl ether.[106] When europium chloride, $EuCl_3$, is treated with sodium methylborohydride in DME or THF, a yellow or green solid, respectively, is obtained. However, no volatile material was collected from either reaction mixture after the solvent was removed and the resulting solid was heated to 120 °C under vacuum. Fluorescent green crystals were grown from the THF solution by slow diffusion of pentane. Unfortunately, no satisfactory elemental analysis or structural data could be obtained.

Crystal Structures. The scandium complex $Sc(H_3BCH_3)_3(THF)$, **1**, is monomeric in the solid state and contains three κ^3*H*-methylborohydride groups (Sc···B, average 2.3054 Å) and one bound THF molecule. The one oxygen atom and three boron atoms describe a distorted tetrahedron about the scandium center.

The neodymium complex $Nd(H_3BCH_3)_3(THF)_2$, **3**, is a methylborohydride-bridged dimer. Each Nd center is bound to two THF molecules, two κ^3*H*-methylborohydride groups (average Nd···B 2.605(2) Å) and two κ^2*H*-methylborohydride groups in a distorted octahedral arrangement; the latter groups bridge between the two Nd centers. If one regards each Nd-H interaction as occupying one coordination site, then each neodymium atom is 12-coordinate. The bridging κ^2*H*-methylborohydride

groups are bound symmetrically between the two metal centers: the Nd···B distances of 2.968(2) and 3.031(2) Å differ by only 0.063 Å.

When the neodymium complex $Nd(H_3BCH_3)_3(DME)_{1.5}$, **3′**, is crystallized from diethyl ether, some of the DME molecules are replaced by Et_2O, resulting in the monomeric complex $Nd(H_3BCH_3)_3(DME)(Et_2O)$, **3′·Et₂O**. The three oxygen atoms and three boron atoms describe a distorted *fac*-octahedral coordination geometry. If one regards each Nd-H interaction as occupying one coordination site, the neodymium center is 12-coordinate with three κ^3*H*-methylborohydride groups (average Nd···B 2.618 Å), one chelating DME molecule, and one Et_2O molecule.

The yttrium complex, **2**, crystalizes as a charge separated ion pair, $[Y(H_3BCH_3)_2(THF)_4][Y(H_3BCH_3)_4]$ similar to its BH_4^- analog.[86] All the methylborohydride ligands are bound in a κ^3*H* fashion. The coordination geometry of the Y cation can be described as a distorted *trans*-octahedron in which the two boron atoms occupy the axial vertices and the four THF oxygens describe the equatorial plane. The average Y···B distance is 2.502 Å and the B···Y···B angle is 163.9 °. The anion can be described as a distorted tetrahedron; the average Y···B distance 2.488 Å. If one regards each Y-H interaction as involving a coordination site, then the geometry of the 12-coordinate yttrium center in the $[Y(H_3BCH_3)_4]$ anion is best described as a distorted cuboctahedron.

The gadolinium complex $Gd(H_3BCH_3)_3(THF)_2$, **4**, and the erbium complex, **5**, also crystallize as charge separated ion pairs, $[M(H_3BCH_3)_2(THF)_4][RE(H_3BCH_3)_4]$ M = Gd, Er,

with the same connectivity and geometry as the yttrium complex, **2**. The average Gd···B distance in the cation is 2.541 Å and the average Er···B distance in the cation is 2.486 Å. The B···Gd···B angle is 167.04 ° and the B···Er···B angle is 163.1 °. The average Gd···B and Er···B distances in the anion of 2.525 Å and 2.467 Å, respectively, are slightly shorter than those in the cation. Crystals of **5** were grown by two methods: cooling a saturated toluene solution and by sublimation. Crystals grown by both methods have identical unit cells, indicating that the charge separated ion pair forms directly as the sublimed product.

NMR Spectra. The ^{11}B NMR spectra of the scandium complex **1** in toluene shows an unresolved multiplet at δ -9.1, which is significantly deshielded relative to the chemical shifts seen for other diamagnetic methylborohydride complexes reported in this thesis. The ^{11}B NMR spectrum of the yttrium complex **2** contains a 1:3:3:1 quartet at δ -15.3. This result suggests that the structure of the yttrium complex in THF is different from the charge separated ion pair which exists in the solid state. The Nd complexes **3** and **3'** as well as the Er complex **5** show resonances at δ 207, 198, and 300 that are highly shifted and broadened by the paramagnetism. No ^{11}B NMR resonance could be observed for the f^7 Gd complex **4**.

IR Spectra. The IR spectra of sublimed samples of complexes **2 – 5** and **3'** each contain two strong B-H stretches, which can be assigned to the A_1 and E modes of the κ^3-*H*-methylborohydride group. These peaks appear at 2180 and 2112 cm^{-1} for the Y

complex **2**, at 2201 and 2107 cm^{-1} for the Nd complex **3**, at 2200 and 2129 cm^{-1} for the Nd complex **3'**, at 2179 and 2103 cm^{-1} for the Gd complex **4**, and at 2183 and 2115 cm^{-1} for the Er complex **5**.[108-110] Although the Nd complex **3** crystalizes as a dimer with κ^2H,κ^2H methylborohydride bridges, there is no IR evidence of this bridging interaction; this behavior is similarly to that reported for the related methylborohydride bridged dimers $[Th(H_3BCH_3)_4]_2(Et_2O)$ and $[Th(H_3BCH_3)_4(THF)]_2$.[111] The IR spectrum of the Er complex **5** is unchanged after the complex is resublimed.

The IR spectrum of the Sc complex **1** is different from those of the lanthanide methylborohydride complexes: there are three strong B-H stretches at 2201, 2120, and 2049 cm^{-1}, which are not typical of a κ^3H-methylborohydride, although the crystal data shows the molecule has three κ^3H-methylborohydride groups in the solid state.

Chemical Vapor Deposition Using the New $Er(H_3BCH_3)_3(THF)_2$ Precursor

Deposition Method. Chemical vapor deposition was carried out using a Schlenk tube deposition chamber and a tube furnace. The Schlenk tube was approximately 25 cm long from the bottom of the ground glass joint with a 2.6 cm outer diameter. A silicon wafer with native oxide was loaded into the deposition tube and approximately 20 to 25 mg of $Er(H_3BCH_3)_3(THF)_2$ was loaded into the precursor reservoir and the deposition tube was sealed under argon in the glove box. The tube was evacuated to approximately 10 mTorr on a Schlenk line and the deposition tube was heated to the

desired set point. The precursor was heated between 75 and 85 °C with heating tape while the deposition tube was under active vacuum. After approximately 15 minutes only traces of the precursor remained in the reservoir. Heating was then discontinued and the deposition tube was allowed to cool under vacuum. Once cooled to room temperature the deposition tube was backfilled and the silicon wafer retrieved. A schematic of the deposition tube can be seen in Figure 3.1.

Chemical Vapor Deposition Results and Discussion. Thin films deposited at 250 °C were thin, <10 nm, and rough. (Figure 3.2) After sputtering the surface of the film to remove atmospheric contaminants, a film composition of 11% Er, 71.6% B, and 17.4% O was measured by x-ray photoelectron spectroscopy, XPS. Films deposited at 300 °C were considerably thicker, 70 to 90 nm, and appear to be smooth and dense. (Figure 3.2) After removal of the surface layer by sputtering, a fairly uniform amount of Er was observed in the film, (13.3 to 13.9%). However, a large amount of oxygen, and smaller amount of boron, was measured near the surface of the film, 61.8% and 24.3%, respectively. Although sputtering deeper into the film show a reversal, where the boron content increases to 72.6% and oxygen decreases to 14%. (Figure 3.3). Films deposited at 350 °C were thick, greater than 350 nm, and poorly adhered to the surface. After sputtering the surface of the film to remove atmospheric contaminants, a film composition of 11.2 % Er, 51% B, 28.6% O, and 9.2% C was measured by XPS. Unlike the films grown at 250 and 300 °C, which had a carbon content near zero, this film had

considerable amounts of carbon which may have come from the decomposition of THF or from the methylborohydride.

Figure 3.1. Schematic depicting a Schlenk tube chemical vapor deposition chamber.

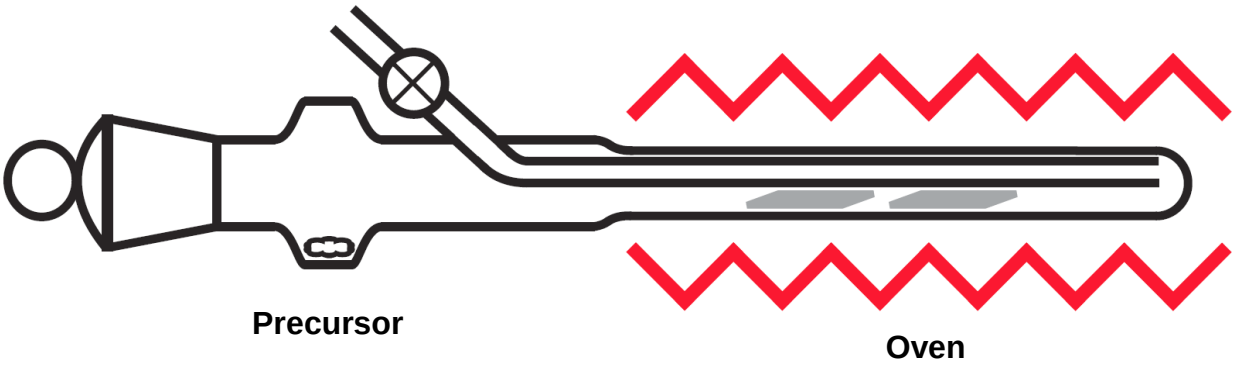

Figure 3.2. Images of the film deposited at 250 °C (top) and 300 °C (bottom).[112]

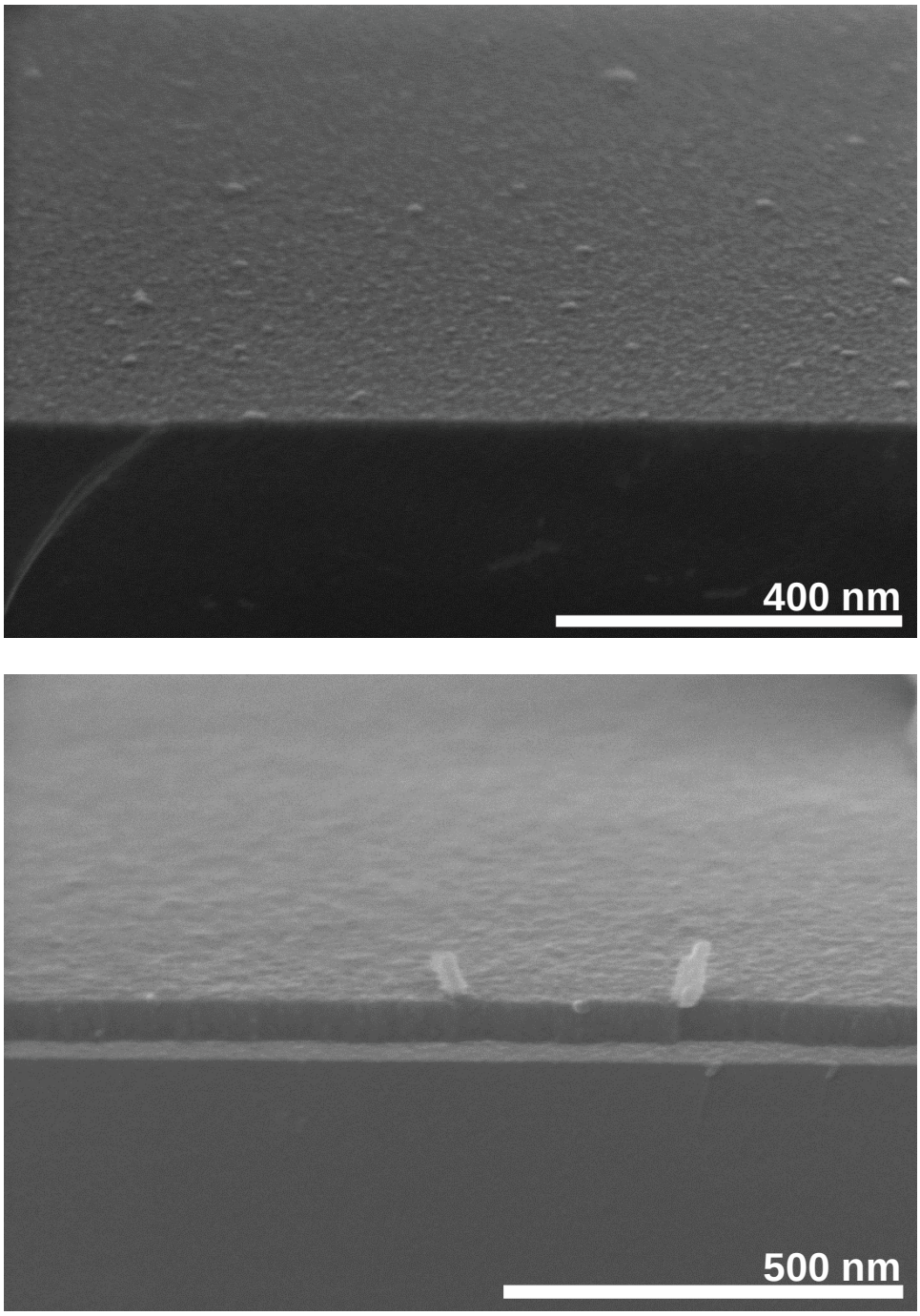

Figure 3.3. XPS depth profile of films grown at 300 °C.[112]

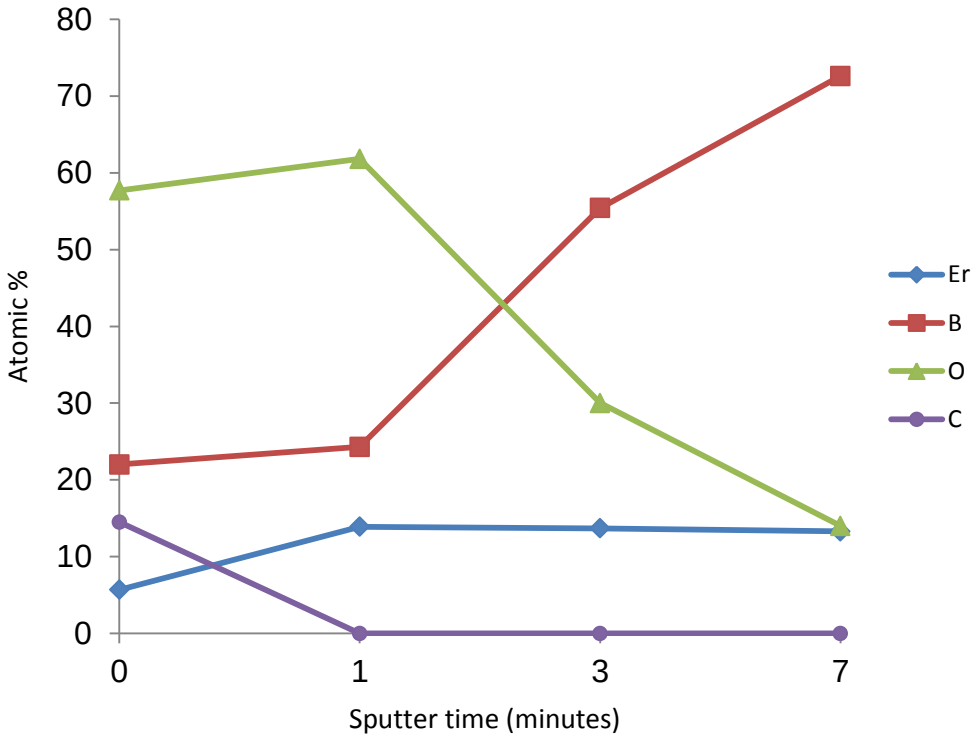

Conclusions

The THF adducts of Sc, Y, Nd, Gd, and Er trismethylborohydride have been successfully isolated and characterized. All five complexes are highly volatile, subliming at or below 60 °C, making them promising candidates for CVD precursors. Preliminary CVD experiments with erbium methylborohydride have been successful in demonstrating film growth at temperatures as low as 250 °C.

Experimental

All operations were carried out in a vacuum or under argon using standard Schlenk and glove box techniques. All glassware was dried in an oven at 150 °C, assembled hot, and allowed to cool under a vacuum before use. Pentane, diethyl ether, tetrahydrofuran, and 1,2-dimethoxyethane were distilled under nitrogen from sodium/benzophenone, and toluene was distilled under nitrogen from molten sodium. All solvents were degassed with argon immediately before use. All anhydrous rare earth metal chlorides were used as received with the exception of yttrium chloride, which was contaminated with nitrogen (probably as ammonia or ammonium); washing with THF removed most of this impurity and afforded samples of $YCl_3(THF)_{3.25}$ that still contained approximately 0.5 weight % of a nitrogen impurity. Sodium methylborohydride was prepared as described in Chapter 2 of this thesis.

Elemental analyses were carried out by the University of Illinois Microanalytical Laboratory. Crystallographic data were collected by the University of Illinois X-Ray Facility. The IR spectra were recorded on a Thermo Nicolet IR200 infrared spectrometer as Nujol mulls between NaCl salt plates. The ^{1}H NMR spectra were obtained on a Varian VXR 500 instrument at 11.7 T and ^{11}B NMR spectra were obtained on a Varian Unity 400 instrument at 9.4 T. The chemical shifts are reported in δ units (positive shifts to high frequency) relative to $SiMe_4$ (^{1}H NMR) or $BF_3{\cdot}Et_2O$ (^{11}B NMR).

Tris(methylborohydride)(tetrahydrofuran)scandium(III), $Sc(H_3BCH_3)_3(THF)$, 1. To a solid mixture of $ScCl_3$ (0.20 g, 1.3 mmol) and $Na(H_3BCH_3)$ (0.274 g, 5.3 mmol) was added THF (30 mL) to give a white suspension. The slurry was stirred for 2 days at room temperature and then allowed to settle to afford a clear solution and white precipitate. The solution was filtered and the filtrate was dried under reduced pressure to a tacky white solid. The solid was sublimed onto a cold finger at 50 °C and ca 10^{-2} Torr to afford a white sublimate. Yield 0.200 g (74%). Mp: 112 – 115 °C. Anal. Calcd. for $Sc(H_3BCH_3)_3(THF)$: C, 41.3; H, 12.87. Found: C, 40.5; H, 13.04. ^{1}H NMR (d_8-toluene): δ 0.4 (m, 9H, BCH_3), 0.92 (m, 4H, β-CH_2), 1.24 (br s, BH_3) 3.43 (m, 4H, α-CH_2). ^{11}B NMR (d_8-toluene): δ -9.1 (br s). IR (Nujol, cm^{-1}): 2201 m, 2120 s, 2049 m, 1312 s, 1271 s, 1176 w, 1105 m, 1040 w, 1012 m, 972 m, 923 w, 853 s.

Tris(methylborohydride)bis(tetrahydrofuran)yttrium(III), $Y(H_3BCH_3)_3(THF)_2$, 2. To a solid mixture of $YCl_3(THF)_{3.25}$ (0.40 g, 0.93 mmol) and $Na(H_3BCH_3)$ (0.19 g, 3.7

mmol) was added THF (30 mL) to give a white suspension. The slurry was stirred for 2 days at room temperature and allowed to settle to afford a clear solution and white precipitate. The solution was filtered and the filtrate was dried under reduced pressure to a tacky white solid. The solid was sublimed onto a cold finger at ca. 10^{-2} Torr and 50 °C to afford a white sublimate. Yield 0.187 g (62%). Mp: 141 – 145 °C. Anal. Calcd. for $Y(H_3BCH_3)_3(THF)_2$: C, 41.3; H, 10.72; N, 0.0. Found: C, 40.8; H, 10.9; N, 0.57; we believe the nitrogen is due to traces of ammonia present in the YCl_3 starting material. ^{1}H NMR (d_8-toluene): δ 0.42 (m, 9H, B-CH_3), 1.16 (1:1:1:1 q, J_{HB} = 70 Hz, BH_3), 1.19 (m, 8H, β-CH_2), 3.73 (m, 8H, α-CH_2). ^{11}B NMR (d_8-toluene): δ -15.3 (1:3:3:1 q, J_{BH} = 71 Hz). IR (Nujol, cm^{-1}): 2180 s, 2122 s, 1342 m, 1306 s, 1258 s, 1178 m, 1089 m, 1040 m, 1009 s, 942 m, 926 m, 854 s, 670 w.

Tris(methylborohydride)bis(tetrahydrofuran)neodymium(III), $Nd(H_3BCH_3)_3(THF)_2$, 3. To a solid mixture of $NdCl_3$ (0.20 g, 0.98 mmol) and $Na(H_3BCH_3)$ (0.165 g, 3.2 mmol) was added THF (30 mL) to give a green suspension. The slurry was stirred for 2 days at room temperature to afford a blue solution and a white precipitate. The solution was filtered and the filtrate was dried under reduced pressure to a tacky purple solid. The solid was sublimed onto a cold finger at 60 °C and ca. 10^{-2} Torr to afford a sublimate that appeared lavender in sunlight or under incandescent lighting, but blue-purple under fluorescent lighting (Figure 3.4). Yield: 0.065 g, (22%). Mp: 130 – 133 °C. Anal. Calcd. for $Nd(H_3BCH_3)_3(THF)_2$: C, 35.2; H, 9.14. Found: C, 35.3; H, 8.99. ^{1}H NMR (d_8-

toluene): δ 1.36 (m, 16H, α,β-CH_2), 9.21 (s, 9H, B-CH_3), 132.9 (br s, fwhm = 368 Hz, 9H, BH_3). ^{11}B NMR (d_8-toluene): δ 207 (s, fwhm = 146 Hz, BH_3). IR (Nujol, cm^{-1}): 2201 m, 2107 s, 1344 w, 1300 m, 1238 s, 1104 m, 1083 m, 1016 m, 958 w, 924 w, 864 m.

Tris(methylborohydride)sesqui(1,2-dimethoxyethane)neodymium(III), $Nd(H_3BCH_3)_3(DME)_{1.5}$, 3'. To a solid mixture of $NdCl_3$ (0.20 g, 0.98 mmol) and $Na(H_3BCH_3)$ (0.15 g, 2.9 mmol) was added 1,2-dimethoxyethane (30 mL) to give a green suspension. The slurry was stirred for 2 days at room temperature to afford a blue solution and white precipitate. The blue solution was filtered and the filtrate was dried to a tacky purple solid under reduced pressure. The solid was sublimed onto a cold finger at 115 °C and ca. 10^{-2} Torr to afford a purple sublimate. Upon exposure to sunlight or incandescent lighting, the solutions and solids appeared lavender. Yield 0.12 g (31%). Mp: 160 – 162 °C. Anal. Calcd. for $Nd(H_3BCH_3)_3(DME)_{1.5}$: Nd, 39.4; B, 8.86; C, 29.5; H, 9.09. Found: Nd, 39.9; B, 8.1; C, 29.4; H, 9.13. IR (Nujol, cm^{-1}): 2200 m, 2129 s, 1301 s, 1238 s, 1188 m, 1153 w, 108 m, 1051 s, 1044 s, 926 w, 903 m, 856 m, 923 w, 784 w. ^{1}H NMR (d_3-acetonitrile): δ 3.24 (s, 9H, OCH_3), 3.63 (s, 6H, OCH_2), 5.56 (s, 9H, B-CH_3), 92.5 (br s, 9H, fwhm = 311 Hz, BH_3). ^{11}B NMR (d_3-acetonitrile): δ 198 (s, fwhm = 163 Hz, BH_3). Crystals suitable for X-ray diffraction studies were grown by dissolving **3'** in a minimal amount of diethyl ether, concentrating the solution to saturation, and cooling the solution to -20 °C. This method of crystallization resulted in the replacement of

some of the DME with diethyl ether, affording the adduct $Nd(H_3BCH_3)_3(DME)(Et_2O)$, **3′·Et₂O**.

Tris(methylborohydride)bis(tetrahydrofuran)gadolinium(III), Gd(H₃BCH₃)₃(THF)₂, 4. To a solid mixture of $GdCl_3$ (0.20 g, 0.76 mmol) and $Na(H_3BCH_3)$ (0.157 g, 3.0 mmol) was added THF (30 mL) to give a white suspension. The slurry was stirred for 2 days at room temperature to afford a clear solution and white precipitate. The slurry was filtered and the filtrate was dried to a tacky white solid under reduced pressure. The solid was sublimed onto a cold finger at 60 °C and ca. 10^{-2} Torr to afford a white sublimate. Yield 0.140 g (48%). Mp: 144 – 147 °C. Anal. Calcd. for $Gd(H_3BCH_3)_3(THF)_2$: C, 34.0; H, 8.83. Found: C, 34.0; H, 8.72. IR (Nujol, cm^{-1}): 2179 m, 2103 s, 1745 w, 1305 s, 1249 s, 1085 m, 1039 w, 1009 s, 939 m, 925 m, 852 s, 773 w, 669 w.

Tris(methylborohydride)bis(tetrahydrofuran)erbium(III), Er(H₃BCH₃)₃(THF)₂, 5. To a solid mixture of $ErCl_3$ (0.40 g, 1.5 mmol) and $Na(H_3BCH_3)$ (0.30 g, 5.8 mmol) was added THF (30 mL) to give a pink suspension. The slurry was stirred for 2 days at room temperature to afford a pink solution and white precipitate. The pink solution was filtered and the filtrate was dried to a tacky pink solid under reduced pressure. The solid was sublimed onto a cold finger at 60 °C and ca. 10^{-2} Torr to afford a pink solid. Yield 0.24 g (41%). Mp: 136 – 139 °C. Anal. Calcd. for $Er(H_3BCH_3)_3(THF)_2$: C, 33.2; H, 8.61. Found: Er, C, 32.7; H, 8.62. ^{11}B NMR (d_8-toluene): δ 211 (s, fwhm = 300 Hz, BH_3). IR

(Nujol, cm^{-1}): 2183 m, 2115 s, 1343 sh, 1307 s, 1260 s, 1173 sh, 1089 m, 1040 w, 1008 m, 942 w, 926 w, 852 m.

Figure 3.4. $Nd(H_3BCH_3)_3(THF)_2$, **3**, under fluorescent light (top) and incandescent light (bottom).

Crystallographic Studies.[113] Single crystals of **1** and **5** were obtained by saturating a solution of toluene under partial vacuum while at room temperature. Single crystals of **2**, **3**, and **4** were obtained by cooling a saturated solution of toluene to -20 °C. Crystals of **3'** were obtained by cooling a saturated solution of diethyl ether to -20 °C. The single crystals were mounted on a nylon loop with Krytox oil (DuPont), and immediately cooled to -80 °C in a cold nitrogen gas stream on the diffractometer. Standard peak search and indexing procedures followed by least square refinement yielded the cell dimensions given in Tables 3.1 and 3.2. Data were collected with an area detector by using the measurement parameters listed in Tables 3.1 and 3.2. The measured intensities were reduced to structure factor amplitudes and their estimated standard deviations by correction for background, and Lorentz and polarization effects. Systematically absent reflections were deleted and symmetry equivalent reflections were averaged to yield the sets of unique data. A face-indexed absorption correction was applied.

All structures were solved using the SHELXTL software package, followed by least-squares refinement and difference Fourier calculations. Non-hydrogen atoms were refined with independent anisotropic displacement parameters. All the hydrogen atoms attached to boron were located in the E-map and their locations were refined without constraints unless otherwise noted. Other hydrogen atoms were placed in "idealized positions" with the idealized methyl groups allowed to rotate about their respective C-

X axes to find the best least-squares positions. Hydrogen atoms attached to boron were assigned independent isotropic displacement parameters; the displacement parameters for other hydrogen atoms were set equal to 1.3 times that of the attached carbon atom (for methylene groups) or 1.5 times that of the attached carbon atom (for methyl groups). Successful convergence was indicated by the maximum shift/error of less than 0.01 for the last cycle of least squares refinement. Aspects of the refinements unique to each structure are detailed below.

$Sc(H_3BCH_3)_3(THF)$, 1. The orthorhombic lattice and systematic absences $0kl$ ($k \neq 2n$), $h0l$ ($l \neq 2n$), and $hk0$ ($h \neq 2n$) were uniquely consistent with the space group *Pbca*. The quantity minimized by the least-squares program was $\Sigma w(F_o^2 - F_c^2)^2$, where $w = \{[\sigma(F_o)]^2 + (0.0345P)^2 + 1.10P\}^{-1}$ and $P = (F_o^2 + 2F_c^2)/3$. The largest peak in the final Fourier difference map (0.73 e $Å^{-3}$) was located 0.93 Å from C5.

$Y(H_3BCH_3)_3(THF)_2$, 2. The orthorhombic lattice and systematic absences $h00$ ($h \neq 2n$), $0k0$ ($k \neq 2n$), and $00l$ ($l \neq 2n$) were uniquely consistent with the space group $P2_12_12_1$. Many of the carbon atoms of the THF ligands were disordered over two sites. Four different site occupancy factors were refined (one for each THF ligand); the sum of the occupancy factors for every pair of disordered sites was restrained to add to 1. Within the THF ligands, the C-C distances were restrained to be 1.54(1) Å and the C-O distances were restrained to be similar; a few restraints on the C-C-C angles were also applied as needed. The quantity minimized by the least-squares program was $\Sigma w(F_o^2 -$

$F_c^2)^2$, where $w = \{[\sigma(F_o)]^2 + (0.0441P)^2 + 6.75P\}^{-1}$ and $P = (F_o^2 + 2F_c^2)/3$. The displacement parameters of neighboring atoms were restrained to be similar. Hydrogen atoms were placed in idealized positions (borane and methyl groups were allowed to rotate about the C-B bond) with B-H = 1.12 Å, and C-H = 0.99 and 0.98 Å for methylene and methyl groups, respectively. The data crystal was an inversion twin; the volume fraction of the major twin individual refined to 51(1). The largest peak in the final Fourier difference map (0.63 e Å^{-3}) was located 0.98 Å from C11.

$Nd(H_3BCH_3)_3(THF)_2$, 3. The monoclinic lattice and systematic absences $0k0$ ($k \neq 2n$) and $h0l$ ($h + l \neq 2n$) were uniquely consistent with the space group $P2_1/n$. The reflections -1 0 1 and 0 1 1 are statistical outliers and were omitted. The quantity minimized by the least-squares program was $\Sigma w(F_o^2 - F_c^2)^2$, where $w = \{[\sigma(F_o)]^2 + (0.0144P)^2 + 0.70P\}^{-1}$ and $P = (F_o^2 + 2F_c^2)/3$. The largest peak in the final Fourier difference map (0.82 e Å^{-3}) was located 1.48 Å from H6B.

$Nd(H_3BCH_3)_3(DME)(Et_2O)$, 3′·$Et_2O$. The data crystal was a non-merohedral twin, and the structure was solved using data derived only form the primary domain. The monoclinic lattice and systematic absences $0k0$ ($k = 2n$) were uniquely consistent with the space group $P2_1$. The reflections -5 3 5 and -3 0 1 are statistical outliers and were omitted. The quantity minimized by the least-squares program was $\Sigma w(F_o^2 - F_c^2)^2$, where $w = \{[\sigma(F_o)]^2 + (0.0268)^2 + 0.60\}^{-1}$ and $P = (F_o^2 + 2F_c^2)/3$. The largest peak in the final Fourier difference map (1.44 e Å^{-3}) was located 1.11 Å from Nd1.

$Gd(H_3BCH_3)_3(THF)_2$, 4. The monoclinic lattice and systematic absences $0k0$ ($k \neq 2n$) and $h0l$ ($l \neq 2n$) were uniquely consistent with the space group $P2_1/c$. An isotropic extinction parameter refined to a final value of $x = 6.5(3) \times 10^{-4}$, where F_c is multiplied by the factor $k[1 + F_c^2 x\lambda^3/\sin 2\theta]^{-1/4}$ with k being the overall scale factor. The quantity minimized by the least-squares program was $\Sigma w(F_o^2 - F_c^2)^2$, where $w = \{[\sigma(F_o)]^2 + (0.0082P)^2 + 3.76P\}^{-1}$ and $P = (F_o^2 + 2F_c^2)/3$. The largest peak in the final Fourier difference map (0.83 e $Å^{-3}$) was located 0.45 Å from C17.

$Er(H_3BCH_3)_3(THF)_2$, 5. The orthorhombic lattice and systematic absences $h00$ ($h \neq 2n$), $0k0$ ($k \neq 2n$), and $00l$ ($l \neq 2n$) were uniquely consistent with the space group $P2_12_12_1$. Many of the carbon atoms of the THF ligands were disordered over two sites. Four different site occupancy factors were refined (one for each THF ligand); the sum of the occupancy factors for every pair of disordered sites was restrained to add to 1. Within the THF ligands, the C-C distances were restrained to be 1.54(1) Å and the C-O distances were restrained to be similar; a few restraints on the C-C-C angles were also applied as needed. The quantity minimized by the least-squares program was $\Sigma w(F_o^2 - F_c^2)^2$, where $w = \{[\sigma(F_o)]^2 + (0.0063P)^2 + 23.11P\}^{-1}$ and $P = (F_o^2 + 2F_c^2)/3$. The displacement parameters of neighboring atoms were restrained to be similar. Hydrogen atoms were placed in idealized positions (borane and methyl groups were allowed to rotate about the C-B bond) with B-H = 1.12 Å, and C-H = 0.99 and 0.98 Å for methylene and methyl groups, respectively. The data crystal was an inversion twin; the volume fraction of the

major twin individual refined to 53(3). The largest peak in the final Fourier difference map (1.64 e $Å^{-3}$) was located 0.7 Å from Er2.

Table 3.1. Crystallographic data for the new methylborohydride complexes **1**, **3**, and **3′·Et$_2$O**.

	1	**3**	**3′**·Et$_2$O
Formula	$ScB_3C_7H_{26}O$	$Nd_2B_6C_{22}H_{68}O_4$	$NdB_3C_{11}H_{38}O_3$
FW (g mol^{-1})	203.669	750.116	395.089
T (K)	100(2)	100(2)	100(2)
λ (Å)	0.71073	0.71073	0.71073
Crystal system	orthorhombic	monoclinic	monoclinic
Space group	*Pbca*	$P2_1/n$	$P2_1$
a (Å)	13.5719(8)	9.6374(5)	7.9614(5)
b (Å)	13.7669(9)	15.8707(8)	12.1811(6)
c (Å)	14.6121(10)	12.5198(6)	10.4823(6)
β(deg)	90	111.023(2)	101.980(2)
V, (Å^3)	2730.2(3)	1787.47(16)	994.42(10)
Z	8	2	2
ρ_{calc} (g cm^{-3})	0.991	1.394	1.319
μ (mm^{-1})	0.501	2.894	2.608
Max./min transm. factors	0.908, 0.7442	0.900, 0.799	0.746, 0.519
Data/restraints/params	4174/0/149	5478/36/193	4928/1/206
GOF on F^2	1.066	1.068	1.081
R_1 [$I > 2\sigma(I)$]	0.0318	0.0198	0.0205
wR_2 (all data)	0.0814	0.0385	0.0489
max, min $\Delta\rho_{electron}$ (e · Å^{-3})	0.725, -0.259	0.824, -0.563	1.443, -0.460

Table 3.2. Crystallographic data for the new methylborohydride complexes **2**, **4**, and **5**.

	2	**4**	**5**
Formula	$Y_2B_6C_{22}H_{68}O_4$	$Gd_2B_6C_{22}H_{68}O_4$	$Er_2B_6C_{22}H_{68}O_4$
FW (g mol^{-1})	639.455	776.136	796.154
T (K)	173(2)	173(2)	173(2)
λ (Å)	0.71073	0.71073	0.71073
Crystal system	orthorhombic	monoclinic	orthorhombic
Space group	$P2_12_12_1$	$P2_1/c$	$P2_12_12_1$
a (Å)	9.7522(13)	9.1542(11)	9.8003(9)
b (Å)	15.1561(18)	24.891(3)	15.2087(15)
c (Å)	25.051(3)	16.492(2)	25.178(2)
β(deg)	90	104.884(4)	90
V, (Å^3)	3702.7(8)	3631.8(8)	3752.8(6)
Z	4	4	4
ρ_{calc} (g cm^{-3})	1.147	1.419	1.409
μ (mm^{-1})	3.140	3.642	4.462
Max./min transm. factors	0.784, 0.398	0.999, 0.824	0.655, 0.550
Data/restraints/params	6822/504/407	11256/0/386	7543/504/407
GOF on F^2	1.115	1.126	1.164
R_1 [$I > 2\sigma(I)$]	0.0502	0.0205	0.0472
wR_2 (all data)	0.1217	0.0441	0.0875
max, min $\Delta\rho_{electron}$ (e · Å^{-3})	0.632, -0.644	0.833, -0.770	1.639, -1.760

Table 3.3. Selected distances and angles for $Sc(H_3BCH_3)_3(THF)$, **1.**

Distances (Å)			
Sc(1)···B(1)	2.3094(1)	B(1)-H(11)	1.158(14)
Sc(1)···B(2)	2.3053(1)	B(1)-H(12)	1.170(15)
Sc(1)···B(3)	2.3015(1)	B(1)-H(13)	1.159(15)
Sc(1)-O(1)	2.1208(8)	B(2)-H(21)	1.146(15)
Sc(1)-H(11)	2.068(15)	B(2)-H(22)	1.152(16)
Sc(1)-H(12)	2.102(17)	B(2)-H(23)	1.164(16)
Sc(1)-H(13)	2.035(15)	B(3)-H(31)	1.133(15)
Sc(1)-H(21)	2.062(16)	B(3)-H(32)	1.170(15)
Sc(1)-H(22)	2.020(15)	B(3)-H(33)	1.153(15)
Sc(1)-H(23)	2.096(16)	B(1)-C(1)	1.5875(17)
Sc(1)-H(31)	2.096(16)	B(2)-C(2)	1.5863(19)
Sc(1)-H(32)	2.085(16)	B(3)-C(3)	1.5875(18)
Sc(1)-H(33)	1.993(15)		
Angles (deg)			
B(1)···Sc(1)···B(2)	114.09(5)	B(1)···Sc(1)-O(1)	104.26(4)
B(1)···Sc(1)···B(3)	115.61(5)	B(2)···Sc(1)-O(1)	101.23(4)
B(2)···Sc(1)···B(3)	116.13(5)	B(3)···Sc(1)-O(1)	102.73(4)

Table 3.4. Selected distances and angles for $Y(H_3BCH_3)_3(THF)_2$, **2.**

	Distances (Å)		
Y(1)···B(1)	2.503(7)	Y(2)-H(33)	2.3506
Y(1)···B(2)	2.500(7)	Y(2)-H(41)	2.3535
Y(1)-O(1)	2.353(3)	Y(2)-H(42)	2.3672
Y(1)-O(2)	2.370(4)	Y (2)-H(43)	2.3681
Y(1)-O(3)	2.392(4)	Y(2)-H(51)	2.3618
Y(1)-O(4)	2.348(4)	Y(2)-H(52)	2.3682
Y(1)-H(11)	2.3808	Y(2)-H(53)	2.3710
Y(1)-H(12)	2.3666	Y(2)-H(61)	2.3666
Y(1)-H(13)	2.3827	Y(2)-H(62)	2.3612
Y(1)-H(21)	2.3699	Y(2)-H(63)	2.3659
Y(1)-H(22)	2.3745	B(3)-H(31)	1.1146
Y(1)-H(23)	2.3774	B(3)-H(32)	1.1161
B(1)-H(11)	1.1144	B(3)-H(33)	1.1145
B(1)-H(12)	1.1161	B(4)-H(41)	1.1158
B(1)-H(13)	1.1149	B(4)-H(42)	1.1145
B(2)-H(21)	1.1154	B(4)-H(43)	1.1145
B(2)-H(22)	1.1150	B(5)-H(51)	1.1158
B(2)-H(23)	1.1146	B(5)-H(52)	1.1144
B(1)-C(1)	1.623(9)	B(5)-H(53)	1.1145
B(2)-C(2)	1.610(10)	B(6)-H(61)	1.1145
Y(2)···B(3)	2.482(6)	B(6)-H(62)	1.1148
Y(2)···B(4)	2.488(7)	B(6)-H(63)	1.1161
Y(2)···B(5)	2.493(7)	B(3)-C(3)	1.611(10)
Y(2)···B(6)	2.490(7)	B(4)-C(4)	1.632(11)
Y(2)-H(31)	2.3627	B(5)-C(5)	1.603(9)
Y(2)-H(32)	2.3601	B(6)-C(6)	1.626(10)
	Angles (deg)		
B(1)···Y(1)···B(2)	163.9(3)	O(1)-Y(1)-O(4)	77.17(14)
B(1)···Y(1)-O(1)	96.09(19)	O(2)-Y(1)-O(3)	117.06(19)
B(1)···Y(1)-O(2)	84.3(2)	O(2)-Y(1)-O(4)	159.48(17)
B(1)···Y(1)-O(3)	84.3(2)	O(3)-Y(1)-O(4)	83.39(16)
B(1)···Y(1)-O(4)	96.8(2)	B(3)···Y(2)···B(4)	108.2(4)
B(2)···Y(1)-O(1)	95.9(2)	B(3)···Y(2)···B(5)	109.5(3)
B(2)···Y(1)-O(2)	86.7(2)	B(3)···Y(2)···B(6)	107.8(3)
B(2)···Y(1)-O(3)	88.0(2)	B(4)···Y(2)···B(5)	109.7(3)
B(2)···Y(1)-O(4)	96.3(2)	B(4)···Y(2)···B(6)	110.8(4)
O(1)-Y(1)-O(2)	82.32(17)	B(5)···Y(2)···B(6)	110.8(3)
O(1)-Y(1)-O(3)	160.48(15)		

Table 3.5. Selected distances and angles for $Nd(H_3BCH_3)_3(THF)_2$, **3.**

Distances (Å)			
Nd(1)···B(1)	2.605(2)	B(1)-H(11)	1.166(9)
Nd(1)···B(2)	2.605(2)	B(1)-H(12)	1.161(9)
Nd(1)···B(3)	2.9682(19)	B(1)-H(13)	1.168(9)
Nd(1A)···B(3)	3.0312(19)	B(2)-H(21)	1.168(9)
Nd(1)-O(1)	2.4689(11)	B(2)-H(22)	1.158(9)
Nd(1)-O(2)	2.4979(11)	B(2)-H(23)	1.166(9)
Nd(1)-H(11)	2.290(19)	B(3)-H(31)	1.164(9)
Nd(1)-H(12)	2.41(2)	B(3)-H(32)	1.166(9)
Nd(1)-H(13)	2.32(2)	B(3)-H(33)	1.164(9)
Nd(1)-H(21)	2.350(18)	B(1)-C(1)	1.596(3)
Nd(1)-H(22)	2.35(2)	B(2)-C(2)	1.599(3)
Nd(1)-H(23)	2.29(2)	B(3)-C(3)	1.603(3)
Nd(1)-H(33)	2.561(17)		
Nd(1)-H(32)	2.360(19)		
Nd(1A)-H(31)			
Nd(1A)-H(32)			
Angles (deg)			
B(1)···Nd(1)···B(2)	100.48(6)	B(2)···Nd(1)-O(1)	102.93(5)
B(1)···Nd(1)···B(3)	107.83(6)	B(2)···Nd(1)-O(2)	88.44(5)
B(1)···Nd(1)···B(3A)	89.38(6)	B(3)···Nd(1)···B(3A)	79.44(6)
B(1)···Nd(1)-O(1)	86.88(5)	B(3)···Nd(1)-O(1)	159.56(4)
B(1)···Nd(1)-O(2)	160.32(5)	B(3)···Nd(1)-O(2)	89.75(5)
B(2)···Nd(1)···B(3)	88.59(6)	O(1)-Nd(1)-O(2)	73.97(4)
B(2)···Nd(1)···B(3A)	166.41(6)		

Table 3.6. Selected distances and angles for $Nd(H_3BCH_3)_3(DME)(Et_2O)$, **3′·Et₂O.**

Distances (Å)			
Nd(1)···B(1)	2.622(4)	B(1)-H(11)	1.18(4)
Nd(1)···B(2)	2.619(3)	B(1)-H(12)	1.21(3)
Nd(1)···B(3)	2.612(4)	B(1)-H(13)	1.08(5)
Nd(1)-O(1)	2.588(2)	B(2)-H(21)	1.10(3)
Nd(1)-O(2)	2.567(2)	B(2)-H(22)	1.13(4)
Nd(1)-O(3)	2.561(2)	B(2)-H(23)	1.08(4)
Nd(1)-H(11)	2.35(3)	B(3)-H(31)	1.15(4)
Nd(1)-H(12)	2.27(3)	B(3)-H(32)	1.09(4)
Nd(1)-H(13)	2.39(5)	B(3)-H(33)	1.17(5)
Nd(1)-H(21)	2.29(3)	B(1)-C(1)	1.604(5)
Nd(1)-H(22)	2.44(4)	B(2)-C(2)	1.602(5)
Nd(1)-H(23)	2.34(4)	B(3)-C(3)	1.598(5)
Nd(1)-H(31)	2.34(3)		
Nd(1)-H(32)	2.42(5)		
Nd(1)-H(33)	2.38(5)		
Angles (deg)			
B(1)···Nd(1)···B(2)	102.26(11)	B(2)···Nd(1)-O(3)	87.94(9)
B(1)···Nd(1)···B(3)	100.56(11)	B(3)···Nd(1)-O(1)	93.04(10)
B(2)···Nd(1)···B(3)	101.64(11)	B(3)···Nd(1)-O(2)	85.63(10)
B(1)···Nd(1)-O(1)	93.40(9)	B(3)···Nd(1)-O(3)	159.01(10)
B(1)···Nd(1)-O(2)	157.68(9)	O(1)-Nd(1)-O(2)	64.70(7)
B(1)···Nd(1)-O(3)	95.50(9)	O(1)-Nd(1)-O(3)	72.46(7)
B(2)···Nd(1)-O(1)	156.05(9)	O(2)-Nd(1)-O(3)	74.54(7)
B(2)···Nd(1)-O(2)	97.37(9)		

Table 3.7. Selected distances and angles for $Gd(H_3BCH_3)_3(THF)_2$, **4.**

	Distances (Å)		
Gd(1)···B(1)	2.537(2)	Gd(2)-H(33)	2.31(3)
Gd(1)···B(2)	2.544(2)	Gd(2)-H(41)	2.27(3)
Gd(1)-O(1)	2.3848(14)	Gd(2)-H(42)	2.26(3)
Gd(1)-O(2)	2.4048(14)	Gd(2)-H(43)	2.31(3)
Gd(1)-O(3)	2.4326(14)	Gd(2)-H(51)	2.22(3)
Gd(1)-O(4)	2.4075(14)	Gd(2)-H(52)	2.24(3)
Gd(1)-H(11)	2.31(2)	Gd(2)-H(53)	2.28(3)
Gd(1)-H(12)	2.28(2)	Gd(2)-H(61)	2.30(3)
Gd(1)-H(13)	2.19(3)	Gd(2)-H(62)	2.27(3)
Gd(1)-H(21)	2.31(2)	Gd(2)-H(63)	2.24(3)
Gd(1)-H(22)	2.25(3)	B(3)-H(31)	1.15(3)
Gd(1)-H(23)	2.29(2)	B(3)-H(32)	1.13(3)
B(1)-H(11)	1.17(2)	B(3)-H(33)	1.15(3)
B(1)-H(12)	1.13(2)	B(4)-H(41)	1.14(3)
B(1)-H(13)	1.17(3)	B(4)-H(42)	1.16(3)
B(2)-H(21)	1.16(2)	B(4)-H(43)	1.10(3)
B(2)-H(22)	1.15(3)	B(5)-H(51)	1.14(3)
B(2)-H(23)	1.13(2)	B(5)-H(52)	1.14(3)
B(1)-C(1)	1.586(3)	B(5)-H(53)	1.17(3)
B(2)-C(2)	1.586(3)	B(6)-H(61)	1.14(3)
Gd(2)···B(3)	2.522(3)	B(6)-H(62)	1.12(3)
Gd(2)···B(4)	2.532(3)	B(6)-H(63)	1.15(3)
Gd(2)···B(5)	2.528(3)	B(3)-C(3)	1.583(4)
Gd(2)···B(6)	2.517(3)	B(4)-C(4)	1.587(4)
Gd(2)-H(31)	2.20(3)	B(5)-C(5)	1.588(4)
Gd(2)-H(32)	2.23(3)	B(6)-C(6)	1.584(3)
	Angles (deg)		
B(1)···Gd(1)···B(2)	167.04(7)	O(1)-Gd(1)-O(4)	81.47(5)
B(1)···Gd(1)-O(1)	93.38(7)	O(2)-Gd(1)-O(3)	85.31(5)
B(1)···Gd(1)-O(2)	94.94(7)	O(2)-Gd(1)-O(4)	157.11(5)
B(1)···Gd(1)-O(3)	85.80(7)	O(3)-Gd(1)-O(4)	117.52(5)
B(1)···Gd(1)-O(4)	88.71(7)	B(3)···Gd(2)···B(4)	111.79(10)
B(2)···Gd(1)-O(1)	97.44(6)	B(3)···Gd(2)···B(5)	108.15(9)
B(2)···Gd(1)-O(2)	94.62(6)	B(3)···Gd(2)···B(6)	106.90(9)
B(2)···Gd(1)-O(3)	86.28(7)	B(4)···Gd(2)···B(5)	110.04(9)
B(2)···Gd(1)-O(4)	85.87(6)	B(4)···Gd(2)···B(6)	110.10(9)
O(1)-Gd(1)-O(2)	75.76(5)	B(5)···Gd(2)···B(6)	109.78(9)
O(1)-Gd(1)-O(3)	160.93(5)		

Table 3.8. Selected distances and angles for $Er(H_3BCH_3)_3(THF)_2$, **5.**

Bond Lengths (Å)			
Er(1)···B(1)	2.481(10)	Er(2)-H(33)	2.3422
Er(1)···B(2)	2.490(10)	Er(2)-H(41)	2.3386
Er(1)-O(1)	2.357(5)	Er(2)-H(42)	2.3448
Er(1)-O(2)	2.374(7)	Er (2)-H(43)	2.3431
Er(1)-O(3)	2.395(6)	Er(2)-H(51)	2.3519
Er(1)-O(4)	2.351(6)	Er(2)-H(52)	2.3541
Er(1)-H(11)	2.3580	Er(2)-H(53)	2.3534
Er(1)-H(12)	2.3548	Er(2)-H(61)	2.3418
Er(1)-H(13)	2.3583	Er(2)-H(62)	2.3386
Er(1)-H(21)	2.3631	Er(2)-H(63)	2.3443
Er(1)-H(22)	2.3642	B(3)-H(31)	1.1200
Er(1)-H(23)	2.3678	B(3)-H(32)	1.1200
B(1)-H(11)	1.1200	B(3)-H(33)	1.1201
B(1)-H(12)	1.1200	B(4)-H(41)	1.1200
B(1)-H(13)	1.1200	B(4)-H(42)	1.1200
B(2)-H(21)	1.1200	B(4)-H(43)	1.1200
B(2)-H(22)	1.1200	B(5)-H(51)	1.1200
B(2)-H(23)	1.1200	B(5)-H(52)	1.1200
B(1)-C(1)	1.646(13)	B(5)-H(53)	1.1200
B(2)-C(2)	1.629(14)	B(6)-H(61)	1.1200
Er(2)···B(3)	2.465(9)	B(6)-H(62)	1.1200
Er(2)···B(4)	2.464(10)	B(6)-H(63)	1.1200
Er(2)···B(5)	2.476(9)	B(3)-C(3)	1.615(14)
Er(2)···B(6)	2.463(9)	B(4)-C(4)	1.657(16)
Er(2)-H(31)	2.3462	B(5)-C(5)	1.596(14)
Er(2)-H(32)	2.3413	B(6)-C(6)	1.629(14)
Angles (deg)			
B(1)···Er(1)···B(2)	163.1(4)	O(1)-Er(1)-O(4)	76.9(2)
B(1)··· Er(1)-O(1)	96.7(3)	O(2)-Er(1)-O(3)	117.4(3)
B(1)···Er(1)-O(2)	84.3(3)	O(2)-Er(1)-O(4)	159.5(3)
B(1)···Er(1)-O(3)	84.0(3)	O(3)-Er(1)-O(4)	83.1(2)
B(1)···Er(1)-O(4)	96.8(3)	B(3)···Er(2)···B(4)	108.2(6)
B(2)···Er(1)-O(1)	96.7(4)	B(3)···Er(2)···B(5)	109.7(4)
B(2)···Er(1)-O(2)	87.0(3)	B(3)···Er(2)···B(6)	108.4(5)
B(2)···Er(1)-O(3)	87.0(4)	B(4)···Er(2)···B(5)	109.4(5)
B(2)···Er(1)-O(4)	96.4(3)	B(4)···Er(2)···B(6)	110.6(6)
O(1)-Er(1)-O(2)	82.6(3)	B(5)···Er(2)···B(6)	110.4(5)
O(1)-Er(1)-O(3)	159.9(2)		

Figure 3.5. Molecular structure of $Sc(H_3BCH_3)_3(THF)$, **1**. The 35 % probability density surfaces are shown; hydrogen atoms are represented by arbitrarily sized spheres or are omitted for clarity.

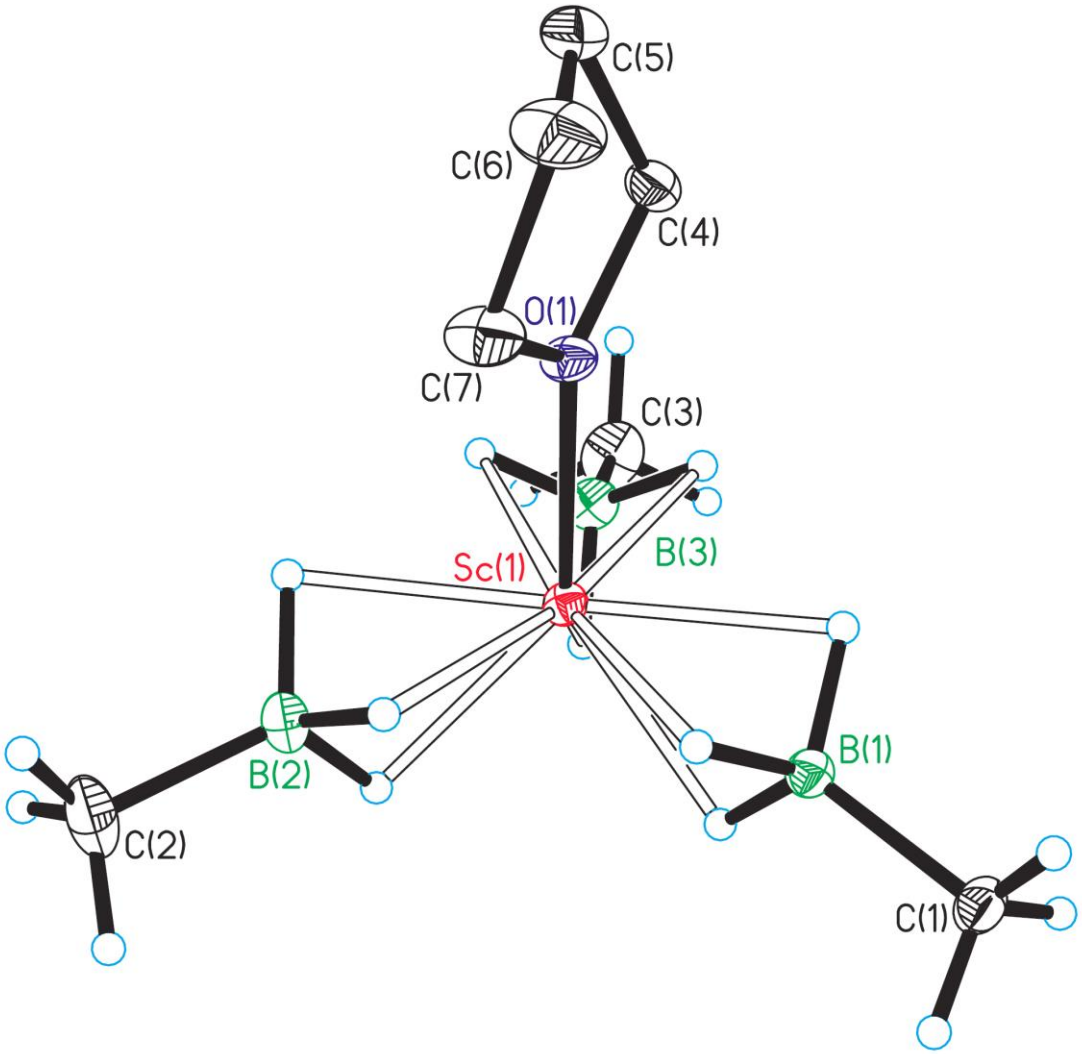

Figure 3.6. Molecular structure of $[Y(H_3BCH_3)_2(THF)_4][Y(H_3BCH_3)_4]$, **2**. The 35 % probability density surfaces are shown; hydrogen atoms are represented by arbitrarily sized spheres or are omitted for clarity.

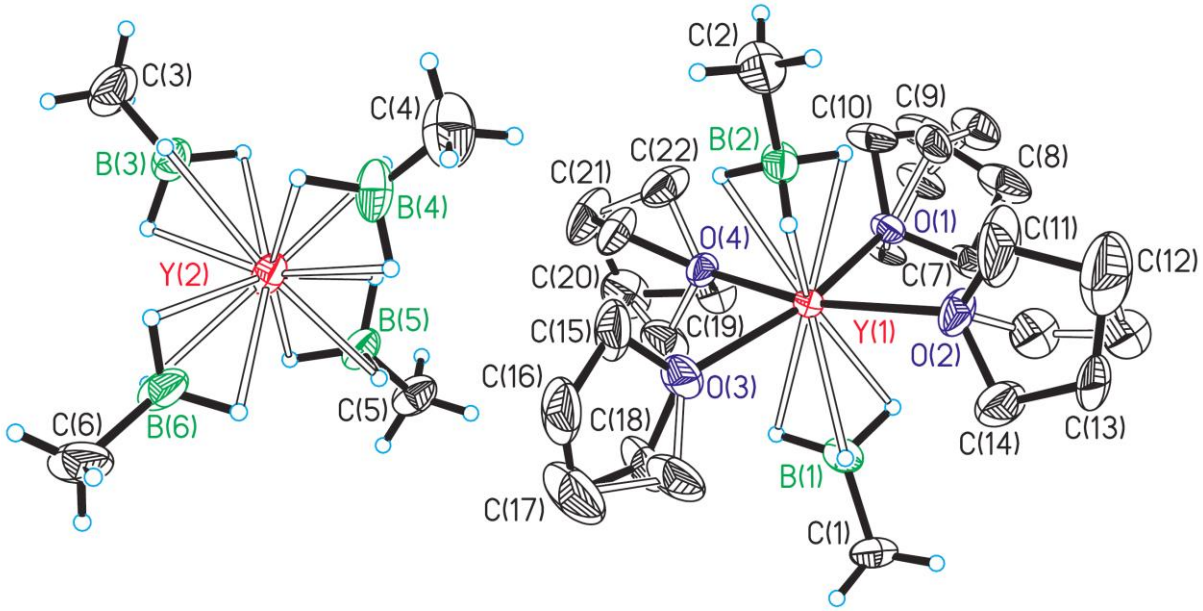

Figure 3.7. Molecular structure of $[Nd(H_3BCH_3)_3(THF)_2]_2$, **3**. The 35 % probability density surfaces are shown; hydrogen atoms are represented by arbitrarily sized spheres or are omitted for clarity.

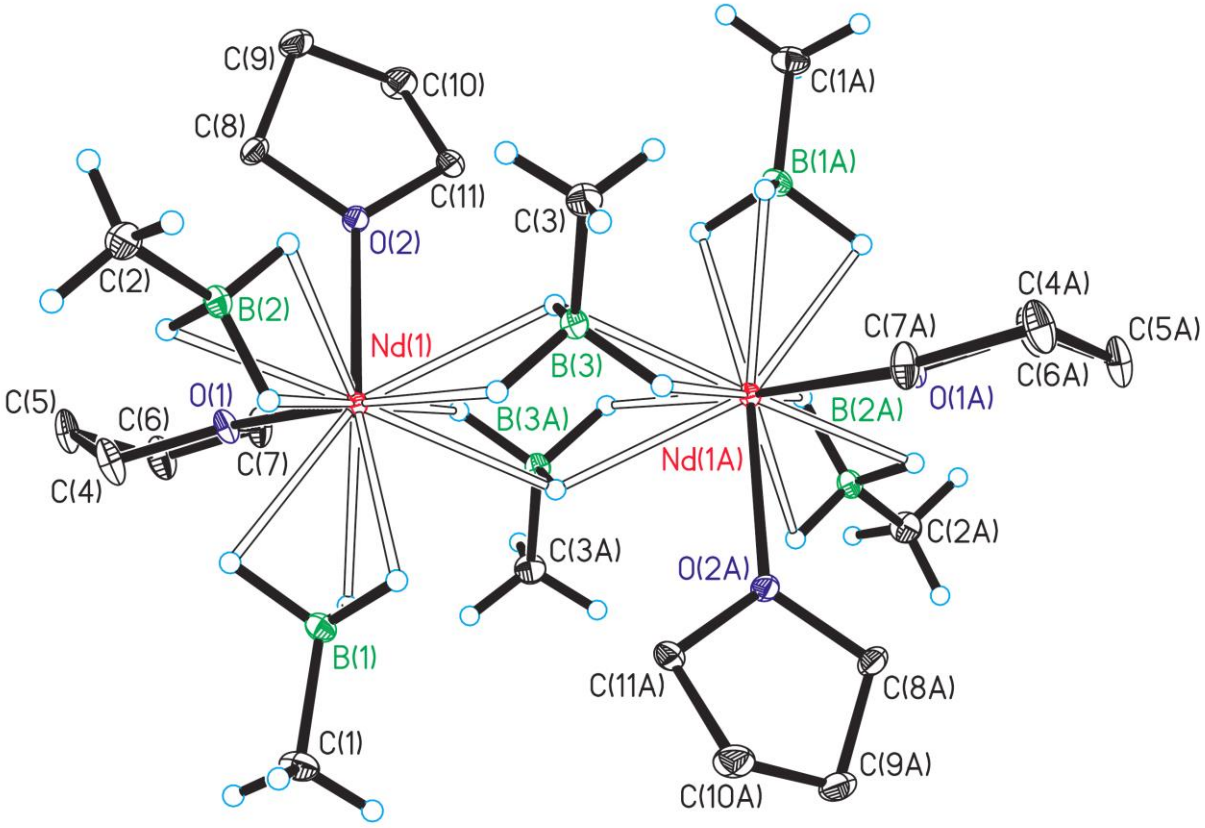

Figure 3.8. Central core of $[Nd(H_3BCH_3)_3(THF)_2]_2$, **3**. The 35 % probability density surfaces are shown; hydrogen atoms are represented by arbitrarily sized spheres.

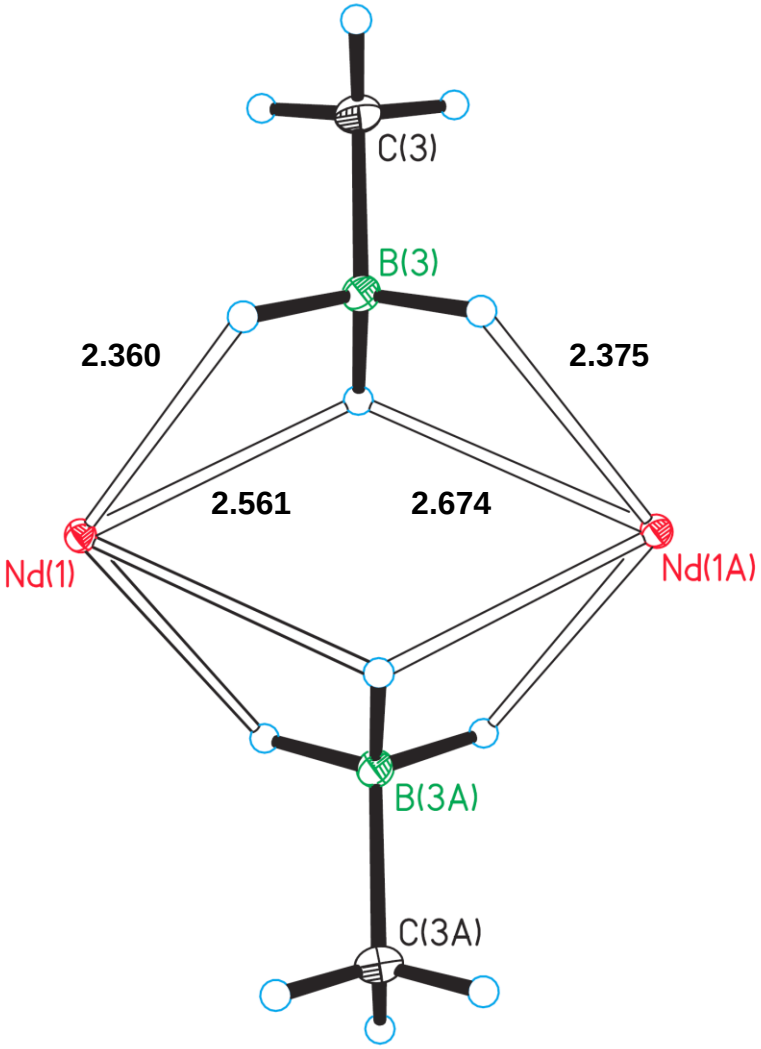

Figure 3.9. Molecular structure of $Nd(H_3BCH_3)_3(DME)(Et_2O)$, **3′**·$Et_2O$. The 35 % probability density surfaces are shown; hydrogen atoms are represented by arbitrarily sized spheres or are omitted for clarity.

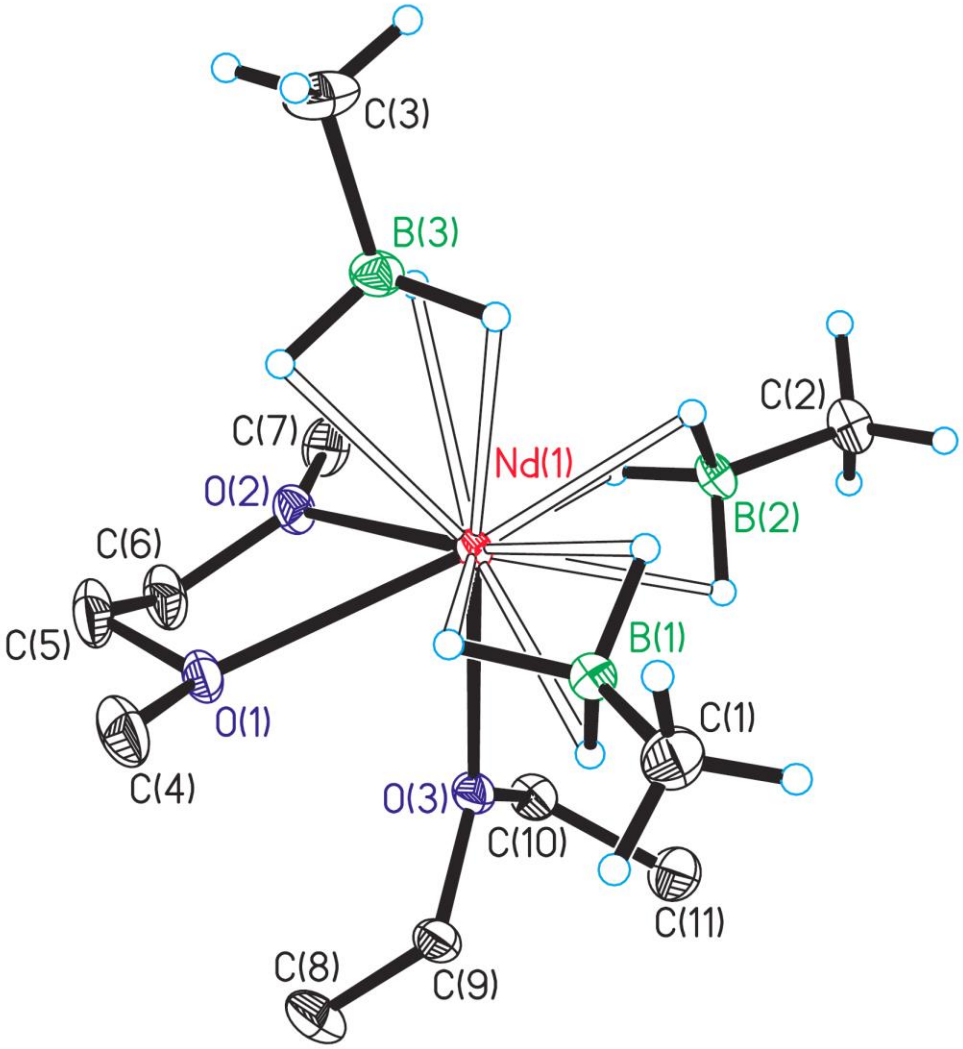

Figure 3.10. Molecular structure of $[Gd(H_3BCH_3)_2(THF)_4][Gd(H_3BCH_3)_4]$, **4**. The 35 % probability density surfaces are shown; hydrogen atoms are represented by arbitrarily sized spheres or are omitted for clarity.

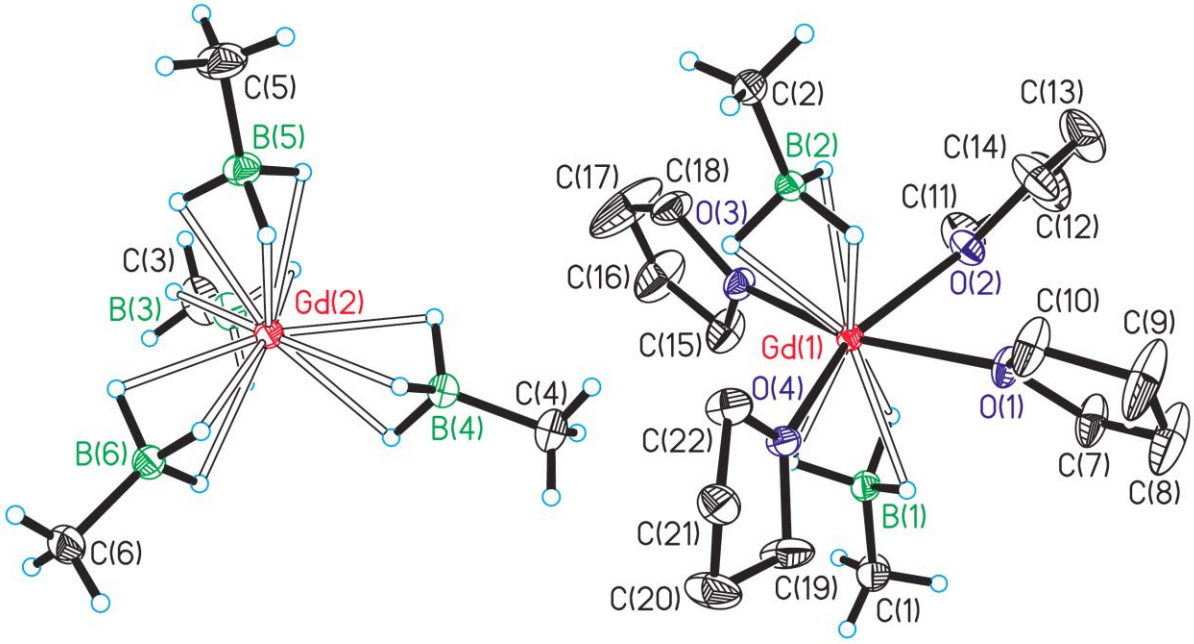

Figure 3.11. Molecular structure of $[Er(H_3BCH_3)_2(THF)_4][Er(H_3BCH_3)_4]$, **5**. The 35 % probability density surfaces are shown; hydrogen atoms are represented by arbitrarily sized spheres or are omitted for clarity.

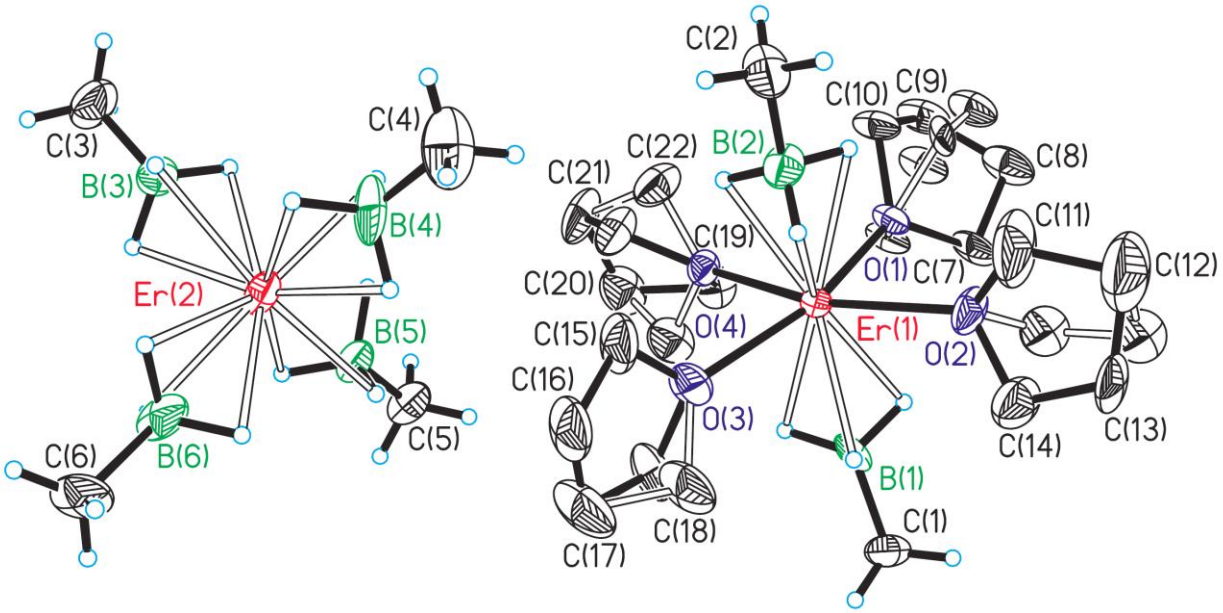

References

(1) Weiss, C. J.; Marks, T. J. *Dalton Trans.* **2010**, *39*, 6553-6892.

(2) Ward, B. D.; Gade, L. H. *Chem. Commun.* **2012**, *48*, 10587-10599.

(3) Sousa-Aguiar, E. F.; Trigueiro, F. E.; Zotin, F. M. Z. *Catal. Today* **2013**, *218–219*, 115-122.

(4) Yoldjian, G. *J. Less-Common Met.* **1985**, *111*, 17-22.

(5) Suresh, G.; Seenivasan, G.; Krishnaiah, M. V.; Murti, P. S. *J. Alloys Compd.* **1998**, *269*, L9-L12.

(6) Sun, W. Z.; Chen, Y. H.; Wu, L. E.; Lu, Y. J.; Jiang, Y.; Huang, Z. K. *J. Mater. Sci.* **2011**, *46*, 6273-6276.

(7) Härkönen, G.; Leppänen, M.; Soininen, E.; Törnqvist, R.; Viljanen, J. *J. Alloys Compd.* **1995**, *225*, 552-554.

(8) Ronda, C. R.; Jüstel, T.; Nikol, H. *J. Alloys Compd.* **1998**, *275–277*, 669-676.

(9) Yan, B.; Lin, L.; Wu, J.; Lei, F. *J. Fluoresc.* **2011**, *21*, 203-211.

(10) Sun, H.; Chen, Y.; Xu, C.; Zhu, D.; Huang, L. *J. Solid State Electrochem.* **2012**, *16*, 1247-1254.

(11) Ding, Y.; Zhang, P.; Jiang, Y.; Gao, D. *Solid State Ionics* **2007**, *178*, 967-971.

(12) Sasidharan, M.; Gunawardhana, N.; Inoue, M.; Yusa, S.; Yoshio, M.; Nakashima, K. *Chem. Commun.* **2012**, *48*, 3200-3202.

(13) Curry, R. J.; Gillin, W. P. *Curr. Opin. Solid State Mater. Sci.* **2001**, *5*, 481-486.

(14) de Bettencourt-Dias, A. *Dalton Trans.* **2007**, 2229-2241.

(15) Li, L.; Zhang, J.; Zi, W.; Gan, S.; Ji, G.; Zou, H.; Xu, X. *Solid State Sci.* **2014**, *29*, 58-65.

(16) Müller, K. H.; Krabbes, G.; Fink, J.; Gruß, S.; Kirchner, A.; Fuchs, G.; Schultz, L. *J. Magn. Magn. Mater.* **2001**, *226–230*, 1370-1376.

(17) Dent, P. C. *J. Appl. Phys.* **2012**, *111*, 07A721.

(18) Sugimoto, S. *J. Phys. D: Appl. Phys.* **2011**, *44*, 064001.

(19) Yi, W.; Yang, J.; Shen, X.; Lu, W.; Li, Z.; Ren, Z.; Che, G.; Dong, X.; Zhou, F.; Sun, L.; Zhao, Z. *Supercond. Sci. Technol.* **2008**, *21*, 125022.

(20) Kadomtseva, A. M.; Kolmakova, N. P.; Krynetskii, I. B.; Levitin, R. Z.; Snegirev, V. V.; Zvezdin, A. K. *Physica C: Superconductivity* **1989**, *162–164*, 1361-1362.

(21) Cava, R. J.; Krajewski, J. J.; Peck Jr., W. F.; Batlogg, B.; Rupp Jr., L. W. *Physica C: Superconductivity* **1989**, *159*, 372-374.

(22) Adachi, Y.; Su, D.; Muralt, P.; Setter, N. *Appl. Phys. Lett.* **2005**, *86*, 172904.

(23) Yan, F.; Lai, M. O.; Lu, L. *J. Phys. D: Appl. Phys.* **2012**, *45*, 325001.

(24) Bayart, A.; Saitzek, S.; Ferri, A.; Pouhet, R.; Chambrier, M.; Roussel, P.; Desfeux, R. *Thin Solid Films* **2014**, *553*, 71-75.

(25) Albert, M.; Atta, M. A. *Metals and Materials* **1967**, *1*, 43-49.

(26) Schmidt, P. H.; Joy, D. C. *J. Vac. Sci. Technol.* **1978**, *15*, 1809-1810.

(27) Ghanashyam Krishna, M.; Rajendran, M.; Pyke, D. R.; Bhattacharya, A. K. *Sol. Energy Mater. Sol. Cells* **1999**, *59*, 337-348.

(28) Leskelä, M.; Kukli, K.; Ritala, M. *J. Alloys Compd.* **2006**, *418*, 27-34.

(29) Chin, W. C.; Cheong, K. Y.; Hassan, Z. *Mater. Sci. Semicond. Process.* **2010**, *13*, 303-314.

(30) Wiemer, C.; Lamagna, L.; Fanciulli, M. *Semicond. Sci. Technol.* **2012**, *27*, 074013.

(31) Zhao, Y. *Materials* **2012**, *5*, 1413-1438.

(32) Lee, P. S.; Chan, M. Y.; Damarwan, P. *High-k Gate Dielectrics for CMOS Technology*; Wiley-VCH Verlag GmbH & Co. KGaA: 2012, 501-530.

(33) Arda, L.; Heiba, Z. K. *Thin Solid Films* **2010**, *518*, 3345-3350.

(34) Dargis, R.; Arkun, E. F.; Roucka, R.; Smith, R.; Williams, D.; Clark, A.; Lebby, M. *Phys. Status Solidi C.* **2012**, *9*, 2031-2035.

(35) Bitnar, B.; Durisch, W.; Mayor, J. C.; Sigg, H.; Tschudi, H. R. *Sol. Energy Mater. Sol. Cells* **2002**, *73*, 221-234.

(36) Guo, H.; Zhang, W.; Lou, L.; Brioude, A.; Mugnier, J. *Thin Solid Films* **2004**, *458*, 274-280.

(37) Pénard, A.; Gacoin, T.; Boilot, J. *Acc. Chem. Res.* **2007**, *40*, 895-902.

(38) Lei, K.; Chow, C.; Tsang, K.; Lei, E. N. Y.; Roy, Y. A. L.; Lam, M. H. W.; Lee, C. S.; Pun, E. Y. B.; Li, J. *J. Mater. Chem.* **2010**, *20*, 7526-7529.

(39) Singh, R.; Sinha, S.; Hsu, N. J.; Chou, P.; Singh, R. K.; Narayan, J. *J. Appl. Phys.* **1990**, *67*, 1562-1565.

(40) Zhang, K.; Kwak, B. S.; Boyd, E. P.; Wright, A. C.; Erbil, A. *Appl. Phys. Lett.* **1989**, *54*, 380-382.

(41) Watanabe, K.; Yamane, H.; Kurosawa, H.; Hirai, T.; Kobayashi, N.; Iwasaki, H.; Noto, K.; Muto, Y. *Appl. Phys. Lett.* **1989**, *54*, 575-577.

(42) Tsuruoka, T.; Takahashi, H.; Kawasaki, R.; Kanamori, T. *Appl. Phys. Lett.* **1989**, *54*, 1808-1809.

(43) Tsuruoka, T.; Kawasaki, R.; Abe, H. *Jpn. J. Appl. Phys.* **1989**, *28*, L1800-L1802.

(44) Kanehori, K.; Sughii, N.; Fukazawa, T.; Miyauchi, K. *Thin Solid Films* **1989**, *182*, 265-270.

(45) Yamane, H.; Masumoto, H.; Hirai, T.; Iwasaki, H.; Watanabe, K.; Kobayashi, N.; Muto, Y.; Kurosawa, H. *Appl. Phys. Lett.* **1988**, *53*, 1548-1550.

(46) Deacon, G. B.; MacKinnon, P.; Dickson, R. S.; Pain, G. N.; West, B. O. *Appl. Organomet. Chem.* **1990**, *4*, 439-449.

(47) Gun'ko, Y. K.; Edelmann, F. T. *Comments Inorg. Chem.* **1997**, *19*, 153-184.

(48) Tiitta, M.; Niinistou, L. *Chem. Vap. Deposition* **1997**, *3*, 167-182.

(49) Jones, A. C.; Aspinall, H. C.; Chalker, P. R.; Potter, R. J.; Kukli, K.; Rahtu, A.; Ritala, M.; Leskela, M. *J. Mater. Chem.* **2004**, *14*, 3101-3112.

(50) Jones, A. C.; Aspinall, H. C.; Chalker, P. R.; Potter, R. J.; Kukli, K.; Rahtu, A.; Ritala, M.; Leskelä, M. *Mater. Sci. Eng., B* **2005**, *118*, 97-104.

(51) Jones, A. C.; Aspinall, H. C.; Chalker, P. R.; Potter, R. J.; Manning, T. D.; Loo, Y. F.; O'Kane, R.; Gaskell, J. M.; Smith, L. M. *Chem. Vap. Deposition* **2006**, *12*, 83-98.

(52) Lo Nigro, R.; Malandrino, G.; Toro, R. G.; Fragalà, I. L. *Chem. Vap. Deposition* **2006**, *12*, 109-124.

(53) Malandrino, G.; Fragalà, I. L. *Coord. Chem. Rev.* **2006**, *250*, 1605-1620.

(54) Aspinall, H. C. *Top. Appl. Phys.* **2007**, *106*, 53-72.

(55) Edelmann, F. T. *Chem. Soc. Rev.* **2009**, *38*, 2253-2268.

(56) Edelmann, F. T. *Chem. Soc. Rev.* **2012**, *41*, 7649-7964.

(57) Condorelli, G. G.; Malandrino, G.; Fragalà, I. L. *Coord. Chem. Rev.* **2007**, *251*, 1931-1950.

(58) Niinistö, J.; Putkonen, M.; Niinistö, L. *Chem. Mater.* **2004**, *16*, 2953-2958.

(59) Losurdo, M.; Giangregorio, M. M.; Bruno, G.; Yang, D.; Irene, E. A.; Suvorova, A. A.; Saunders, M. *Appl. Phys. Lett.* **2007**, *91*, 091914.

(60) Jamerson, J. D.; Masino, A. P.; Takats, J. *J. Organomet. Chem.* **1974**, *65*, C33-C36.

(61) Uwai, K.; Nakagome, H.; Takahei, K. *Appl. Phys. Lett.* **1987**, *50*, 977-979.

(62) Weber, A.; Suhr, H.; Schumann, H.; Köhn, R. D. *Appl. Phys. A* **1990**, *51*, 520-525.

(63) Weber, J.; Moser, M.; Stapor, A.; Scholz, F.; Bohnert, G.; Hangleiter, A.; Hammel, A.; Wiedmann, D.; Weidlein, J. *J. Cryst. Growth* **1990**, *104*, 815-819.

(64) Weber, J.; Moser, M.; Stapor, A.; Scholz, F.; Hörcher, G.; Forchel, A.; Bohnert, G.; Hangleiter, A.; Hammel, A.; Weidlein, J. *J. Cryst. Growth* **1990**, *100*, 467-470.

(65) Aspinall, H. C.; Williams, P. A.; Gaskell, J.; Jones, A. C.; Roberts, J. L.; Smith, L. M.; Chalker, P. R.; Critchlow, G. W. *Chem. Vap. Deposition* **2003**, *9*, 7-10.

(66) Aspinall, H. C.; Gaskell, J.; Williams, P. A.; Jones, A. C.; Chalker, P. R.; Marshall, P. A.; Smith, L. M.; Critchlow, G. W. *Chem. Vap. Deposition* **2004**, *10*, 83-89.

(67) Kukli, K.; Ritala, M.; Pilvi, T.; Sajavaara, T.; Leskelä, M.; Jones, A. C.; Aspinall, H. C.; Gilmer, D. C.; Tobin, P. J. *Chem. Mater.* **2004**, *16*, 5162-5168.

(68) Anwander, R.; Munck, F. C.; Priermeier, T.; Scherer, W.; Runte, O.; Herrmann, W. A. *Inorg. Chem.* **1997**, *36*, 3545-3552.

(69) Aspinall, H. C.; Gaskell, J.; Williams, P. A.; Jones, A. C.; Chalker, P. R.; Marshall, P. A.; Bickley, J. F.; Smith, L. M.; Critchlow, G. W. *Chem. Vap. Deposition* **2003**, *9*, 235-238.

(70) Aspinall, H. C.; Bickley, J. F.; Gaskell, J. M.; Jones, A. C.; Labat, G.; Chalker, P. R.; Williams, P. A. *Inorg. Chem.* **2007**, *46*, 5852-5860.

(71) Suhr, H.; Weber, A. *Mod. Phys. Lett. B* **1989**, *03*, 1001-1008.

(72) Malandrino, G.; Lo Nigro, R.; Fragalà, Ignazio L.; Benelli, C. *Eur. J. Inorg. Chem.* **2004**, 500-509.

(73) Meng, Q.; Witte, R. J.; Gong, Y.; Day, E. L.; Chen, J.; May, P. S.; Berry, M. T. *Chem. Mater.* **2010**, *22*, 6056-6064.

(74) Belot, J. A.; Wang, A.; McNeely, R. J.; Liable-Sands, L.; Rheingold, A. L.; Marks, T. J. *Chem. Vap. Deposition* **1999**, *5*, 65-69.

(75) Edleman, N. L.; Wang, A.; Belot, J. A.; Metz, A. W.; Babcock, J. R.; Kawaoka, A. M.; Ni, J.; Metz, M. V.; Flaschenriem, C. J.; Stern, C. L.; Liable-Sands, L. M.; Rheingold, A. L.; Markworth, P. R.; Chang, R. P. H.; Chudzik, M. P.; Kannewurf, C. R.; Marks, T. J. *Inorg. Chem.* **2002**, *41*, 5005-5023.

(76) Lim, B. S.; Rahtu, A.; Park, J.; Gordon, R. G. *Inorg. Chem.* **2003**, *42*, 7951-7958.

(77) Paivasaari, J.; Dezelah, I. V. C. L.; Back, D.; El-Kaderi, H. M.; Heeg, M. J.; Putkonen, M.; Niinisto, L.; Winter, C. H. *J. Mater. Chem.* **2005**, *15*, 4224-4233.

(78) Milanov, A. P.; Thiede, T. B.; Devi, A.; Fischer, R. A. *J. Am. Chem. Soc.* **2009**, *131*, 17062-17063.

(79) Milanov, A. P.; Fischer, R. A.; Devi, A. *Inorg. Chem.* **2008**, *47*, 11405-11416.

(80) Milanov, A. P.; Toader, T.; Parala, H.; Barreca, D.; Gasparotto, A.; Bock, C.; Becker, H.; Ngwashi, D. K.; Cross, R.; Paul, S.; Kunze, U.; Fischer, R. A.; Devi, A. *Chem. Mater.* **2009**, *21*, 5443-5455.

(81) Daly, S. R. Ph.D. Thesis, University of Illinois at Urbana-Champaign, **2010**.

(82) Daly, S. R.; Kim, D. Y.; Yang, Y.; Abelson, J. R.; Girolami, G. S. *J. Am. Chem. Soc.* **2010**, *132*, 2106-2107.

(83) Daly, S. R.; Kim, D. Y.; Girolami, G. S. *Inorg. Chem.* **2012**, *51*, 7050-7065.

(84) Steele, J. L. Ph.D. Thesis, University of Illinois at Urbana-Champaign, **2013**.

(85) Morris, J. H.; Smith, W. E. *J. Chem. Soc. Chem. Commun.* **1970**, 245.

(86) Lobkovskii, É. B.; Kravchenko, S. E.; Kravchenko, O. V. *J. Struct. Chem.* **1983**, *23*, 582-586.

(87) Makhaev, V. D.; Borisov, A. P.; Semenenko, K. N. *Russ. J. Inorg. Chem.* **1986**, *31*, 908-910.

(88) Zange, E. *Chem. Ber.* **1960**, *93*, 652-657.

(89) Kapur, S.; Kalsotra, B. L.; Multani, R. K.; Jain, B. D. *J. Inorg. Nucl. Chem.* **1973**, *35*, 1689-1691.

(90) Marks, T. J.; Grynkewich, G. W. *Inorg. Chem.* **1976**, *15*, 1302-1307.

(91) Manzer, L. E. *J. Organomet. Chem.* **1976**, *110*, 291-294.

(92) Segal, B. G.; Lippard, S. J. *Inorg. Chem.* **1978**, *17*, 844-850.

(93) Lappert, M. F.; Singh, A.; Atwood, J. L.; Hunter, W. E. *J. Chem. Soc., Chem. Commun.* **1983**, 206-207.

(94) White III, J. P.; Deng, H.; Shore, S. G. *Inorg. Chem.* **1991**, *30*, 2337-2342.

(95) Gun'ko, Y. K.; Bulychev, B. M.; Soloveichik, G. L.; Belsky, V. K. *J. Organomet. Chem.* **1992**, *424*, 289-300.

(96) Laske, D. A.; Duchateau, R.; Teuben, J. H.; Spek, A. L. *J. Organomet. Chem.* **1993**, *462*, 149-153.

(97) Daoli, D.; Xiaofan, Z.; Changtao, Q.; Jie, S.; Li, Z. *J. Organomet. Chem.* **1994**, *466*, 95-100.

(98) Cendrowski-Guillaume, S. M.; Nierlich, M.; Lance, M.; Ephritikhine, M. *Organometallics* **1998**, *17*, 786-788.

(99) Schumann, H.; Keitsch, M. R.; Demtschuk, J.; Mühle, S. *Z. Anorg. Allg. Chem.* **1998**, *624*, 1811-1818.

(100) Khvostov, A. V.; Nesterov, V. V.; Bulychev, B. M.; Sizov, A. I.; Antipin, M. Y. *J. Organomet. Chem.* **1999**, *589*, 222-225.

(101) Schumann, H.; Keitsch, M. R.; Muhle, S. H. *Acta Crystallographica Section C* **2000**, *C56*, 48-49.

(102) Jaroschik, F.; Bonnet, F.; Le Goff, X.; Ricard, L.; Nief, F.; Visseaux, M. *Dalton Trans.* **2010**, *39*, 6761-6766.

(103) Arliguie, T.; Belkhiri, L.; Bouaoud, S.; Thuéry, P.; Villiers, C.; Boucekkine, A.; Ephritikhine, M. *Inorg. Chem.* **2008**, *48*, 221-230.

(104) Cendrowski-Guillaume, S. M.; Le Gland, G.; Nierlich, M.; Ephritikhine, M. *Organometallics* **2000**, *19*, 5654-5660.

(105) Sato, T.; Miwa, K.; Nakamori, Y.; Ohoyama, K.; Li, H.; Noritake, T.; Aoki, M.; Towata, S.; Orimo, S. *Phys. Rev. B* **2008**, *77*, 104114.

(106) Shinomoto, R.; Zalkin, A.; Edelstein, N. M. *Inorg. Chim. Acta* **1987**, *139*, 97-101.

(107) Shinomoto, R. S. Ph.D. Thesis, University of California, Berkely, **1984**.

(108) Marks, T. J.; Kennelly, W. J.; Kolb, J. R.; Shimp, L. A. *Inorg. Chem.* **1972**, *11*, 2540-2546.

(109) Banks, R.; Edelstein, N. *J. Chem. Phys.* **1980**, *73*, 3589-3599.

(110) Marks, T. J.; Kolb, J. R. *Chem. Rev.* **1977**, *77*, 263-293.

(111) Shinomoto, R.; Brennan, J. G.; Edelstein, N. M.; Zalkin, A. *Inorg. Chem.* **1985**, *24*, 2896-2900.

(112) Data collected by Elham Mohimi.

(113) Brumaghim, J. L.; Priepot, J. G.; Girolami, G. S. *Organometallics* **1999**, *18*, 2139-2144.

CHAPTER 4: Synthesis and Characterization of Sodium Aminodiboranates with Sterically Bulky or Electron Withdrawing Substituents on Nitrogen.

Introduction

The synthesis of sodium *N*,*N*-dimethylaminodiboranate, Na[H_3B-NMe_2-BH_3], NaDMADB, was first achieved by Keller in 1969.[1] This salt was obtained by two different synthetic routes: by addition of sodium hydride, NaH, or sodium borohydride, $NaBH_4$, to μ-(dimethylamino)diborane, μ-$(Me_2N)B_2H_5$:

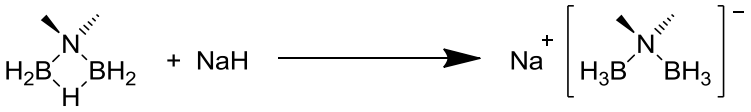

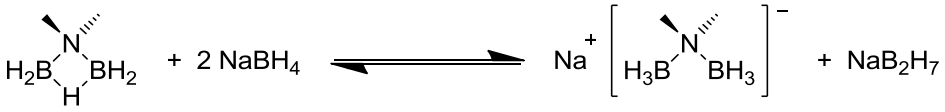

Later, Nöth reported an alternative, more convenient, preparation of NaDMADB by reduction of dimethylamine borane, $Me_2NH{\cdot}BH_3$, with sodium metal in refluxing THF.[2]

Our group has synthesized a large number of homoleptic and heteroleptic DMADB complexes by salt metathesis reactions of sodium *N*,*N*-dimethylamino-diboranate with alkaline earth, transition metal, rare earth metal, and actinide halides.[3-16] Figure 1.5 in Chapter 1 of this thesis shows all the DMADB complexes which have

been isolated by our group to date. Many of these complexes are volatile, and already some metal DMADB complexes have been used as CVD precursors for the deposition of thin films of metal borides and metal oxides.[5,17,18] A more extended discussion of these results can be found in Chapter 1.

The DMADB anion can be thought of as a dimethylamide anion whose two electron pairs each donate to a BH_3 Lewis acceptor. Alternatively, it can be thought of as containing a four-coordinate quaternary ammonium center bonded to two four-coordinate borate groups. The electronegativity difference between B and H means that there are partial negative charges on the hydrogen atoms of the BH_3 groups, similar to those found in the borohydride anion, BH_4^-. The DMADB anion can chelate to a metal center by means of both BH_3 groups; in such cases, geometric constraints limit the number of metal-hydrogen interactions to four (two on each BH_3 group). Typically, the DMADB ligand binds to single metal centers in a κ^2H,κ^2H binding mode, but κ^2H,κ^1H and κ^1H,κ^1H binding modes are also known.[3,16] In oligomeric and polymeric species, however, the DMADB ligand can bridge between two (or more) metal centers. For example, a DMADB ligand can chelate to one metal center and also use some of the remaining B-H units to bridge to other metal centers; alternatively, a DMADB ligand can use its two BH_3 group to bind to different metal centers in a non-chelating fashion.[3-5,12,16]

In addition to NaDMADB, our group has described several sodium aminodiboranates derived from other amines, including ammonia, methylamine, ethylamine, ethylmethylamine, diethylamine, piperidine, and pyrrolidine.[4,5,19] All of these sodium aminodiboranates are synthesized by Nöth's method of refluxing the amine borane with sodium in THF, except $Na[H_3B\text{-}NH_2\text{-}BH_3]$, which is best made by treating ammonia borane, $H_3N{\cdot}BH_3$, with sodium amine, $NaNH_2$, in refluxing THF.[19] Although these results demonstrate that sodium aminodiboranates can have a variety of substituents on nitrogen, the electronic and steric properties of these substituents all fall in a relatively limited range. Thus, the pK_a's of the listed amines are quite similar: ammonia (9.24), methylamine (10.66), ethylamine (10.65), ethylmethylamine (est. 10.7), diethylamine (10.84), piperidine (11.12), and pyrrolidine (11.31).[20] The substituents on nitrogen, either a hydrogen atom or a primary alkyl group, are sterically similar as well.

Here I describe our efforts to extend the electronic and steric properties of aminodiboranate groups outside the current range, with the goal of exerting greater control over the binding mode of aminodiboranate ligands, as well as the physical properties (such as volatility and thermal stability) of the metal aminodiboranate complexes. Specifically, the successful synthesis of three new sodium aminodiboranate salts containing secondary alkyl substituents is reported: sodium *N*-isopropyl-*N*-methylaminodiboranate, **1**; sodium *N*,*N*-diisopropylaminodiboranate, **2**; and sodium *cis*-2,6-dimethylpiperidinodiboranate, **3**. I also describe our efforts to prepare other

sterically hindered sodium aminodiboranates, including sodium *N*-isopropylaminodiboranate and sodium *N*-*tert*-butylaminodiboranate, as well as sodium aminodiboranates with electron withdrawing substituents, including sodium *N*-benzylaminodiboranate, sodium *N*-benzyl-*N*-methylaminodiboranate, and sodium 2,2-difluoroethylaminodiboranate. Finally, we detail the synthesis of magnesium *cis*-2,6-dimethylpiperidinyldiboranate and our attempts to synthesize magnesium, titanium, and manganese complexes containing the *N*,*N*-diisopropylaminodiboranate anion.

Results and Discussion

Synthesis of Sterically Hindered Aminodiboranates: Initial Results. To make sterically bulky aminodiboranates by Nöth's method, we attempted the reduction of *N*-*tert*-butylamine-borane, (t-Bu)NH_2-BH_3, and *N*,*N*-diisopropylamine-borane, (i-Pr)$_2$NH-BH_3, with sodium in refluxing THF. After three days, the ^{11}B NMR spectra indicated that more than 90% of the starting material remained; minor amounts of the corresponding iminoborane, $R_1R_2N{=}BH_2$, and sodium borohydride were present. At best, only traces of the desired aminodiboranate product were observed.

Why do these reactions proceed so differently compared with primary alkyl- and dialkyl-amine boranes? The pK_a's of *tert*-butylamine (10.68) and diisopropylamine (11.05)[20] are similar to those of piperidine and pyrrolidine (for which Nöth's method works just fine). Presumably, then, the drastically reduced rate at which bulky amine-

boranes react with sodium in refluxing THF must be attributed to the steric hinderance of the amine alkyl groups, although why steric effects should affect the rate of a redox reaction in this way is not clear.

We therefore investigated whether Keller's method could be used to synthesize sodium aminodiboranates with bulky alkyl groups on nitrogen. This method employs the corresponding μ-aminodiborane, μ-(R_1R_2N)B_2H_5, as a starting material. We have found that bulky μ-aminodiboranes can be made, but the preferred method differs depending on the nature of substituents on nitrogen.

The complex μ-(*N*-isopropyl-*N*-methylamino)diborane can be prepared in good yield by treatment of *N*-isopropyl-*N*-methylamine-borane with BH_3·THF. This reaction proceeds slowly at room temperature, as evidenced by the slow formation of bubbles, presumably H_2, but proceeds much more quickly at 50 °C:[21]

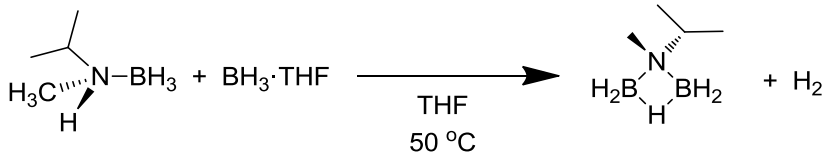

The complexes μ-(*N*-*tert*-butylamino)diborane and μ-(*N*-isopropylamino)diborane can also be prepared by this method. However, with more sterically hindered amine-boranes, such as *N*,*N*-diisopropylamine-borane and *cis*-2,6-dimethylpiperidine-borane, little or no reaction takes place with BH_3·THF, even at elevated temperatures.

More sterically hindered μ-(amino)diboranes are best made in two steps. Heating *N*,*N*-diisopropylamine-borane to 160 °C or higher in the absence of solvent causes the 1:1 amine-borane adduct to melt and lose H_2, forming *N*,*N*-diisopropyliminoborane, $(i\text{-}Pr)_2N{=}BH_2$.[22] As it is generated, the *N*,*N*-diisopropyliminoborane product can be distilled from the melt and collected as a colorless liquid (less sterically hindered iminoboranes typically form cyclic dimers and solidify at room temperature). Treatment of *N*,*N*-diisopropyliminoborane with BH_3·THF generates the desired μ-(*N*,*N*-diisopropylamino)diborane:

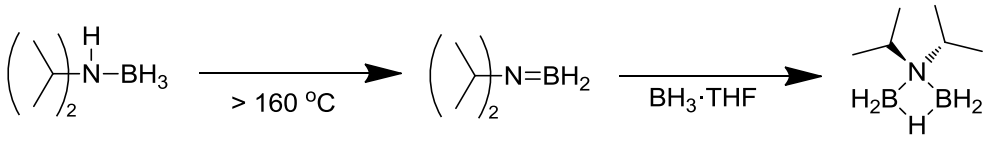

A similar reaction sequence can be used to prepare μ-(*cis*-2,6-dimethyl-piperidino)diborane, except that, during the first step, the *cis*-2,6-dimethylpiperidine-borane adduct must be heated to 180 °C before distillate is collected. This is because, unlike *N*,*N*-diisopropyliminoborane, *cis*-2,6-dimethylpiperidinoiminoborane is not sufficiently sterically bulky to prevent dimerization of the iminoborane intermediate, which, as a result, has a relatively high boiling (and melting) point. At lower temperatures, the iminoborane dimer tends to solidify in the still head.

Synthesis of Sterically Hindered Aminodiboranates: Success. With the sterically bulky μ-aminodiboranes in hand, we find that the corresponding sodium aminodiboranates can be prepared in good yield by Keller's method, hydride insertion with sodium hydride:

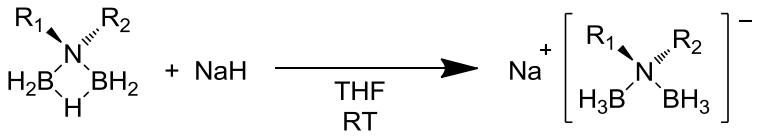

The products, sodium *N*-isopropyl-*N*-methylaminodiboranate, **1**, sodium *N*,*N*-diisopropylaminodiboranate, **2**, and sodium *cis*-2,6-dimethylpiperidinyldiboranate, **3**, are best purified by crystallization from diethyl ether. Sodium *N*-isopropyl-aminodiboranate and sodium *N*-*tert*-butylaminodiboranate can be synthesized by a method similar to that used to synthesize **1**; however, they are much more difficult to purify.

The new sodium aminodiboranate salts are air and water sensitive. They are all soluble in THF but have varying solubilities in diethyl ether: **1** and **2** are soluble, **3** is only moderately soluble, and sodium *N*-*tert*-butylaminodiboranate and *N*-isopropylaminodiboranate are only sparingly soluble. ^{1}H NMR data for the new complexes are given in the Experimental Section.

Synthesis of Sodium Aminodiboranates with Electron Withdrawing Substituents. Syntheses of sodium *N*-benzylaminodiboranate, sodium *N*-benzyl-*N*-methylaminodiboranate, and sodium 2,2-difluoroethylaminodiboranate were attempted by refluxing the respective amine-borane adduct with sodium metal in THF and also by the route discussed above in which BH_3·THF is added to the respective amine-borane followed by treatment of the resulting μ-aminodiborane with NaH. The sodium reduction method produced the desired sodium aminodiboranate but also afforded a number of unidentifiable byproducts, as judged by ^{11}B NMR spectroscopy, from which the product could not be separated.

Fortunately, the sodium hydride addition route did afford the desired sodium aminodiboranate, as judged by the ^{11}B NMR spectra. However, all three complexes decompose slowly at room temperature, preventing analytically pure material from being obtained.

^{11}B NMR Spectra of Sodium Aminodiboranates. The ^{11}B NMR chemical shift and coupling constants of all known sodium aminodiboranates have been compiled in Table 4.1. Except for sodium *cis*-2,6-dimethylpiperidinyldiboranate, **3**, the ^{11}B NMR spectra of the new sodium aminodiboranates consist a single binomial quartet due to coupling with the BH_3 hydrogen atoms. The spectrum of the sodium *cis*-2,6-dimethylpiperidinyldiboranate salt, **3**, features two quartets due to the inequivalent chemical environments produced by the *cis*-methyl groups of the 2,6-

dimethylpiperidine ring. The ^{1}H NMR spectra of **1** and **2** have a single 1:1:1:1 $^{11}BH_3$ resonances superimposed over a broad hump due to the $^{10}BH_3$ resonances which, in these molecules, do not show the expected 1:1:1:1:1:1:1 septet. Again, **3** has two different 1:1:1:1 quartets due to the inequivalence of the BH_3 groups.

The ^{11}B NMR chemical shifts of the sodium aminodiboranates show some systematic trends as a function of the substituents on nitrogen. Using the unsubstituted sodium aminodiboranate, $Na[H_3B\text{-}NH_2\text{-}BH_3]$, as a reference point, an additive trend is observed in which substituting one hydrogen with a methyl group results in a shift ($\Delta\delta$) of +4.2 ppm, and double this amount if two hydrogens are substituted with methyl groups. Similarly, $\Delta\delta$ is +3.4 for benzyl and 2,2-trifluoroethyl, +2.7 for ethyl, +0.5 for isopropyl, and +0.2 for *tert*-butyl (all in ppm). Aminodiboranates with two different substituents on nitrogen, such as $NMe(CH_2Ph)$ and NMe(i-Pr), also obey these additive trends. Aminodiboranates based on pyrrolidinyl and piperidinyl groups, which are electronically similar to NEt_2 groups but with steric sizes intermediate between NMe_2 and NEt_2, have ^{11}B NMR chemical shifts that are intermediate between the NMe_2 and NEt_2 aminodiboranates. Interestingly, the two chemically inequivalent BH_3 groups in *cis*-2,6-dimethylpiperidinyldiboranate have ^{11}B NMR chemical shifts that differ by a relatively large amount, 11 ppm. The average of these two shifts of δ -19.6 is very similar to the ^{11}B NMR shift of the aminodiboranate based on $N(i\text{-}Pr)_2$, which the *cis*-2,6-dimethylpiperidinyl group resembles both sterically and electronically. The 11 ppm

chemical shift difference suggests that inductive effects cannot be the only factor affecting the ^{11}B NMR chemical shifts in these aminodiboranates. In fact, the general trends suggest that electron donating substituents tend to deshield the ^{11}B NMR shift, whereas sterically bulky groups tend to shield the ^{11}B NMR shift, and that electronic (inductive) and steric effects seem to be about equally important.

Table 4.1. ^{11}B NMR chemical shifts and coupling constants of previously reported and new sodium aminodiboranates in THF.

NR_2 group	Chemical shift (ppm)	Coupling constant (J_{BH} Hz)	Reference
NH_2	-19.9	90	5
NHMe	-15.7	91	5
NHEt	-17.2	90	5
NH(i-Pr)	-19.3	90	This work
NH(t-Bu)	-19.7	91	This work
$NH(CH_2CF_2H)$	-16.5	91	This work
$NH(CH_2Ph)$	-16.5	91	This work
NMe_2	-11.5	91	5
NEt_2	-14.8	90	4
$N(i\text{-}Pr)_2$	-19.2	91	This work
$NMe(CH_2Ph)$	-12.1	91	This work
Isopropylmethyl	-14.6	90	This work
Pyrrolidinyl	-12.7	91	5
Piperidinyl	-13.5	90	4
cis-2,6-Dimethylpiperidinyl	-14.2, -25.1	91, 91	This work

Synthesis of New Magnesium Aminodiboranates. Magnesium *N*,*N*-dimethyl-aminodiboranate, $Mg(DMADB)_2$, has been successfully used to deposit conformal thin films of MgO by CVD with water as a co-reactant.[23] The principal advantage of $Mg(DMADB)_2$ is its unusually high vapor pressure (800 mTorr at 25 °C), which is larger than those of other known Mg-containing CVD precursors.[24-32] Unfortunately, attempts to deposit magnesium diboride, MgB_2, using $Mg(DMADB)_2$ as a single source precursor failed: the precursor begins to thermolyze only above ~350 °C and at those temperatures the magnesium sublimes away and the films are mostly boron. Titanium doped magnesium boride films were successfully prepared by the co-deposition of $Mg(DMADB)_2$ and $Ti(DMADB)_2$, resulting in films with the stoichiometry $Mg_{0.88}Ti_{0.19}B_2$. Unfortunately, these films were not superconducting at low temperature.[17] Magnesium aminodiboranate complexes which contain electron withdrawing groups or sterically hindered groups on nitrogen should decompose at lower temperatures and may enable us to deposit pure magnesium diboride thin films.

The reaction of $MgBr_2$ with two equivalents of sodium *cis*-2,6-dimethyl-piperidinyldiboranate in diethyl ether for 24 h, followed by sublimation at 50 °C under vacuum resulted in a sublimate which contained the desired magnesium aminodiboranate product, as judged by the two quartets at δ -15.0 and -23.3, both with J_{BH} = 90 Hz, in its ^{11}B NMR spectrum in C_7D_8. The sublimate was about 85% pure as

judged by ^{11}B NMR spectroscopy, the balance consisting of the hydrolysis/thermolysis product μ-(*cis*-2,6-dimethylpiperidino)diborane.

Attempted Synthesis of $Mg[H_3B\text{-}N(i\text{-}Pr)_2\text{-}BH_3]_2$ and the Ti and Mn Analogs. The reaction of $MgBr_2$ and sodium *N*,*N*-diisopropylaminodiboranate, NaDIPADB, in diethyl ether at room temperature affords a small amount of the hydrolysis/thermolysis product μ-(diisopropylamino)diborane by ^{11}B NMR spectroscopy. It is difficult to determine if the desired product is formed by ^{11}B NMR due to the single resonance which is observed because of rapid chemical exchange between the Na and Mg cations, and the similarity of the chemical shifts of sodium and magnesium aminodiboranates.

The parent aminodiboranate complex, $Mg(DMADB)_2$, can be synthesized in good yield by ball milling $MgBr_2$ with NaDMADB, and isolating the product by sublimation.[11] Similarly, $MgBr_2$ and sodium *N*,*N*-diisopropylaminodiboranate was ball milled for 30 min and then the mixture was heated under a static vacuum at 65 °C in a sublimator. After several hours, a colorless liquid started to condense onto the cold finger, which dripped back into the mixture. The contents of the sublimator were dissolved in diethyl ether; the ^{11}B NMR spectrum (Figure 4.1) showed that the solution contained primarily *N*,*N*-diisopropyliminoborane and magnesium borohydride, $Mg(BH_4)_2$, with smaller amounts of the hydrolysis product μ-(diisopropylamino)diborane and unreacted NaDIPADB.

Figure 4.1. ^{11}B NMR spectrum of the $Mg(DIPADB)_2$ decomposition products: $(i\text{-}Pr)_2N{=}BH_2$, **A**; $Mg(BH_4)_2$, **B**; unreacted starting material NaDIPADB, **C**; and hydrolysis product $\mu\text{-}(i\text{-}Pr)_2NB_2H_5$, **D**.

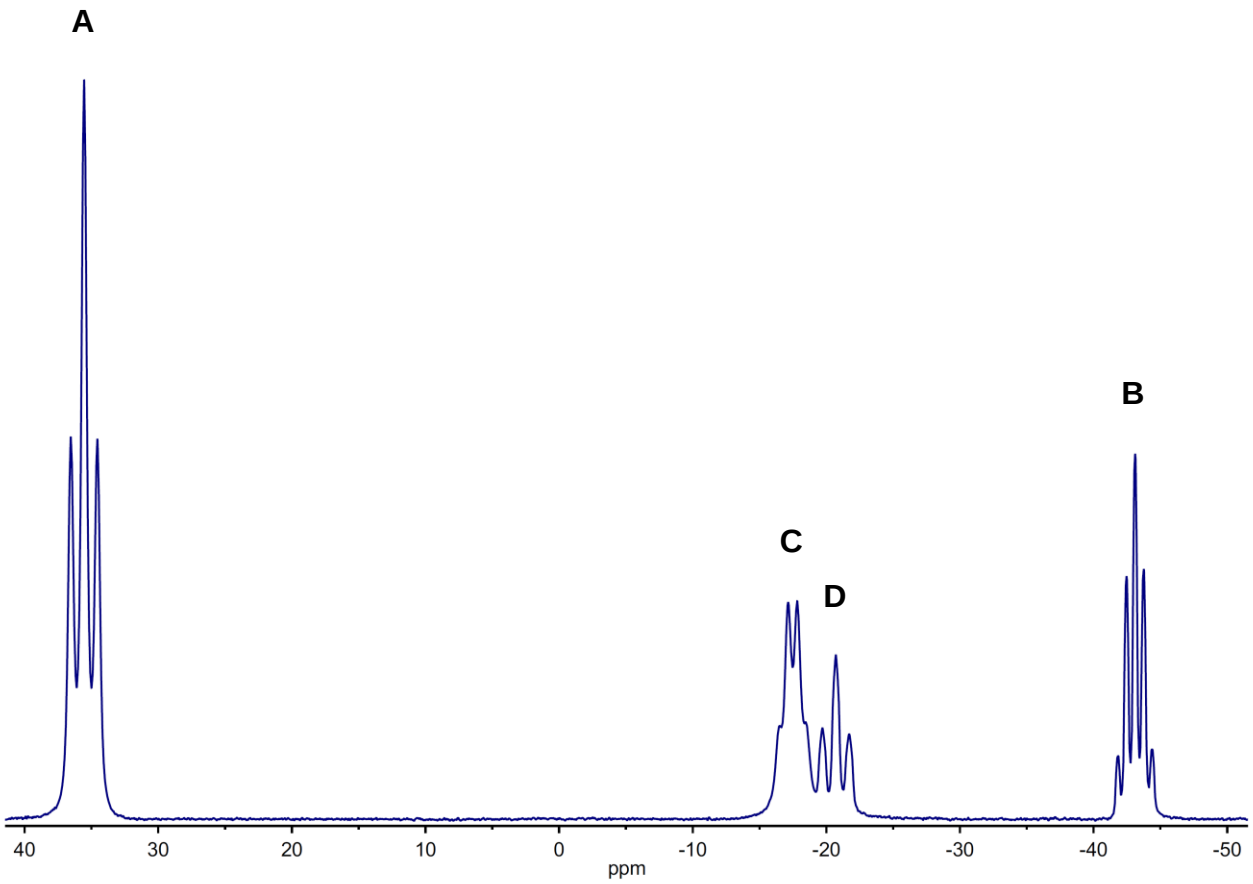

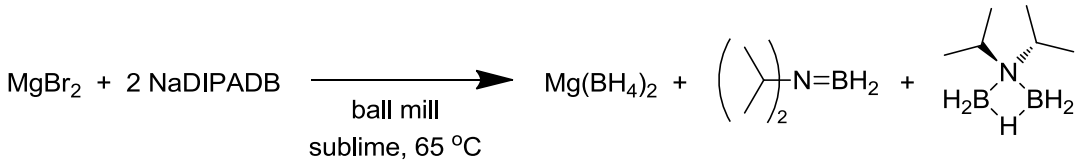

Evidently, the DIPADB ligands decompose by breaking one B-N bond and transferring one BH_3 hydrogen atom to the other BH_3 group; this reaction affords the two principal reaction products $Mg(BH_4)_2$ and $(i\text{-}Pr)_2N{=}BH_2$. This result may be attributed to the steric interaction of the isopropyl groups with the BH_3 groups. Electronically, one would expect the B-N bonds to be stronger than in DMABD owing to the electron donating nature of the isopropyl substituents, which should make the two lone pairs in the $N(i\text{-}Pr)_2$ anion more Lewis basic toward the BH_3 Lewis acids. Interestingly, however, the inductive effects of the larger alkyl groups, which contribute to the electron donating nature of the nitrogen, is secondary to the steric effects the larger alkyl groups have on the N-B bond strength. For example, the relative order of amine base strength with trimethylboron, $B(CH_3)_3$, as the reference acid is $(C_2H_5)_3N < NH_3 < (C_2H_5)_2NH < (C_2H_5)NH_2$. Substituting the substantially more bulky tri-*tert*-butylborane, $B(C_4H_{10})_3$, as the reference acid results in a change in the order of amine base strength: $(C_2H_5)_3N < (C_2H_5)_2NH < (C_2H_5)NH_2 < NH_3$.[33] Similarly, the formation of $(H_3C)_3N\text{-}BH_3$ and $H_2(H_3C)N\text{-}BH_3$ from the respective amines and diborane, B_2H_6, have similar $-\Delta H°$, while the formation of $H(H_3C)_2N\text{-}BH_3$ has a slightly larger $-\Delta H°$ due to a

balance between inductive and steric effects the *N*-methyl groups have on the electron donation of the nitrogen and steric interactions between the methyl groups and BH_3.[34]

Although it is unfortunate that $Mg(DIPADB)_2$ is unsuitable for use as a CVD precursor due to its lack of thermal stability, it is important to note the implication of the above result. It may be possible to adjust the steric bulk of the *N*-alkyl groups to tune the decomposition temperature of magnesium aminodiboranates, resulting in the clean decomposition of the magnesium aminodiboranate to the iminoborane (which typically are volatile liquids) and magnesium borohydride. Thus, it may be possible to deposit a thin film of magnesium borohydride on a substrate by thermal CVD and further anneal the film at atmospheric pressure to produce magnesium diboride without the loss of magnesium to the gas phase typically observed during heating magnesium containing films in vacuum.

The divalent DMADB species $Ti(DMADB)_2$ and $Mn(DMADB)_2$ can be synthesized by the addition of NaDMADB to $TiCl_3(THF)_3$ and $MnCl_2$, respectively.[3] In the titanium reaction, the Ti^{3+} species is reduced to Ti^{2+} by one of the equivalents of NaDMADB.[3] In analogous reactions with NaDIPADB, however, $MnCl_2$ is quickly reduced to what appears to be Mn metal, and Ti is reduced to a black oil and only traces of a blue sublimate could be collected.

Conclusions

Five new sodium aminodiboranates with bulky N-alkyl groups and three new sodium aminodiboranates with electron withdrawing groups on nitrogen have been prepared. The complex, magnesium *cis*-2,6-dimethylpiperidinyldiboranate was able to be prepared although was difficult to isolate. Synthesis of magnesium *N*,*N*-diisopropylaminodiboranate was attempted by ball milling followed by sublimation at 65 °C. Primarily decomposition products, *N*,*N*-dimethylimine and magnesium borohydride, $Mg(BH_4)_4$, were observed by ^{11}B NMR in the reaction mixture, indicating the ligand is less thermally robust relative to the *N*,*N*-dimethylaminodiboranate analog.

Experimental

All operations were carried out in vacuum or under argon using standard Schlenk and glove box techniques. All glassware was dried in an oven at 150 °C, assembled hot, and allowed to cool under a vacuum before use. Diethyl ether and tetrahydrofuran were distilled under nitrogen from sodium/benzophenone and degassed with argon immediately before use. *N*-isopropyl-*N*-methylamine, diisopropylamine, *cis*-2,6-dimethylpiperidine, benzylamine, and *N*-benzyl-*N*-methylamine were distilled from calcium hydride before use. 2,2-difluoroethylamine (Oakwood Chemical Co.) was used as received. *tert*-Butylamine-borane and borane in THF (1.0 M) were purchased from Aldrich and used as received.

Elemental analyses were carried out by the University of Illinois Microanalytical Laboratory. The IR spectra were recorded on a Thermo Nicolet IR200 infrared spectrometer as Nujol mulls between NaCl salt plates. The ^{1}H NMR spectra were obtained on a Varian VXR 500 at 11.75 T and ^{11}B NMR spectra were obtained on a Varian Unity 400 instrument at 9.4 T. The chemical shifts are reported in δ units (positive shifts to high frequency) relative to $SiMe_4$ (^{1}H NMR) or $BF_3{\cdot}Et_2O$ (^{11}B NMR). Multiplets have binomial intensities unless otherwise specified.

General Preparation of Amine-borane Adducts. To a stirred solution of $BH_3{\cdot}THF$ (1 M solution in THF, 1.1 eq) at 0 °C was added the amine (1 eq.) dropwise (the addition can also be done in reverse). The resulting colorless solution can be used as prepared; alternatively, removing the solvent under vacuum affords the product as a white solid.

Isopropylamine-borane. ^{11}B NMR (THF): δ -20.4 (q, J_{BH} = 96 Hz).

***N,N*-Diisopropylamine-borane.** ^{11}B NMR (THF): δ -21.2 (q, J_{BH} = 97 Hz).

***N*-Isopropyl-*N*-methylamine-borane.** ^{11}B NMR (THF): δ -17.0 (q, J_{BH} = 97 Hz).

***cis*-2,6-Dimethylpiperidine-borane.** ^{11}B NMR (THF): δ -17.0 (q, J_{BH} = 97Hz), -25.5 (q, J_{BH} = 97Hz).[35]

N-*B*enzylamine-borane. ^{11}B NMR (THF): δ -18.6 (q, J_{BH} = 96 Hz).

***N*-Benzyl-*N*-methylamine-borane.** ^{11}B NMR (THF): δ -13.2 (q, J_{BH} = 96 Hz).

2,2-Difluoroethylamine-borane. ^{11}B NMR (THF): δ -18.6 (q, J_{BH} = 97 Hz).

Sodium *N*-Isopropyl-*N*-methylaminodiboranate, Na[H_3B-N(i-Pr)Me-BH_3], 1. To BH_3·THF (50 mL of a 1 M solution in THF, 50 mmol) at 0 °C was added *N*-isopropyl-*N*-methylamine (2.4 mL, 23 mmol) dropwise with stirring. After several minutes the solution was warmed, first to room temperature and then to 50 °C for 3 days. During this time gas was evolved to afford μ-(*N*-isopropyl-*N*-methylamino)diborane, μ-(i-Pr)$MeNB_2H_5$. ^{11}B NMR (THF): δ -17.9 (dt, J_{BH} = 32, 130 Hz).

In a separate flask, NaH (2.6 g of a 60 wt.% dispersion in mineral oil, 65 mmol) was washed with pentane (50 mL), collected by filtration, and dried under vacuum. The μ-(*N*-isopropyl-*N*-methylamino)diborane solution from the previous step was cooled to 0 °C and added to NaH. The resulting slurry was stirred for 4 hrs at room temperature. The slurry was filtered, and the colorless filtrate was taken to dryness under vacuum to afford a white solid. Coordinated solvent was removed by heating the solid under vacuum to 40 °C overnight. The white solid was dissolved in Et_2O (50 mL), the solution was filtered, and the colorless filtrate was taken to dryness under vacuum to afford a white powder. Yield: 2.57 g (90%). Mp. >275 °C. Anal. Calcd. for Na[H_3B-N(i-Pr)Me-BH_3]: C, 39.1; H, 13.13; N, 11.41%. Found: C, 39.1; H, 13.12; N, 10.25%. ^{1}H NMR (d_3-MeCN): δ 1.13 (d, J_{BH} = 6.6 Hz, 6H, C-Me), 1.22 (1:1:1:1 q, J_{BH} = 90 Hz, 6H, BH_3), 2.12 (s, 3H, N-Me), 2.66 (septet, J_{BH} = 6.4 Hz, 1H, N-CH). ^{11}B NMR (d_3-MeCN): δ -13.1 (q, J_{BH} = 91

Hz). IR (Nujol, cm^{-1}): 2322 s, 2258 s, 1416 w, 1221 m, 1198 m, 1169 s, 1140, w, 1110, w, 1072 w, 1055 w, 1025 w, 972 w, 826 w, 799 w.

Sodium *N,N*-Diisopropylaminodiboranate, Na[H_3B-N(i-Pr)$_2$-BH_3], 2. *N,N*-Diisopropylamine-borane (4.1 g, 35.7 mmol) was heated to 160 °C; during which time the white solid melted to a colorless liquid and began to evolve gas at ca. 100 °C. A colorless distillate was collected in a Schlenk flask cooled to -78 °C. To the distillate at 0 °C was added BH_3·THF (32 mL of a 1 M solution in THF, 32 mmol). The mixture was warmed to room temperature and then stirred overnight to give a solution of μ-(*N,N*-diisopropylamino)diborane, μ-(i-Pr)$_2$$NB_2H_5$. ^{11}B NMR (THF): δ -20.8 (td, J_{BH} = 128, 33 Hz).

In a separate flask, NaH (1.8 g of a 60 wt.% dispersion in mineral oil, 45 mmol NaH) was washed with pentane (50 mL), collected by filtration, and dried under vacuum. The μ-(*N,N*-diisopropylamino)diborane solution from the previous step was cooled to 0 °C and transferred onto the NaH, and the resulting mixture was stirred for 21 hrs at room temperature. The slurry was filtered, and the colorless filtrate was taken to dryness under vacuum to afford a white solid. Coordinated solvent was removed by heating the solid under vacuum to 40 °C overnight. The white solid was dissolved in Et_2O (50 mL), the solution was filtered, and the colorless filtrate was taken to dryness under vacuum to afford a white powder. Yield: 3.62 g (67%). Analytically pure crystals can be grown by dissolving **2** in Et_2O, concentrating the solution under reduced

pressure to saturation, and cooling to -20 °C. Mp. >275 °C. Anal. Calcd. for Na[H_3B-N(i-Pr)$_2$-BH_3]: C, 47.8; H, 13.4; N, 9.29%. Found: C, 47.7; H, 13.1; N, 9.4%. ^{1}H NMR (d$_3$-MeCN): δ 1.02 (1:1:1:1 q, J_{HB} = 91 Hz, 6H, BH_3), 1.16 (d, J_{HH} = 6.5 Hz, 12H, C-Me), 2.96 (septet, J_{HH} = 6.5 Hz, 2H, N-CH). ^{11}B NMR (d$_3$-MeCN): δ -17.6 (q, J_{BH} = 91 Hz). IR (Nujol, cm^{-1}): 2543 w, 2354 s, 2312 s, 2250 s, 2096 w, 1321 w, 1270 m, 1225 m, 1197 m, 1158 s, 1124 w, 1101 w, 1046 m, 1025 m, 975 m, 941 w, 924 w, 895 w, 822 w, 771 w.

Sodium *cis*-(2,6-Dimethylpiperidinyl)diboranate, Na[H_3B-N(C_7H_{14})-BH_3], 3. *cis*-2,6-Dimethylpiperidine-borane (3.8 g, 30 mmol) was heated to 180 °C during which time the solid melted at 110 °C and began to evolve gas. A clear and colorless liquid, (C_7H_{14})N=BH_2, was distilled off through a heated still head (ca. 100 °C) to prevent condensation of the dimer ((C_7H_{14})N-BH_2)$_2$, into a flask at -78 °C. BH_3·THF (20 mL of a 1M solution in THF, 20 mmol) was added to the distillate and the solution was heated to 50 °C until the conversion of (C_7H_{14})N-BH_2 (δ 1.5 J_{BH} = 160 Hz) to (*cis*-2,6-dimethylpiperidino)diborane (δ -16.7, -20.1 td, J_{BH} = 128, 33 Hz) was complete.

In a separate flask, NaH (0.75 g, 60% in mineral oil, 19 mmol) was washed with pentane (50 mL), collected by filtration, and dried under vacuum. The *cis*-(2,6-dimethylpiperidino)diborane solution was cooled to 0 °C and added to the NaH. The resulting mixture was stirred at room temperature for 3 hrs. The slurry was filtered, and the colorless filtrate was dried under vacuum to afford a white powder. Coordinated solvent was removed by heating the solid under vacuum to 50 °C for 3 days. The solid

was dissolved in Et_2O (50 mL), and the solution was concentrated to ca. 40 mL and cooled to -20 °C. The resulting needles were collected and dried under vacuum. Yield: 1.56 g (32%). Mp. >275 °C. Anal. Calcd. for $Na[H_3B\text{-}N(C_7H_{14})\text{-}BH_3]$: C, 51.6; H, 12.38; N, 8.60%. Found: C, 49.9; H, 12.16; N, 8.40%. ^1H NMR (d_3-MeCN): δ 0.911 (1:1:1:1 q, J_{HB} = 88 Hz, 3H, BH_3), 1.14 (m, 2H, eq-3-CH_2), 1.27 (1:1:1:1 q, J_{HB} = 88 Hz, 3H, BH_3), 1.27 (d, J = 6.5 Hz), 1.36 (m, 1H, ax-4-CH_2), 1.59 (d of septets, J = 12.7 Hz, 2.2 Hz, 1H, eq-4-CH_2), 1.89 (qd, J = 13 Hz, 4.5 Hz, 2H, ax-3-CH_2), 2.4 (m, 2H, ax-2-CH_2). ^{11}B NMR (d_3-MeCN): δ -12.5 (q, J_{BH} = 91 Hz), -23.5 (q, J_{BH} = 90 Hz). IR (Nujol, cm^{-1}): 2343 s, 2309 sh, 2260 s, 1329 w, 1300 w, 1275 m, 1266 m, 1209 sh, 1177 s, 1165 s, 1114 m, 1098 s, 1074 w, 1057 m, 1042 w, 1027 m, 976 m, 951 w, 918 w, 902 w, 868 w, 832 w, 802 w, 768 w.

References

(1) Keller, P. C. *J. Chem. Soc. D* **1969**, *24*, 1465.

(2) Nöth, H.; Thomas, S. *Eur. J. Inorg. Chem.* **1999**, *1999*, 1373-1379.

(3) Kim, D. Y. Ph.D. Thesis, University of Illinois at Urbana-Champaign, **2007**.

(4) Bellott, B. J. Ph.D. Thesis, University of Illinois at Urbana-Champaign, **2010**.

(5) Daly, S. R. Ph.D. Thesis, University of Illinois at Urbana-Champaign, **2010**.

(6) Daly, S. R.; Girolami, G. S. *Inorg. Chem.* **2010**, *49*, 4578-4585.

(7) Daly, S. R.; Girolami, G. S. *Inorg. Chem.* **2010**, *49*, 5157-5166.

(8) Daly, S. R.; Girolami, G. S. *Chem. Commun.* **2010**, *46*, 407-408.

(9) Daly, S. R.; Kim, D. Y.; Yang, Y.; Abelson, J. R.; Girolami, G. S. *J. Am. Chem. Soc.* **2010**, *132*, 2106-2107.

(10) Daly, S. R.; Piccoli, P. M. B.; Schultz, A. J.; Todorova, T. K.; Gagliardi, L.; Girolami, G. S. *Angew. Chem. Int. Ed.* **2010**, *49*, 3379-3381.

(11) Kim, D. Y.; Girolami, G. S. *Inorg. Chem.* **2010**, *49*, 4942-4948.

(12) Dunbar, A. C. Ph.D. Thesis, University of Illinois at Urbana-Champaign, **2011**.

(13) Daly, S. R.; Bellott, B. J.; Nesbit, M. A.; Girolami, G. S. *Inorg. Chem.* **2012**, *51*, 6449-6459.

(14) Daly, S. R.; Kim, D. Y.; Girolami, G. S. *Inorg. Chem.* **2012**, *51*, 7050-7065.

(15) Dunbar, A. C.; Girolami, G. S. *Inorg. Chem.* **2013**, *53*, 888-896.

(16) Steele, J. L. Ph.D. Thesis, University of Illinois at Urbana-Champaign, **2013**.

(17) Yang, Y. Ph.D. Thesis, University of Illinois at Urbana-Champaign, **2007**.

(18) Wang, W. B.; Yang, Y.; Yanguas-Gil, A.; Chang, N. N.; Girolami, G. S.; Abelson, J. R. *Appl. Phys. Lett.* **2013**, *102*, 101605.

(19) Daly, S. R.; Bellott, B. J.; Kim, D. Y.; Girolami, G. S. *J. Am. Chem. Soc.* **2010**, *132*, 7254-7255.

(20) Haynes, W. M. *CRC Handbook of Chemistry and Physics, 94th Edition*; Taylor & Francis Limited, 2013.

(21) Malcolm, A. C.; Sabourin, K. J.; McDonald, R.; Ferguson, M. J.; Rivard, E. *Inorg. Chem.* **2012**, *51*, 12905-12916.

(22) Wrackmeyer, B.; Molla, E.; Thoma, P.; Klimkina, E. V.; Tok, O. L.; Bauer, T.; Kempe, R. *Z. Anorg. Allg. Chem.* **2011**, *637*, 401-405.

(23) Wang, W. B.; Yang, Y.; Yanguas-Gil, A.; Chang, N. N.; Girolami, G. S.; Abelson, J. R. *Appl. Phys. Lett.* **2013**, *102*, 101605.

(24) Zhao, Y.; Suhr, H. *Appl. Phys. A* **1992**, *54*, 451-454.

(25) Boo, J.; Lee, S.; Yu, K.; Koh, W.; Kim, Y. *Thin Solid Films* **1999**, *341*, 63-67.

(26) Babcock, J. R.; Benson, D. D.; Wang, A.; Edleman, N. L.; Belot, J. A.; Metz, M. V.; Marks, T. J. *Chem. Vap. Deposition* **2000**, *6*, 180-183.

(27) Davies, H. O.; Jones, A. C.; Leedham, T. J.; Crosbie, M. J.; Wright, P. J.; Boag, N. M.; Thompson, J. R. *Chem. Vap. Deposition* **2000**, *6*, 71-75.

(28) Matthews, J. S.; Just, O.; Obi-Johnson, B.; Rees Jr., W. S. *Chem. Vap. Deposition* **2000**, *6*, 129-132.

(29) Wang, L.; Yang, Y.; Ni, J.; Stern, C. L.; Marks, T. J. *Chem. Mater.* **2005**, *17*, 5697-5704.

(30) Carta, G.; El Habra, N.; Crociani, L.; Rossetto, G.; Zanella, P.; Zanella, A.; Paolucci, G.; Barreca, D.; Tondello, E. *Chem. Vap. Deposition* **2007**, *13*, 185-189.

(31) Kim, D. Y.; Yang, Y.; Abelson, J. R.; Girolami, G. S. *Inorg. Chem.* **2007**, *46*, 9060-9066.

(32) Mathur, S.; Rügamer, T.; Braunschweig, H.; D'Andola, G. *Z. Anorg. Allg. Chem.* **2007**, *633*, 2459-2462.

(33) Brown, H. C. *J. Am. Chem. Soc.* **1945**, *67*, 1452-1455.

(34) McCoy, R. E.; Bauer, S. H. *J. Am. Chem. Soc.* **1956**, *78*, 2061-2065.

(35) Flores-Parra, A.; Farfán, N.; I. Hernández-Bautista, A.; Fernández-Sánchez, L.; Contreras, R. *Tetrahedron* **1991**, *47*, 6903-6914.

CHAPTER 5: Superconformal Coating of Hafnium Diboride or Iron by Static Chemical Vapor Deposition.

Introduction

Chemical vapor deposition, CVD, is a highly useful technique that is employed to deposit thin films for a wide variety of applications, a number of which have been discussed in Chapter 1 of this thesis. One of the advantages of CVD is that, unlike physical vapor deposition methods, it is not a line-of-sight technique and thus can coat deep and hidden features on surfaces with complex topologies. This ability to coat deep features is particularly useful in the fabrication of microelectronic devices, in which trenches and vias are created that subsequently must be coated or filled.

As microelectronic devices become smaller, however, the aspect ratios of deep features tend to increase, and uniformly coating these features becomes more difficult.[1,2] The difficulty arises due to a competition between the rate at which precursor vapor diffuses into relief features, the rate at which precursor decomposition occurs on the surface, and the rate at which unreacted precursor is removed from the system. During precursor dosing, the flux is largest at the opening of the trench and diminishes to negligible amounts deep in the trench. This leads to pinch off, a phenomenon where the opening of a trench is completely infilled with film and a void space with little or no film is left deeper in the trench because of the higher growth rate on high flux surfaces.

Chemical vapor deposition is typically carried out in two kinds of apparatus: open systems and closed systems;[3] these two alternatives can also be referred to as continuous flow and batch processing, respectively. Open system CVD, which is the much more common of the two methods, involves flowing a precursor (or precursors) through a chamber where it comes into contact with a hot surface. A solid film is deposited on the surface, and the volatile byproducts that desorb from the surface are removed from the chamber either by entrainment in a carrier gas, in the case of atmospheric CVD, or by vacuum pumping, in the case of low pressure, LP, or ultra high vacuum, UHV, CVD.[4-6] A wide array of variants of open-system CVD have been described, including thermally activated,[7] plasma enhanced,[8] photo-assisted,[9] and microwave assisted CVD.[10]

Examples of closed system deposition techniques include chemical vapor transport, CVT, and atomic layer deposition, ALD. In closed-system methods, the surface is exposed to the precursor(s) for some period of time without a net flow through the reaction chamber. CVT is often used for the crystal growth of materials with negligible vapor pressure: at elevated temperatures, a reaction occurs between the non-volatile solid and a transport agent to form a volatile intermediate. The volatile intermediate diffuses to a cooler region of the closed system where it decomposes into a crystalline solid, releasing the transport agent back into the gas phase for re-use.[11-14] An

example of this technique, shown below, involves the use of chlorine gas as a transport agent to grow crystalline uranium oxide, UO_2, from powder.[12]

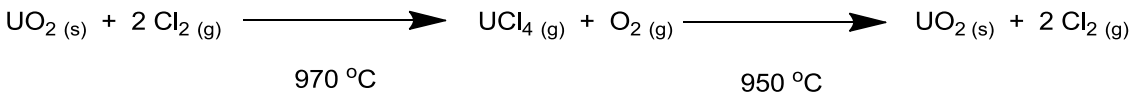

In ALD, two or more molecular precursors are individually dosed into a closed chamber during alternate cycles. Once the requisite time has elapsed for complete saturation of the surface (e.g., by diffusion of the precursor into any deep features that are present), the chamber is evacuated and purged to remove unreacted precursor. The exposure process is then repeated with the other precursor. Repeated cycles of dosing and purging the chamber are performed until the desired film thickness is achieved. This process is often described as "self-limiting" because the precursors do not decompose unimolecularly, but instead react with reactive functional groups left on the surface by the other precursor. Thus, growth stops once the reactive surface groups have been completely consumed.[15-17]

To extend the capabilities of the CVD method, we have investigated a little-explored pressure and flow regime in which a substrate is exposed to the precursor at its equilibrium vapor pressure in a closed system. Although closed system CVD studies have been done with silane, SiH_4, in a closed chamber, plasma enhanced CVD reactor

and by condensation of digermane, Ge_2H_6 into complex structures,[18,19] neither study involved the deposition of thin films from complex molecular precursors that produce byproducts other than hydrogen. In this process regime the rate at which precursor molecules come in contact with the surface is much more uniform throughout the entire trench or via. This minimizes the depletion effects, which are typically seen in an actively pumped system, where newly injected precursor molecules have a high probability of decomposing near the entrance of the trench rather than diffusing down the trench prior to decomposition.

In this chapter, we report the growth of conformal thin films of both hafnium diboride, HfB_2, and iron metal, Fe, by static chemical vapor deposition, static CVD. Hafnium diboride is an interesting material due to its high hardness (29 GPa),[20] high melting point, high wear resistance,[21] refractory properties, and fairly high thermal[22] and electrical conductivities.[23] Additionally, crystalline HfB_2 has a lattice mismatch with GaN of only 1.4%.[24] These characteristics give HfB_2 the potential to be used in wear resistant hard coatings, refractory linings, and diffusion barriers.[25,26]

Iron and iron alloy thin films have numerous applications in solid state microelectronic device including interconnects, thin film capacitors, sensors, microactuators, nanostructured high-density digital storage devices, spintronics, and in high activity catalysts.[27-34]

Results

Hafnium Diboride Thin Films Grown by Static CVD. Whereas bulk samples of the metallic ceramic hafnium diboride, HfB_2, are typically synthesized by sintering at high temperature and pressure,[35,36] thin films of HfB_2 can deposited by flow CVD from the molecular precursor hafnium borohydride, $Hf(BH_4)_4$.[23,24,37] The molecule $Hf(BH_4)_4$ is an excellent static CVD precursor due to its high vapor pressure (15 Torr at 25 °C),[38] a low onset temperature for deposition (200 °C), and the thermal stability of the reaction byproducts at these low growth temperatures.[24] Although films grown at 200 °C are amorphous, crystalline thin films can be obtained if the substrate temperature is greater than 400 °C, or if the amorphous films are annealed at 600 °C in vacuum.[39-41] The idealized CVD reaction leading to HfB_2 is shown below.

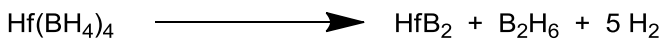

Static CVD of HfB_2 was carried out by loading substrates of interest (planar substrates, microtrenches, macrotrenches, colloidal crystals, and silica aerogels) into a tube furnace with an interior volume of 0.092 L. After being baked out, the furnace was charged with an equilibrium vapor pressure (15 Torr, ca. 75 μmol) of the $Hf(BH_4)_4$ precursor. The furnace was then sealed and heated at 1 °C/minute to 200 °C; this relatively low temperature was chosen to minimize incorporation of excess boron into

the film by means of thermal decomposition of the boron hydride byproducts.[37,42] After the set temperature was reached, deposition was carried out for 2 hours.

Chemical analysis by Auger electron spectroscopy, AES, of films deposited on planar substrates showed that they are chemically similar to films deposited from $Hf(BH_4)_4$ by LPCVD (Figures 5.1 and 5.2). Time-of-flight secondary ion mass spectrometry, TOF-SIMS, showed that about two or three times as much hydrogen is present in the static CVD films in comparison to those deposited by LPCVD at the same growth temperature (Figure 5.3). Small amounts of oxygen were present on the surface of the film but not the interior, presumably as a result of post-growth atmospheric exposure. This result is interesting because the partial pressure of oxygen and residual water in the glassware system used for these experiments is most likely orders of magnitude higher than what is typically found in a turbo-pumped high vacuum system. The observed low incorporation of oxygen into the films is likely due to the high reactivity of $Hf(BH_4)_4$ toward water and oxygen. Evidently, residual water and oxygen in the vacuum background is immediately consumed by the $Hf(BH_4)_4$ when the deposition tube is charged with precursor.

We next turned to experiments with non-flat substrates. Microtrenches of aspect ratio of 2:1, 3:1, and 13:1 coated by static CVD with 80 nm of HfB_2 are shown in Figure 5.4. Remarkably, the films are essentially perfectly conformal, and the 13:1 microtrench is completely infilled with HfB_2 with no void space due to pinch off.

In order to explore higher aspect ratios, a silicon macrotrench (Figure 5.5)[43] was coated with HfB_2 by static CVD. The film thickness decreases from 52 nm at the opening to approximately one half this value at a 200:1 normalized depth (depth in the feature divided by the aperture width). The film thickness is still 20 nm and the step coverage is an impressive 40% at a normalized depth of 1000:1 (Figure 5.6).

The ability to deposit highly conformal films in high aspect ratio structures is the key to fabricating inverse opal crystals with photonic bandgaps.[44-46] The deposited material must be narrow band emitter and thermally robust to temperatures of 1000 °C and above, and HfB_2 is an excellent material on both counts. Therefore, a colloidal crystal composed of a seven-layer stack of 635 nm SiO_2 microspheres was infilled with HfB_2 by static CVD (Figure 5.7). The colloidal crystal was completely coated with a conformal thin film, approximately 90 nm thick, throughout the structure (including the underlying substrate). Impressively, a second colloidal crystal consisting of more than 50 layers of SiO_2 microspheres, with a total depth of ca. 23 μm, could also be uniformly infilled with HfB_2 (Figure 5.8) For comparison, attempts to infill the photonic crystal with HfB_2 from $Hf(BH_4)_4$ by LPCVD are shown in Figure 5.7. There is an overlayer of HfB_2 on the surface of the colloidal crystal and a diminishingly thin film of HfB_2 penetrating approximately 3 layers deep, beyond which no film is observed. Precursor utilization was also very high (ca. one gram), most of which passed through the reaction chamber without contributing to film growth.

Even higher aspect ratios are characteristic of aerogels. We investigated the coating of a silica aerogel composed of interconnected 20 nm voids, resulting in greater than 90% void space by volume. Due to the large surface area and poor thermal conductivity of the aerogel, it was heated under vacuum for several hours to remove residual water before the deposition was carried out. During deposition, the tube furnace ramp rate was 0.1 °C/minute to maintain thermal equilibrium throughout the silica aerogel. The set point was 150 °C and the dwell time was 40 hours. After the deposition was complete, the sample was evacuated for several hours to remove unreacted precursor and volatile byproducts. X-ray computed tomography (CT; Figure 5.9) shows that HfB_2 has been deposited inside the aerogel to a depth of ca. 1 mm: there is bright ring around the outside of the aerogel, and an uncoated interior having the same cross-sectional intensity as the uncoated aerogel. We estimate that HfB_2 has been deposited inside the aerogel to an effective aspect ratio estimated to be greater than 10^5:1. Although ALD has been used to achieve similar results with various precursors,[47-52] there are no reports of thermal CVD achieving such highly conformal films.

Figure 5.1. An Auger electron spectroscopy profile of a HfB_2 film deposited by static CVD.[53]

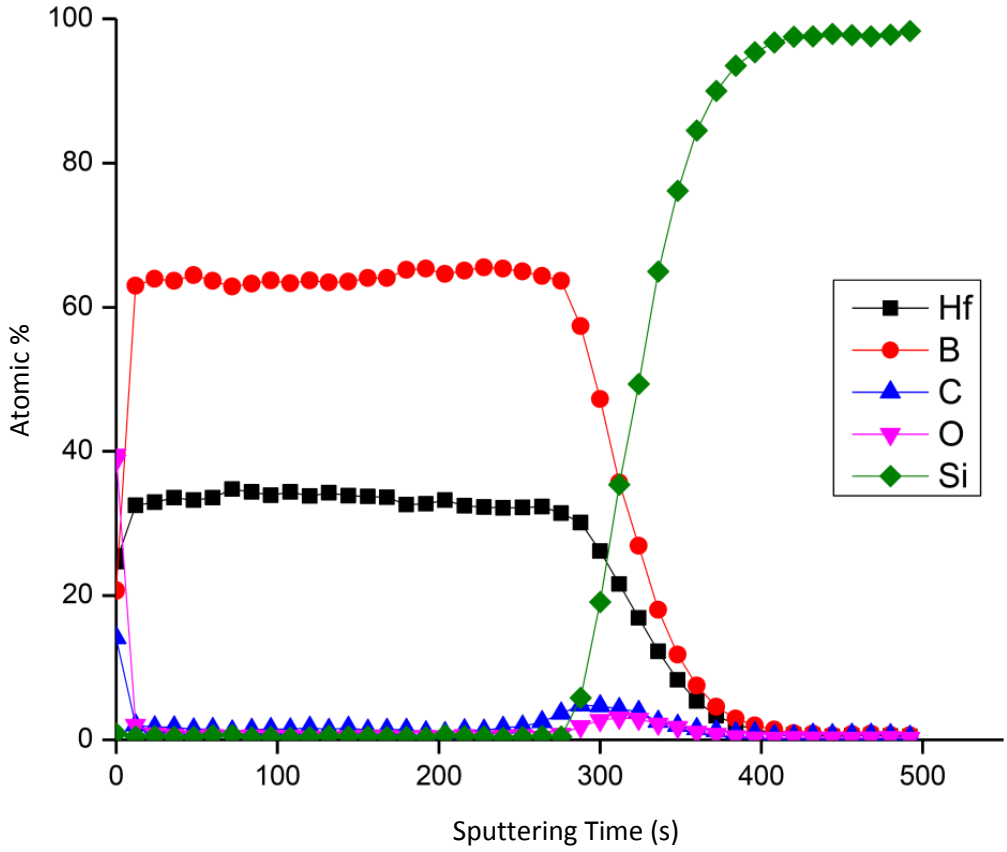

Figure 5.2. An Auger electron spectroscopy profile of a HfB_2 film deposited by LPCVD.[53]

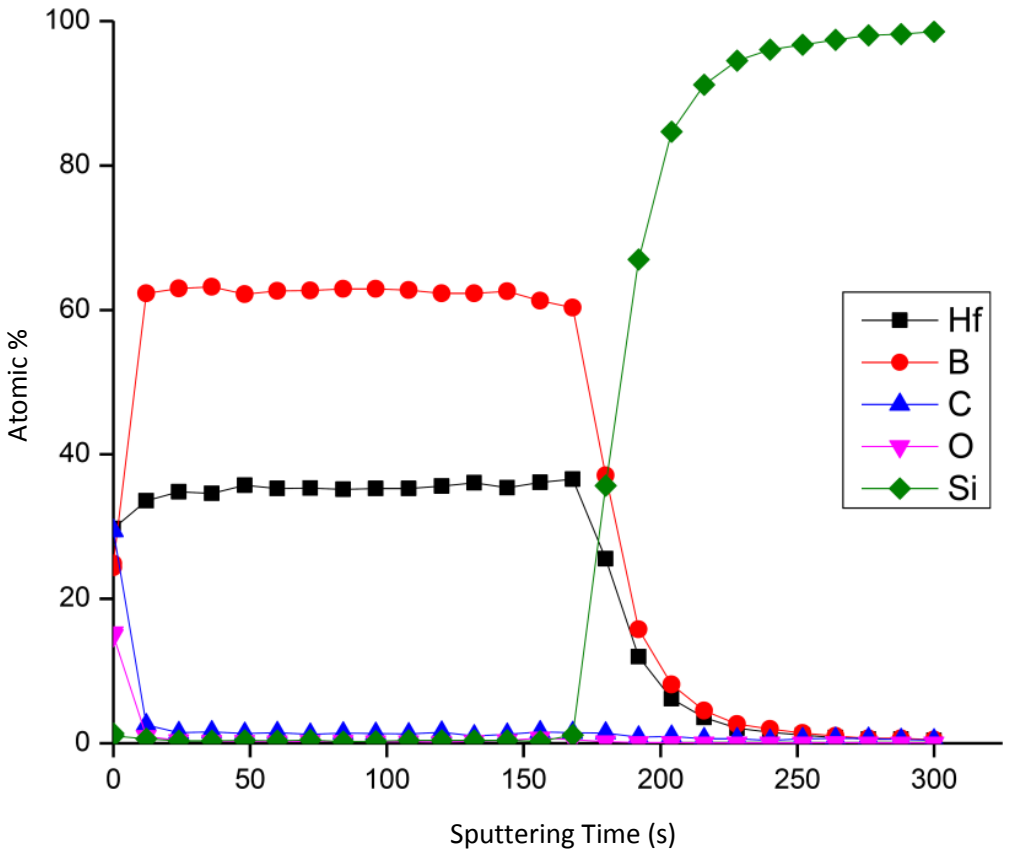

Figure 5.3. A TOF-SIMS profile of the hydrogen to boron ratio found in films grown by LPCVD and static CVD.[53]

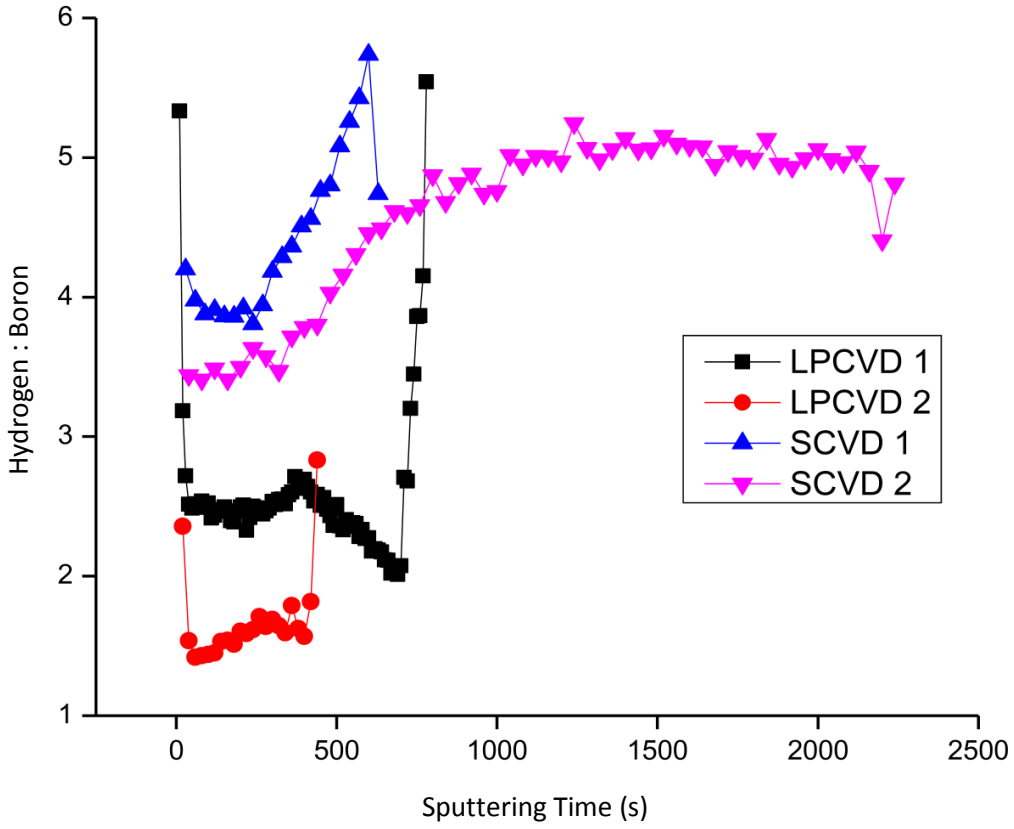

Figure 5.4. Microtrenches with aspect ratios of 2:1 (top), 3:1 (middle), and 13:1 (bottom), all infilled with ca. 80 nm of HfB_2.[53]

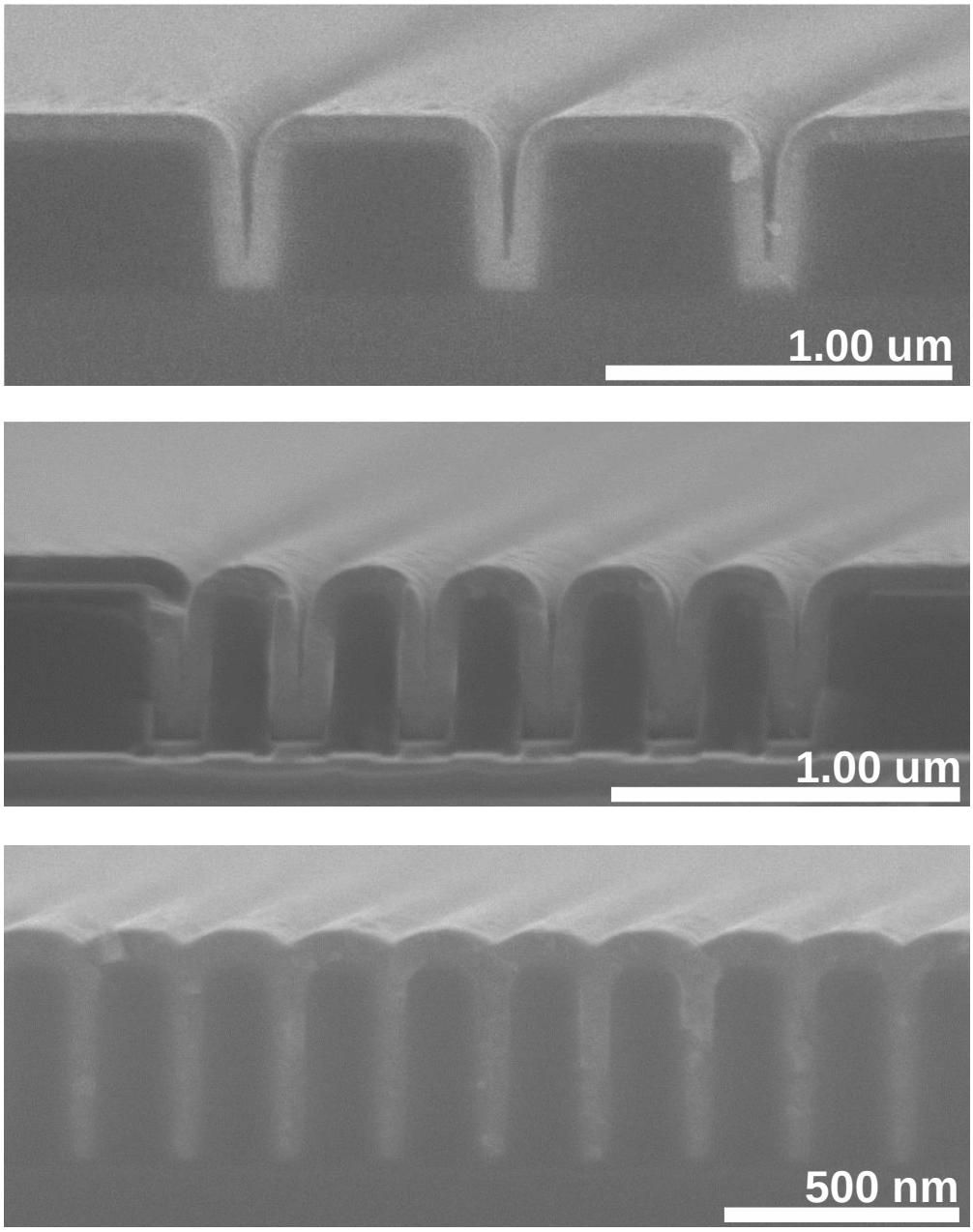

Figure 5.5. Schematic drawing of a macrotrench. Top: The assembled macrotrench with a d = 25 μm tantalum spacer. Middle: The lower wafer of a disassembled macrotrench, bearing a film of diminishing thickness with increasing distance from the opening. The dashed line is the cleavage plane for cross sectional imaging. Bottom: Cross sectional image of the lower wafer of the macrotrench. The arrow points from the opening of the trench to the bottom of the trench.[43]

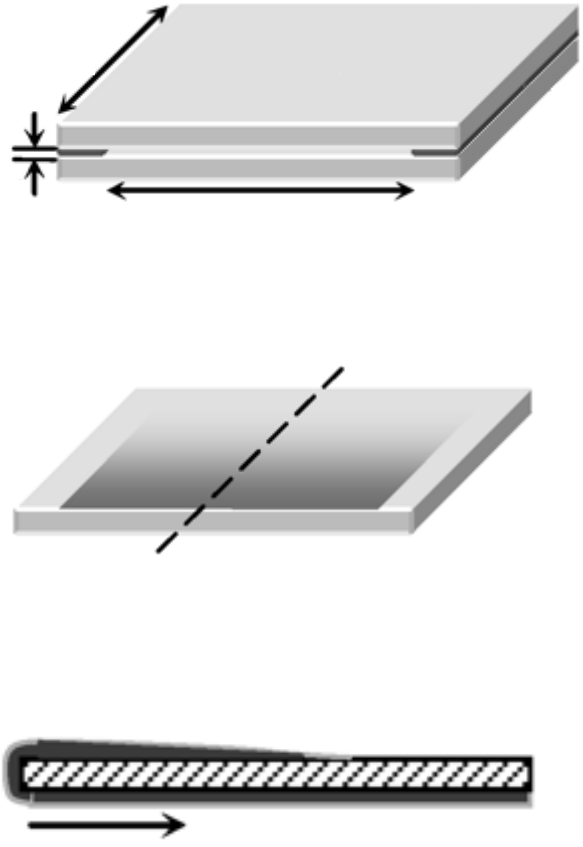

Figure 5.6. The cross sectional HfB_2 film profile from a macrotrench with an aspect ratio of 1000:1.[53]

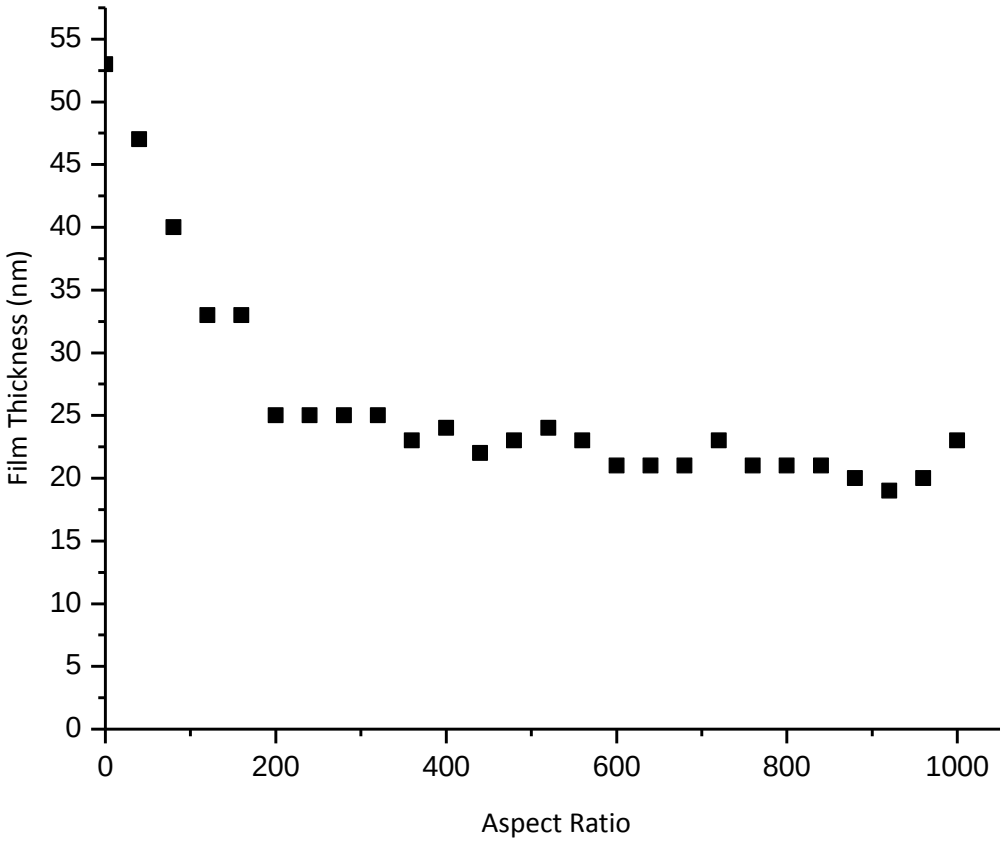

Figure 5.7. Opal photonic crystal coated with HfB_2. Top: by LPCVD. Bottom: by static CVD.[53]

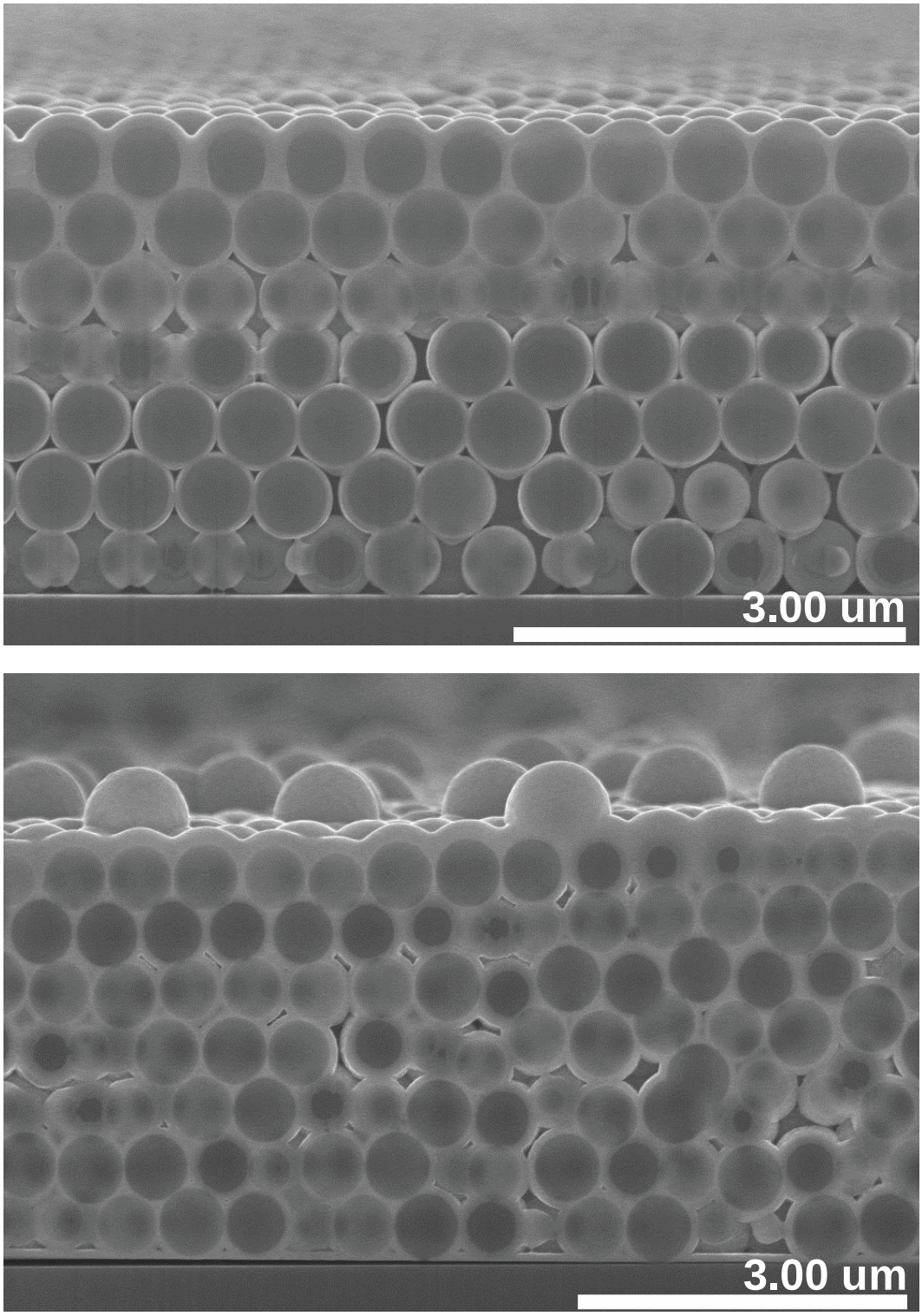

Figure 5.8. Opal photonic crystal 50 layers (ca. 23 μm) thick conformally coated with HfB_2 by static CVD.[53]

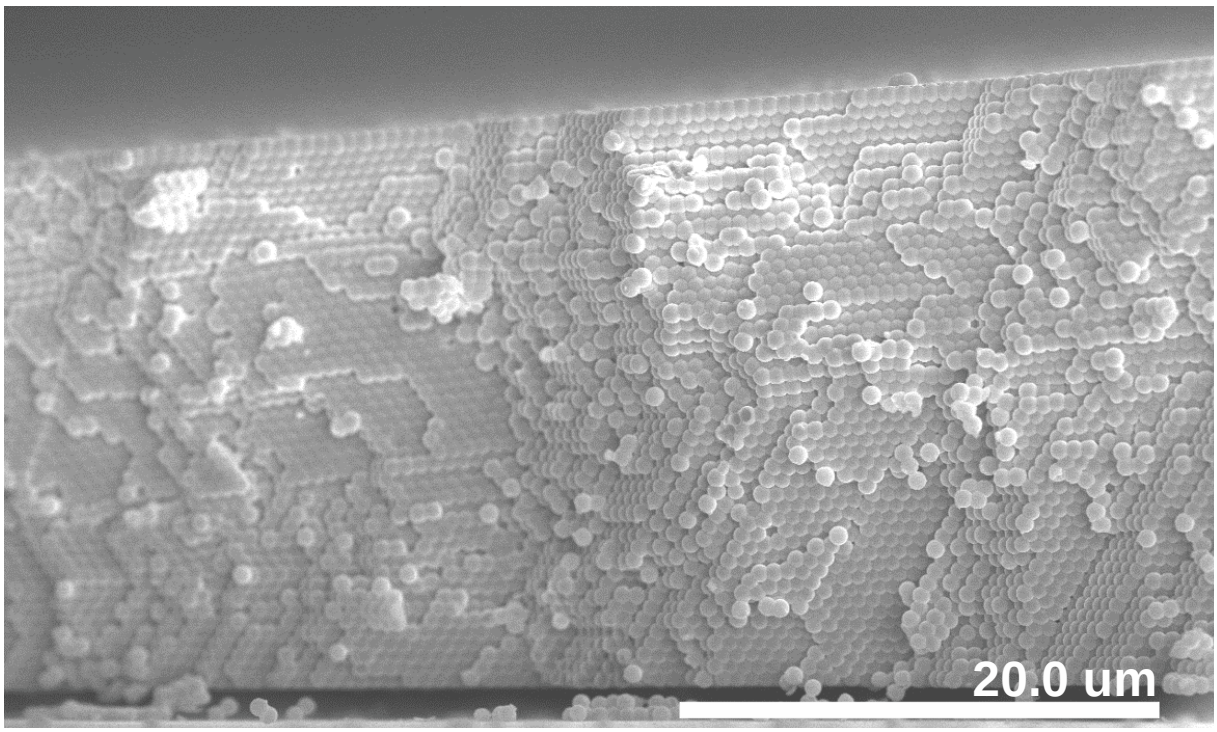

Figure 5.9. Top: CT scan image of coated and uncoated silica aerogels. Middle: The CT scan cross sectional trace intensity. Bottom: An image of an aerogel coated with HfB_2 by static CVD.

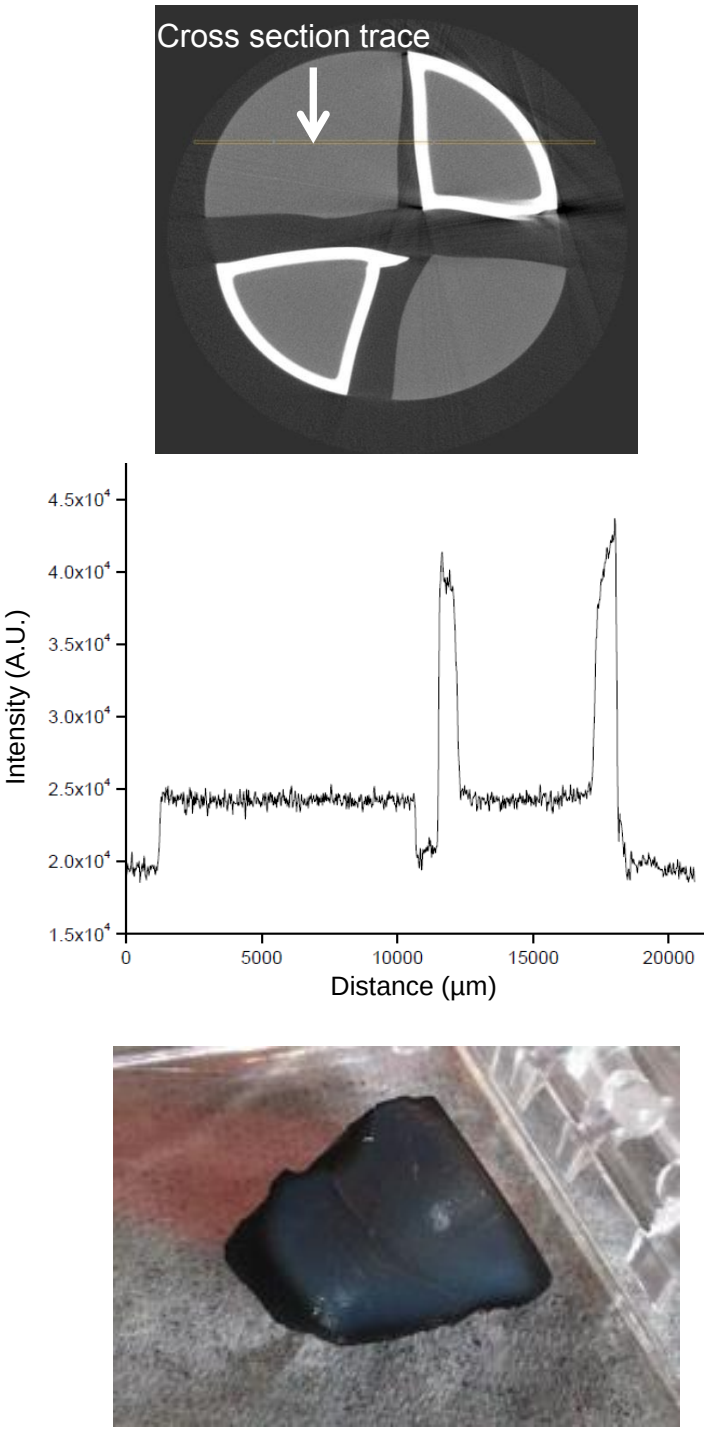

Iron Thin Films Grown by Static CVD. Highly pure Fe thin films have previously been grown by CVD from the molecular precursor iron pentacarbonyl, $Fe(CO)_5$, both in low pressure and atmospheric pressure CVD systems.[54-56] Like hafnium borohydride, $Fe(CO)_5$ is an excellent precursor for static CVD experiments due to its high vapor pressure (25 Torr at 20 °C),[28] low decomposition temperature, and relatively inert carbon monoxide byproduct. However, at substrate temperatures below 250 °C, the films deposited by conventional CVD methods tend to be discontinuous and therefore poorly conducting: for example, a resistivity of 250 μΩ-cm was observed for films deposited at 200 °C,[57-59] vs. a value of 9.7 μΩ-cm for pure iron. At higher substrate temperatures the films are also resistive but for a different reason: incorporation of carbon and oxygen contaminants.

The idealized CVD reaction stoichiometry for the deposition of iron carbonyl is shown below.

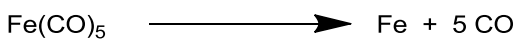

Static CVD experiments with $Fe(CO)_5$ were performed between 100 and 150 °C with a ramp rate of 1 °C/minute and a dwell time typically of two hours. Unlike $Hf(BH_4)_4$, which acts as its own water and oxygen scavenger, $Fe(CO)_5$ is not highly oxygen or water sensitive but the Fe film being deposited is sensitive to oxidation. Thus,

a prolonged bake-out of the deposition chamber and substrate for several hours, followed by cooling to room temperature was performed before each deposition.

Films grown after the tube furnace was thoroughly baked-out were reasonably pure, and consisted of 97 % Fe with only 1.5 % carbon and oxygen each, as shown by X-ray photoelectron spectroscopy, XPS. Presumably, these carbon and oxygen levels arise by means of dissociative chemisorption of carbon monoxide, which is known to occur on iron.[60-63] A 70 nm-thick Fe film had a resistivity of 150 μΩ-cm after being exposed to atmosphere for several hours, similar to what has been reported elsewhere.[57]

Conformal deposition of approximately 100 nm of iron on a relief feature with an aspect ratio of approximately 1:1 is shown in Figure 5.10. The film thickness is remarkably uniform on the substrate surface as well as the walls and bottom of the relief feature. Figure 5.11 depicts a microtrench with an aspect ratio of approximately 8:1. The infilled iron metal exhibits neither pinch off nor voids, although a seam is clearly visible where the side deposits grew together.

Figure 5.12 shows a colloidal crystal uniformally coated with 90 nm of Fe throughout the structure and on the substrate below. Finally, Figure 5.13 show attempts to coat gallium arsenide nanowires with Fe by low pressure and static CVD. Using LPCVD, there was limited film on the nanowires, primarily at the base of the wire and the substrate, and the nanowires themselves are mangled, presumable due to the large precursor flux directed at the surface during deposition. However, coating the

nanowires with Fe by static CVD was highly successful. There is a uniform, 90 nm film on the entire length of the nanowire, as well as a coating on the substrate. Unlike the low pressure CVD sample there is minimal disturbance in the nanowire position or orientation.

Figure 5.10. A microtrench coated with ca. 100 nm of Fe by static CVD.[53]

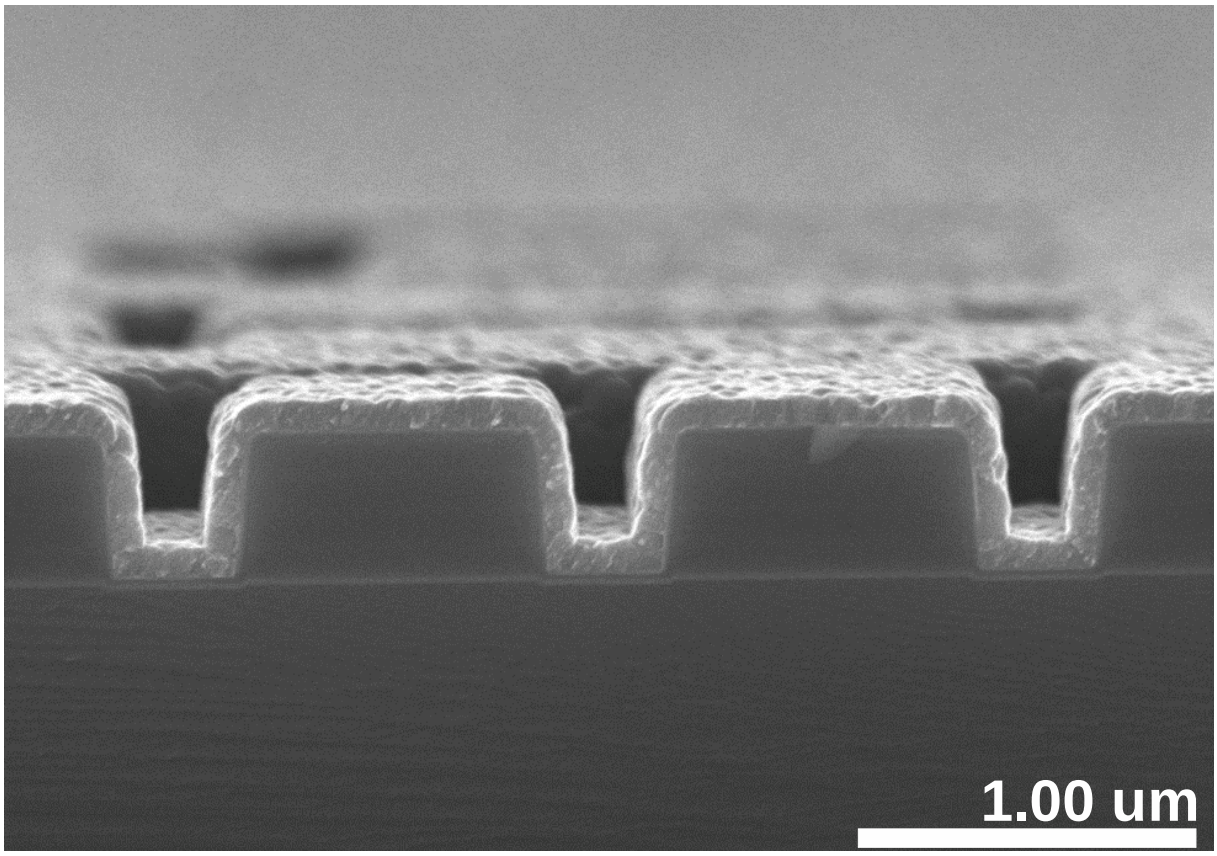

Figure 5.11. An 8:1 microtrench infilled with Fe by static CVD.[53]

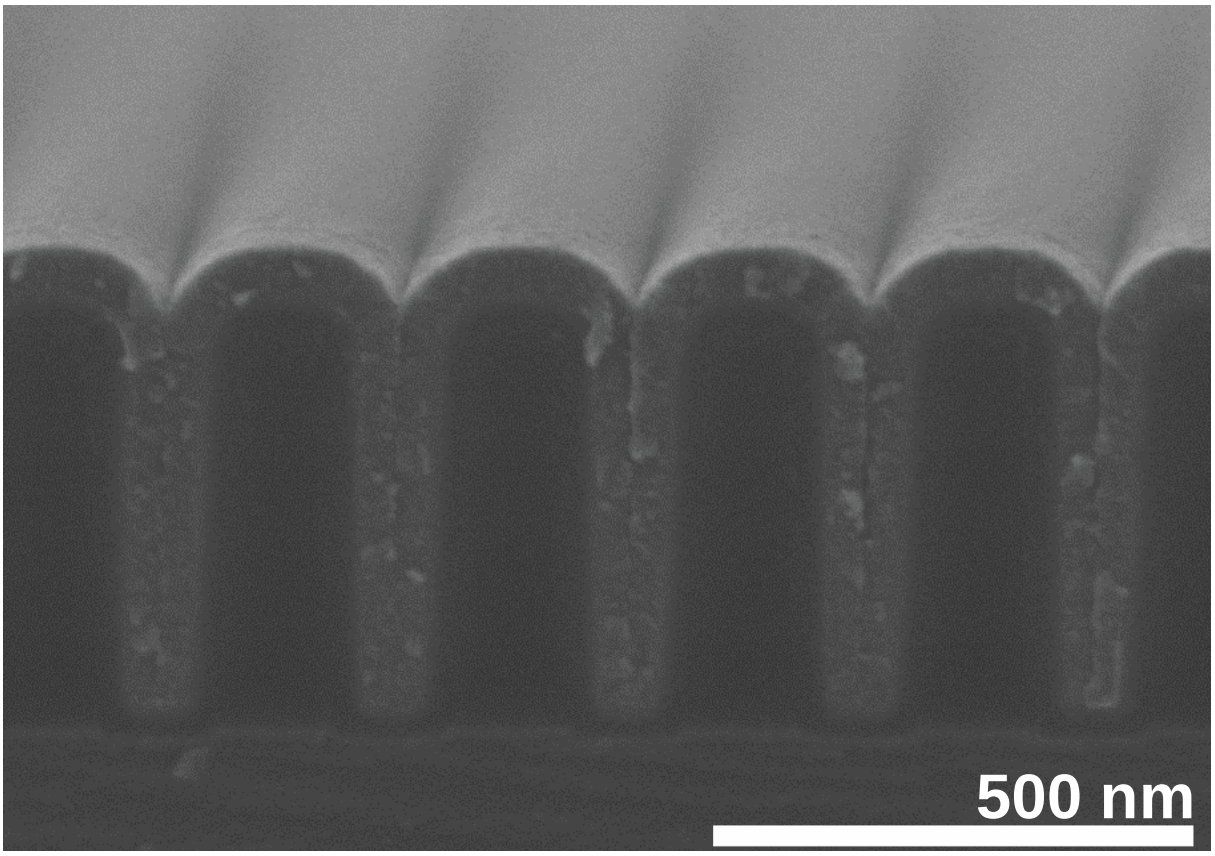

Figure 5.12. A photonic crystal uniformly infilled with Fe by static CVD.[53]

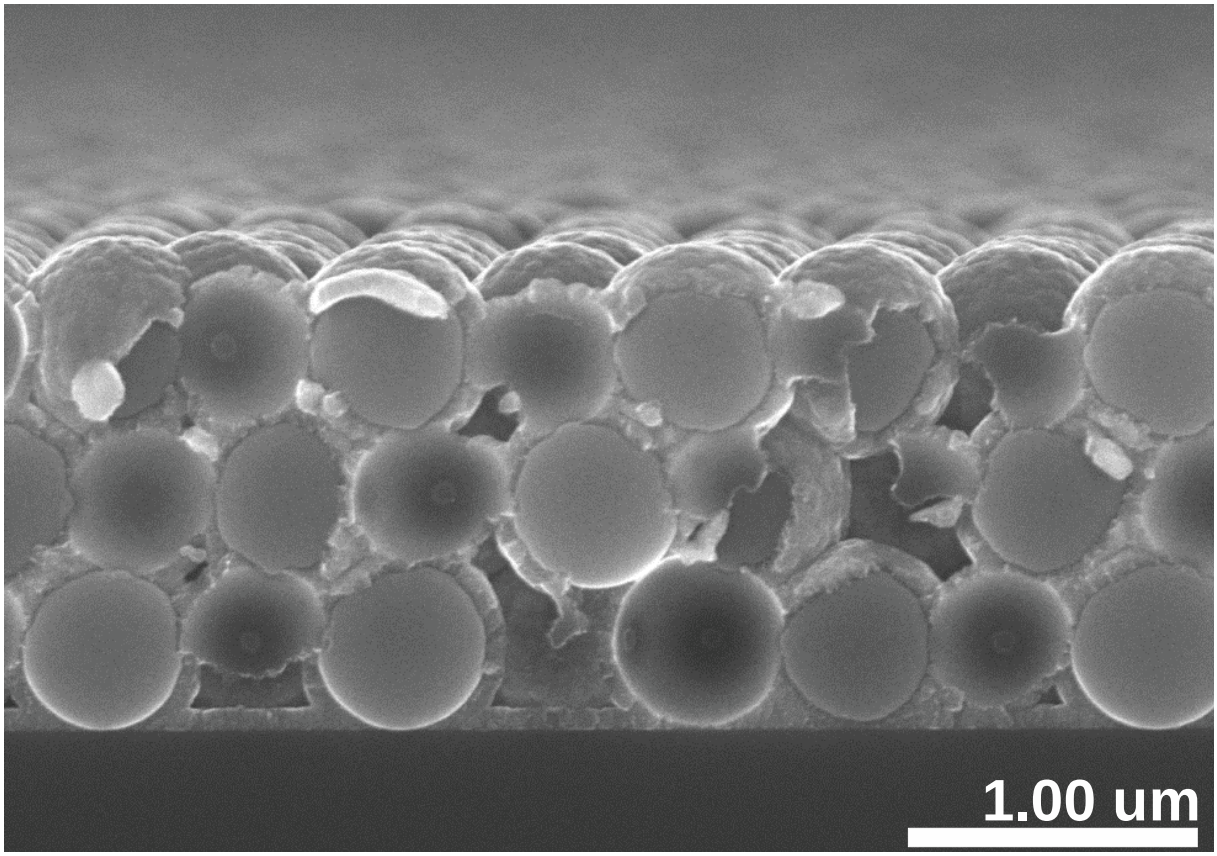

Figure 5.13. Top: Uncoated GaAs nanowires. Middle: Attempt to coat the nanowires with Fe by LPCVD. Bottom: GaAs nanowires conformally coated with Fe by static CVD.[53]

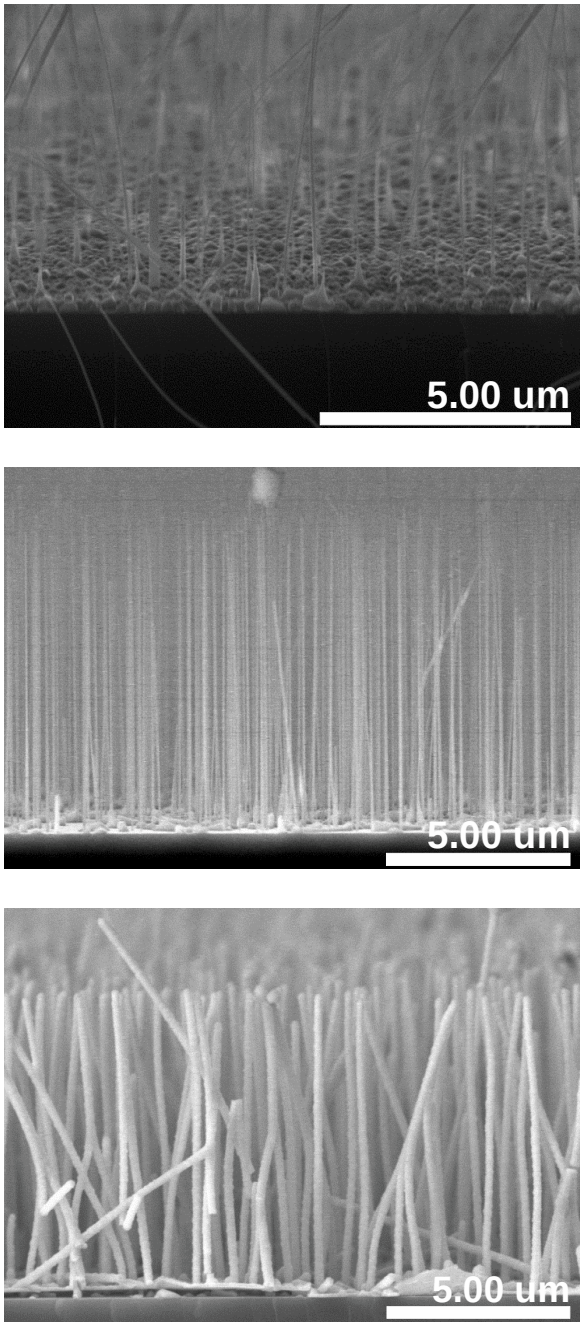

Discussion

Recently, Abelson and Girolami have demonstrated that the addition of a growth inhibitor, such as ammonia or 1,2-dimethoxyethane, slows film growth on high flux surfaces due to a site-blocking effect. The addition of a growth inhibitor enables the precursor to diffuse more deeply into relief features and greatly increases the areal density of nuclei during low temperature CVD. These effects lead to improved film conformality and smoothness in high aspect ratio relief features in comparison to films grown without the addition of an inhibitor.[2,64,65] When using CVD precursors of appropriately high vapor pressure, static CVD offers the further advantages of a low cost and simple setup, high precursor utilization rates, and superior conformality.

Precursor selection is of great importance for static CVD; even more so than with an actively pumped thermal CVD system. Unlike in a flow system where fresh precursor is being continuously introduced to the substrate, the entirety of the precursor available for film growth is sealed in the deposition chamber, without any additional precursor supplied during the deposition. As such, high vapor pressure precursors are required to achieve film thicknesses of several tens of nanometers. Based on our results with $Hf(BH_4)_4$ and $Fe(CO)_5$, lower vapor pressure precursors with a vapor pressure of 1 Torr would produce a film approximately 3 to 6 nm thick. The other consideration is byproduct stability and incorporation. $Hf(BH_4)_4$ and $Fe(CO)_5$ both produce byproducts which are rather stable at 200 °C, neither undergo further

decomposition at an appreciable rate nor become incorporated into the film in significant quantities. However, many organometallic precursors with thermally sensitive ligands may produce byproducts with undergo further decompositions, generating reactive species which will lead to film contamination.

Conclusions

Static chemical vapor deposition has been used to deposit conformal thin films of HfB_2 and Fe metal using $Hf(BH_4)_4$ and $Fe(CO)_5$, respectively. A step coverage of 40% in a macrotrench has been achieved using the $Hf(BH_4)_4$ precursor. In addition to the advantage of conformality when comparison to an actively pumped system, static CVD can be performed with a simple and inexpensive apparatus as well as proved superior precursor utilization rates.

Apparatus and General Procedure

The $Hf(BH_4)_4$ precursor was synthesized by a solid state reaction between $HfCl_4$ and $LiBH_4$.[66,67] Iron pentacarbonyl, $Fe(CO)_5$, was used as received. Surface characterizations (scanning electron microscopy, Auger electron spectroscopy, and x-ray photoelectron spectroscopy) were performed by Andrew Cloud (Abelson Group, UIUC) at the University of Illinois at Urbana-Champaign Materials Research Laboratory. Computed Tomography (CT) imaging was performed at the University of

Illinois at Urbana-Champaign, Beckman Institute Imaging Technology Group. Electrical conductivity was measured using a four-point probe.

Static Chemical Vapor Deposition Apparatus. The apparatus is composed of three parts: a precursor container, a central valve, and a deposition tube. A schematic diagram and photograph of the apparatus are shown in Figures 5.14 and 5.15, respectively. All glass parts were fabricated by the University of Illinois at Urbana-Champaign School of Chemical Sciences glass shop from vacuum compatible borosilicate pieces. The apparatus is connected to a standard Schlenk line (base pressure: ca. 10 mTorr, Welch Duoseal high vacuum pump) by gum rubber tubing. All ground glass joints are lubricated with either Dow Corning high vacuum grease or Apiezon H grease. The precursor container is either a Schlenk tube or 100 mL round-bottomed Schlenk flask. The precursor container is connected to a Schlenk line through a 2 mm ground glass stopcock and to the central valve by a female 24/40 ground glass joint. The deposition tube is 273 mm long, as measured from the inner margin of the 24/40 ground glass joint to the closed end of the tube. For the first 70 mm next to the ground glass joint, the tube has a 28 mm outer diameter; the remaining 200 mm of the tube has a 20 mm outer diameter. The interior volume of the deposition tube is approximately 92 cm^3. The deposition tube is connected to the Schlenk line through a 2 mm ground glass stopcock and to the rest of the apparatus by a female 24/40 ground

glass joint. The central valve connecting the precursor container and deposition tube consists of two male 24/40 ground glass joints joined by a 4 mm ground glass stopcock.

The tube furnace was either a Thermolyne 21100 equipped with a Eurotherm 2116 controller, or a Lindberg Blue tube furnace equipped with a Yokogawa UT150 controller. The deposition hot zone was the distal 170 mm of the deposition tube. Glass wool was packed in the open end of the tube furnace and between the furnace opening and the deposition tube to provide thermal insulation.

Static Chemical Vapor Deposition General Procedure. The precursor container was charged with precursor under argon and fitted with the central valve. The sample substrates were loaded into the center of the hot zone of the deposition tube, and the precursor container and valve assembly were connected to the deposition tube. The entire apparatus was evacuated and sealed under vacuum. The deposition tube was then cycled between an atmosphere of argon and vacuum to remove residual oxygen and water vapor followed by heating the deposition tube to greater than 100 °C while under vacuum using either a heat gun or tube furnace. The tube was subsequently cycled between vacuum and argon while it cooled to room temperature. The deposition tube was sealed under vacuum and the central valve connecting the precursor container to the deposition tube was opened for 15 minutes, after which it was closed, isolating the deposition container.

The tube furnace was programmed with the desired temperature set-point, dwell time, and a ramp rate. When the program ended, the deposition tube was allowed to cool to room temperature. The deposition tube was again evacuated and cycled with argon to remove volatile byproducts. Then the deposition tube was back-filled with argon and detached from the central valve. After the grease was carefully cleaned from the ground glass joint, the samples were retrieved.

Figure 5.14. Schematic depicting a disassembled static CVD apparatus (top) and an assembled static CVD apparatus (bottom).

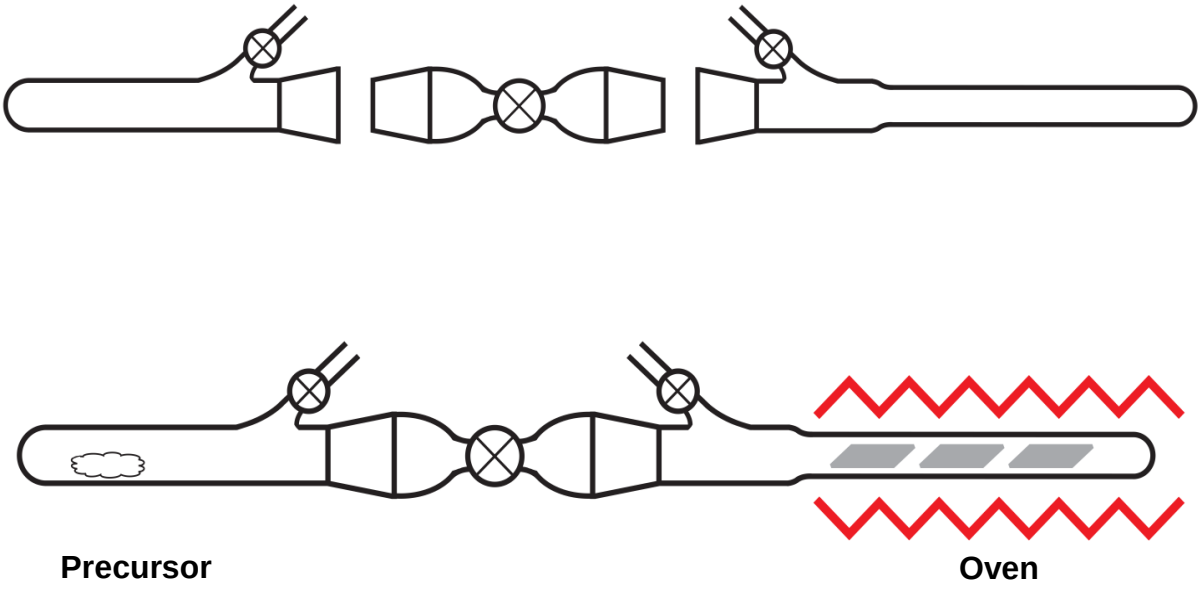

Figure 5.15. Image of the static CVD apparatus during the deposition of HfB_2.

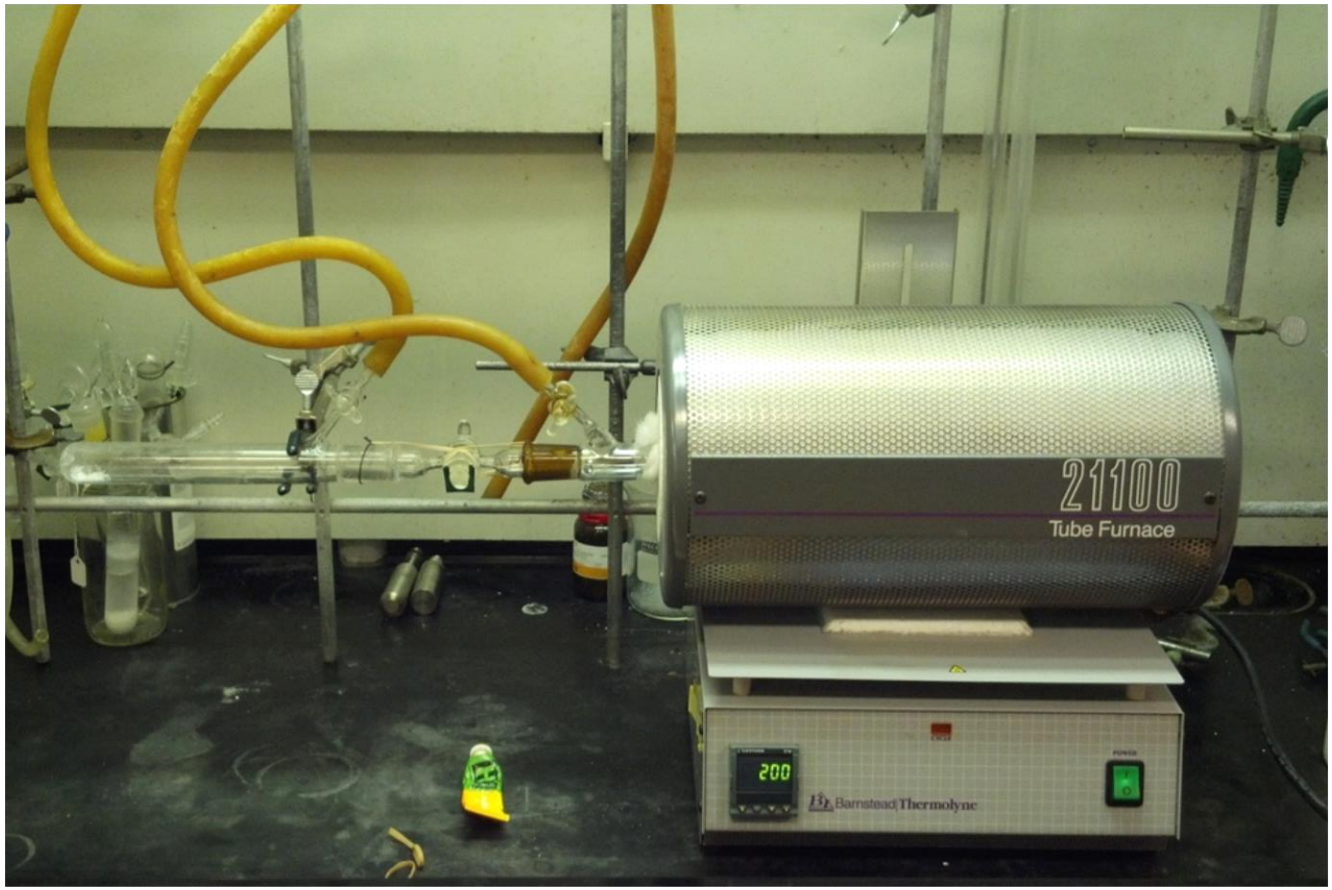

References

(1) Wang, W. B.; Yang, Y.; Yanguas-Gil, A.; Chang, N. N.; Girolami, G. S.; Abelson, J. R. *Appl. Phys. Lett.* **2013**, *102*, 101605.

(2) Babar, S.; Kumar, N.; Zhang, P.; Abelson, J. R.; Dunbar, A. C.; Daly, S. R.; Girolami, G. S. *Chem. Mater.* **2013**, *25*, 662-667.

(3) Pierson, H. O. *Handbook of Chemical Vapor Deposition, 2nd Edition: Principles, Technology and Applications*; Elsevier Science, 1999.

(4) Douard, A.; Maury, F. *Surf. Coat. Technol.* **2005**, *200*, 1407-1412.

(5) Rastogi, A. C.; Dhara, S.; Das, B. K. *J. Electrochem. Soc.* **1995**, *142*, 3148-3156.

(6) Thomas, N. A. *Silicon Heterostructure Handbook*; CRC Press: 2005, 95-105.

(7) Choy, K. L. *Prog. Mater. Sci.* **2003**, *48*, 57-170.

(8) Lundin, D.; Pedersen, H. *Physics Procedia* **2013**, *46*, 3-11.

(9) Irvine, S. J. C.; Lamb, D. *Chemical Vapour Deposition: Precursors*; The Royal Society of Chemistry: 2009, 477-493.

(10) Ndiege, N.; Subramanian, V.; Shannon, M. A.; Masel, R. I. *Thin Solid Films* **2008**, *516*, 8307-8314.

(11) Paorici, C.; Attolini, G. *Mater. Chem.* **1979**, *4*, 301-307.

(12) Singh, R. N.; Coble, R. L. *J. Cryst. Growth* **1974**, *21*, 261-266.

(13) Carlsson, J. *J. Less-Common Met.* **1980**, *71*, 1-14.

(14) Jasinski, J. M.; Meyerson, B. S.; Scott, B. A. *Annu. Rev. Phys. Chem.* **1987**, *38*, 109-140.

(15) Emslie, D. J. H.; Chadha, P.; Price, J. S. *Coord. Chem. Rev.* **2013**, *257*, 3282-3296.

(16) Devi, A. *Coord. Chem. Rev.* **2013**, *257*, 3332-3384.

(17) Li, W. *Chem. Vap. Deposition* **2013**, *19*, 82-103.

(18) Koynov, S.; Schwarz, R.; Fischer, T.; Grebner, S.; Münder, H. *Jpn. J. Appl. Phys.* **1994**, *33*, 4534-4539.

(19) Míguez, H.; Chomski, E.; García-Santamaría, F.; Ibisate, M.; John, S.; López, C.; Meseguer, F.; Mondia, J. P.; Ozin, G. A.; Toader, O.; van Driel, H. M. *Adv. Mater.* **2001**, *13*, 1634-1637.

(20) Kieffer, R.; Benesovsky, F. *Hartstoffe*; Springer-Verlag: Berlin, 1963.

(21) Chatterjee, A.; Jayaraman, S.; Gerbi, J. E.; Kumar, N.; Abelson, J. R.; Bellon, P.; Polycarpou, A. A.; Chevalier, J. P. *Surf. Coat. Technol.* **2006**, *201*, 4317-4322.

(22) Gasch, M.; Johnson, S.; Marschall, J. *J. Am. Ceram. Soc.* **2008**, *91*, 1423-1432.

(23) Wayda, A. L.; Schneemeyer, L. F.; Opila, R. L. *Appl. Phys. Lett.* **1988**, *53*, 361-363.

(24) Jayaraman, S.; Yang, Y.; Kim, D. Y.; Girolami, G. S.; Abelson, J. R. *J. Vac. Sci. Technol., A* **2005**, *23*, 1619-1625.

(25) Wittmer, M. *J. Vac. Sci. Technol., A* **1984**, *2*, 273-280.

(26) Nicolet, M. A. *Thin Solid Films* **1978**, *52*, 415-443.

(27) Teixeira, S. R.; Freire Jr., F. L.; Baumvol, I. J. R. *Appl. Phys. A: Mater. Sci. Process.* **1989**, *48*, 481-488.

(28) Quandt, E. *J. Alloys Compd.* **1997**, *258*, 126-132.

(29) Fomin, L. A.; Malikov, I. V.; Vinnichenko, V. Y.; Mikhailov, G. M. *Russ. Microelectron.* **2008**, *37*, 283-295.

(30) Cadieu, F. J.; Cheung, T. D.; Wickramasekara, L.; Kamprath, N.; Hegde, H.; Liu, N. C. *J. Appl. Phys.* **1987**, *62*, 3866-3872.

(31) Dieny, B.; Speriosu, V. S.; Metin, S.; Parkin, S. S. P.; Gurney, B. A.; Baumgart, P.; Wilhoit, D. R. *J. Appl. Phys.* **1991**, *69*, 4774-4779.

(32) Sato, R.; Mizushima, K. *Appl. Phys. Lett.* **2001**, *79*, 1157-1159.

(33) Zhu, H. J.; Ramsteiner, M.; Kostial, H.; Wassermeier, M.; Schönherr, H. P.; Ploog, K. H. *Phys. Rev. Lett.* **2001**, *87*, 016601.

(34) Xu, M.; Zaera, F. *J. Vac. Sci. Technol., A* **1996**, *14*, 415-424.

(35) Fahrenholtz, W. G.; Hilmas, G. E.; Talmy, I. G.; Zaykoski, J. A. *J. Am. Ceram. Soc.* **2007**, *90*, 1347-1364.

(36) Anselmi-Tamburini, U.; Kodera, Y.; Gasch, M.; Unuvar, C.; Munir, Z. A.; Ohyanagi, M.; Johnson, S. M. *J. Mater. Sci.* **2006**, *41*, 3097-3104.

(37) Jensen, J. A.; Gozum, J. E.; Pollina, D. M.; Girolami, G. S. *J. Am. Chem. Soc.* **1988**, *110*, 1643-1644.

(38) Hoekstra, H. R.; Katz, J. J. *J. Am. Chem. Soc.* **1949**, *71*, 2488-2492.

(39) Yang, Y.; Abelson, J. R. *J. Cryst. Growth* **2008**, *310*, 3197-3202.

(40) Jayaraman, S.; Gerbi, J. E.; Yang, Y.; Kim, D. Y.; Chatterjee, A.; Bellon, P.; Girolami, G. S.; Chevalier, J. P.; Abelson, J. R. *Surf. Coat. Technol.* **2006**, *200*, 6629-6633.

(41) Yang, Y.; Jayaraman, S.; Kim, D. Y.; Girolami, G. S.; Abelson, J. R. *J. Cryst. Growth* **2006**, *294*, 389-395.

(42) Fernández, H.; Grotewold, J.; Previtali, C. M. *J. Chem. Soc., Dalton Trans.* **1973**, 2090-2095.

(43) Yang, Y.; Jayaraman, S.; Kim, D. Y.; Girolami, G. S.; Abelson, J. R. *Chem. Mater.* **2006**, *18*, 5088-5096.

(44) Arpin, K. A.; Losego, M. D.; Cloud, A. N.; Ning, H.; Mallek, J.; Sergeant, N. P.; Zhu, L.; Yu, Z.; Kalanyan, B.; Parsons, G. N.; Girolami, G. S.; Abelson, J. R.; Fan, S.; Braun, P. V. *Nat. Commun.* **2013**, *4*, 3630.

(45) López, C. *Adv. Mater.* **2003**, *15*, 1679-1704.

(46) López-García, M.; Galisteo-López, J. F.; Blanco, Á.; López, C.; García-Martín, A. *Adv. Funct. Mater.* **2010**, *20*, 4338-4343.

(47) Mane, A. U.; Greene, J. P.; Nolen, J. A.; Sampathkumaran, U.; Owen, T. W.; Winter, R.; Elam, J. W. *Appl. Surf. Sci.* **2012**, *258*, 6472-6478.

(48) Ghosal, S.; Baumann, T. F.; King, J. S.; Kucheyev, S. O.; Wang, Y.; Worsley, M. A.; Biener, J.; Bent, S. F.; Hamza, A. V. *Chem. Mater.* **2009**, *21*, 1989-1992.

(49) Kucheyev, S. O.; Biener, J.; Baumann, T. F.; Wang, Y. M.; Hamza, A. V.; Li, Z.; Lee, D. K.; Gordon, R. G. *Langmuir* **2008**, *24*, 943-948.

(50) Elam, J. W.; Libera, J. A.; Pellin, M. J.; Zinovev, A. V.; Greene, J. P.; Nolen, J. A. *Appl. Phys. Lett.* **2006**, *89*, 053124.

(51) Baumann, T. F.; Biener, J.; Wang, Y. M.; Kucheyev, S. O.; Nelson, E. J.; Satcher, J. H.; Elam, J. W.; Pellin, M. J.; Hamza, A. V. *Chem. Mater.* **2006**, *18*, 6106-6108.

(52) Kucheyev, S. O.; Biener, J.; Wang, Y. M.; Baumann, T. F.; Wu, K. J.; van Buuren, T.; Hamza, A. V.; Satcher Jr., J. H.; Elam, J. W.; Pellin, M. J. *Appl. Phys. Lett.* **2005**, *86*, 083108.

(53) Data collected by Andrew Cloud.

(54) Liu, K.; Shen, D.; Zhang, J.; Wu, X.; Li, B.; Li, B.; Lu, Y.; Fan, X. *Solid State Commun.* **2006**, *140*, 33-37.

(55) Delsol, T. *Proc. - Electrochem. Soc.* **2005**, *2005-09*, 638.

(56) Maruyama, T.; Shinyashiki, Y. *Thin Solid Films* **1998**, *333*, 203-206.

(57) Low, Y. H.; Bain, M. F.; Bien, D. C. S.; Montgomery, J. H.; Armstrong, B. M.; Gamble, H. S. *Microelectron. Eng.* **2006**, *83*, 2229-2233.

(58) Bain, M. F.; Low, Y. H.; Bien, D. C. S.; Montgomery, J. H.; Armstrong, B. M.; Gamble, H. S. *Surf. Coat. Technol.* **2007**, *201*, 8998-9002.

(59) Low, Y. H.; Montgomery, J. H.; Gamble, H. S. *ECS Trans.* **2007**, *2*, 167-177.

(60) Zaera, F. *Langmuir* **1991**, *7*, 1188-1191.

(61) Hofer, L. J. E.; Sterling, E.; McCartney, J. T. *J. Phys. Chem.* **1955**, *59*, 1153-1155.

(62) Moon, D. W.; Dwyer, D. J.; Bernasek, S. L. *Surf. Sci.* **1985**, *163*, 215-229.

(63) Rhodin, T. N.; Brucker, C. F. *Solid State Commun.* **1977**, *23*, 275-279.

(64) Abelson, J. R. *ECS Trans.* **2010**, *33*, 307-319.

(65) Kumar, N.; Yanguas-Gil, A.; Daly, S. R.; Girolami, G. S.; Abelson, J. R. *J. Am. Chem. Soc.* **2008**, *130*, 17660-17661.

(66) James, B. D.; Nanda, R. K.; Wallbridge, M. G. H. *J. Chem. Soc., A* **1966**, 182-184.

(67) Reid Jr., W. E.; Bish, J. M.; Brenner, A. *J. Electrochem. Soc.* **1957**, *104*, 21-29.

Appendix A: Preparation of High Purity Hafnium Borohydride for Electron Beam Induced Deposition Using a Scanning Electron Microscope.

Introduction

Hafnium borohydride prepared by the Girolami group is performed in the solid state either by ball milling or stirring hafnium tetrachloride (1 eq.) with lithium borohydride (ca. 5 eq.). Both methods require the use of a Schlenk line and glove box which may contaminate the product with grease and pump oil as well as other unknown chemical contaminates. When $Hf(BH_4)_4$, which has been prepared by our typical methods, is used in scanning tunneling microscope (STM) electron beam induced deposition (EBID) experiments by the Lyding group (UIUC) over a period of weeks to months large, amorphous, non-conductive "blobs" begin to contaminate the UHV-STM system. This requires the system be baked out and the $Hf(BH_4)_4$ precursor be replaced. The following method has successfully been used to synthesize and purify $Hf(BH_4)_4$ suitable for long term use in STM EBID experiments.

Experimental

Hafnium tetrachloride (98 %, Aldrich) and lithium borohydride (>90%, Aldrich) were used as received. The starting materials need to be a fine powder in order for the reaction to proceed in a timely fashion. A fume hood was cleared of all nonessential

equipment and was lined with padding. Stainless steel ball bearings, a scoupula, and the ball milling container were rinsed thoroughly with electronics grade isopropyl alcohol and were allowed to dry at 60 – 80 °C. A glove bag was loaded with a balance, unopened bottles of hafnium tetrachloride and lithium borohydride, weigh boats, stainless steel ball bearings, a scoupula, the ball milling container fitted with a valve and the appropriate hardware and wrenches. The glove bag was inflated with argon and vented to the atmosphere several times and before being sealed. Approximately 1 g of hafnium tetrachloride and 0.34 g of lithium borohydride were weighed out and transferred to the ball milling container. Grinding the reagents to a fine powder was performed using a mortar and pestle prior to transferring the reagents to the ball milling container. The stainless steel ball bearings were transferred to the container and the container was sealed. The ball milling container was gently shaken in the glove bag for approximately 30 min, during which time crystalline hafnium borohydride was observed forming on the upper portion of the container and the white solid remaining in the bottom of the container became tacky. The container was then removed from the glove bag and transported to the Lyding lab.

The STM chamber had been fitted with a precursor container and necessary valves prior to connecting the ball milling container. The ball milling container was attached to the STM chamber and the entire precursor delivery system was baked at >100 °C overnight and allowed to cool to room temperature. The precursor dosing

system was checked for leaks using He and the STM residual gas analyzer (RGA). The vacuum gauges on the STM chamber *MUST* be turned off to avoid damaging them prior to evacuation of the ball milling container. The ball milling container was cooled using dry ice to decrease the vapor pressure of the hafnium borohydride prior to evacuating the container of argon. The container was assumed to be a vacuum when the whine of the turbo pump ceased. The dry ice was removed and the ball milling container and the precursor container was cooled using dry ice. The valves were open between the ball milling container and precursor container until no crystalline hafnium borohydride was visible in the ball milling container (usually 2 to 4 hours). The ball milling container was removed from the system and cleaned. The precursor container remained on the system at room temperature for more than a year without visible degradation of the hafnium borohydride.

Figure A.1. Sublimation system connected to the STM system. All valves are high pressure diaphragm valves.